POLITECNICO DI MILANO

School of Civil, Environmental and Land Management Engineering

Master of Science in Environmental and Land Planning Engineering

POLITECNICO
MILANO 1863

Exploring the water-energy nexus in the Iberian Peninsula under climate change: a deterministic optimization approach

Supervisor: Prof. Andrea Castelletti

Assistant Supervisor: Prof. Peter Bauer-Gottwein

Master Graduation Thesis by:

Federica Bertoni

Student Id n. 837724

Academic Year: 2015-16

Acknowledgments

I will always be grateful to my supervisor Andrea Castelletti for being a great source of inspiration and encouragement, and for his dedication.

Special thanks are also due to Peter Bauer-Gottwein, who hosted me in Copenhagen at the department of Hydrology and Water Resources Management of DTU, supporting and helping me with his valuable advice and meticulous comments.

Long hours at University were livened by all the great people passing through here: my deskmate Raphaël, who helped me out with his smart ideas and brightened up all my days, and “The Three Germans”, who made my life in Copenhagen so much better. And thank you to all my friends in Denmark: you all made this year impossible to forget.

I am extremely grateful to all my family, for their constant and unconditioned love and support. Thank you to all my friends in Italy; life is wonderful when you have real friends. In the end, special thanks are due to Nico, who always had the right words to say to put a smile back on my face.

Abstract

Energy and freshwater resources are strictly interconnected: the former is used to clean and transport freshwater needed, the latter to help produce the energy required. Their policy goals often conflict; their competition is expected to be enhanced especially by climate change-induced alterations in water resources. Climate change might also rise some concerns whether future cooling water needs can be met in thermoelectric power industry, which is responsible for about 80% of global energy generation. Due to the difficulty of the problem, a deeper knowledge of the impacts of water constraints on electricity production and of feasible methods to include water-energy security when planning future energy systems are required for planning purposes. The objective of this thesis is to find a proper method to further improve the modelling of water-energy nexus in order to analyze the effects of thermal cooling constraints on both thermal and overall energy production, as well as on the entire water-power system. In order to achieve this goal, a deterministic, single objective, resource allocation problem is implemented. The single objective consists in minimizing the net costs of the system. The model is optimized through a linear programming solver over both control (1961-1990) and future climate (2036-2065) in order to assess the effects of climate change and compare the consequences of cooling constraints in both time periods. The case study is the Iberian Peninsula. Within control scenario, thermal cooling restrictions do not have a significant impact on the water-power system of the IP. In future climate, these limitations become more binding, mainly due to higher water temperatures and lower inflows induced by climate change. The combination of climate change and thus stricter cooling constraints might have significant effects on several elements of the coupled system (e.g. reduced hydropower production, increased agriculture deficit, increased modelled and residual thermal generation).

***Keywords**:* Water-Energy Nexus, Iberian Peninsula, Thermal Cooling Constraints, Deterministic, Costs Minimization, Climate Change

Sintesi

Energia e risorse idriche sono strettamente interconnesse. La prima è impiegata nella pulizia e nel trasporto delle risorse idriche; le seconde nella produzione di energia elettrica. I loro obiettivi spesso entrano in conflitto. Si prevede che in futuro questa competizione verrà esacerbata dalle alterazioni indotte dal cambiamento climatico nell'ambito delle risorse naturali. Il cambiamento climatico potrebbe inoltre destare preoccupazioni riguardo il soddisfacimento delle future esigenze idriche per il raffreddamento delle industrie termoelettriche che producono circa l'80% dell'energia elettrica globale. A causa della complessità dell'argomento, sono necessari sia una conoscenza più approfondita degli impatti dei vincoli idrici sulla produzione elettrica che l'individuazione di possibili metodi che includano nella pianificazione la sicurezza idrica ed energetica. L'obiettivo di questa tesi è cercare un metodo idoneo all'ulteriore miglioramento della modellizzazione del nesso acqua-energia, al fine di analizzare gli effetti dei vincoli sul raffreddamento termoelettrico sulla produzione elettrica (sia termica che non), nonché sull'intero sistema acqua-energia. Per raggiungere tale obiettivo, è stato implementato un modello di allocazione di risorse di tipo deterministico e a singolo obiettivo. Il singolo obiettivo consiste nella minimizzazione dei costi netti del sistema. Il modello è stato ottimizzato attraverso la programmazione lineare sia su un periodo storico di controllo (1961-1990) che futuro (2036-2065), al fine di valutare gli impatti del cambiamento climatico e confrontare le conseguenze dei vincoli sul raffreddamento termoelettrico in entrambe le finestre temporali. Il caso di studio è la Penisola Iberica. Nello scenario di controllo, le restrizioni sul raffreddamento termoelettrico non hanno determinato impatti significativi sul sistema acqua-energia della Penisola. In quello futuro, invece, queste limitazioni sono diventate più vincolanti, principalmente a causa delle temperature più elevate delle fonti idriche e dei minori afflussi dovuti al cambiamento climatico. La combinazione "cambiamento climatico"-"vincoli più severi" sul raffreddamento hanno avuto conseguenze significative su diversi elementi del sistema accoppiato acqua-energia (e.g. produzione idroelettrica ridotta, deficit agricolo e produzione termica in aumento).

***Parole Chiave**:* Nesso Acqua-Energia, Penisola Iberica, Vincoli Raffreddamento Termoelettrico, Deterministico, Minimizzazione Costi, Cambiamento Climatico

Table of Contents

Part VI - Conclusions

List of Figures

List of Tables

List of Abbreviations

IP	Iberian Peninsula
MIBEL	Iberian Power Market
CF	Change Factor
RCM	Regional Climate Model
HP	Hydropower Plant
TPP	Thermal Power Plant
LP	Linear Programming
IWD	Irrigation Water Demand
CWD	Crop Water Demand
Hw	Waste Heat

Part I

Introduction

Chapter 1

Background and Motivation

Energy and freshwater resources are strictly interconnected: the former is used to clean and transport freshwater needed, the latter to help produce the energy required (Gleick, 1994). Water is an integral element of both energy resource development and utilization (it is used in energy-resource extraction, refining and processing, and transportation) and electric-power generation (it is used directly in hydroelectric generation and for cooling and emissions scrubbing in thermoelectric generation) (US Department of Energy, 2006). On the other hand, energy is essential to extract, treat and distribute drinking water as well as to collect and treat wastewater, even if its dependency on water is less apparent (Olsson, 2012).

Water and energy policy goals often conflict; this discordance originates from the interdependence of water and energy, commonly called the 'water-energy nexus' (Stucki et al., 2012; Scanlon et al., 2013). According to Hoffman (2010), as demand for one increases, so does the demand for the other. The competition between water resources and power generation caused serious conflicts and arose several debates throughout the decades (Gleick, 1993a; King et al., 2008). Rather recent researches (King et al., 2008; van Vliet et al., 2016) suggest that these clashes are expected to be enhanced by climate change-induced alterations in water resources (IPCC, 2007), growing population and rising welfare, which will lead to an increase in the amount and quality of water (Vörösmarty et al., 2000) and energy requested (International Energy Agency, 2008). In particular, global water consumption for power generation is projected to double within the next four decades (Olsson, 2012), leading to an increased scarcity and competition for water across different sectors (e.g., agriculture and energy; van Vliet et al., 2016).

Due to the complicated interconnections between water and power systems, formulating a joint hydrological-energy model is complex. For example, the energy supply sector[1] is the largest contributor to global greenhouse gas emissions, accounting for approximately 35% of total anthropogenic GHG emissions in 2010 (IPCC, 2014). This may contribute to climate change, which might in turn have some negative effects on different sectors: (i) increase in the energy demand (Flörke et al., 2011; Isaac et al., 2009); (ii) reduction in the hydropower generation potential (Lehner et al., 2005; Schaefli et al., 2007; Vicuna et al.,

[1]The energy supply sector comprises all energy extraction, conversion, storage, transmission, and distribution processes that deliver final energy to the end-use sectors (industry, transport, and building, as well as agriculture and forestry) (IPCC, 2014).

2009); (iii) concerns whether future cooling water needs can be met in the thermoelectric power industry (Flörke et al., 2011; Feeley et al., 2008). Moreover, a future change in cooling technology of thermal power plants may lead to a 10% increase in cooling water consumption by the end of the century, which is relevant for already water-stressed systems (Davies et al., 2013). This is an explanatory example of the complexity of the so-called 'water-energy nexus'.

Due to the difficulty of the problem, a deeper knowledge of the impact of water constraints on electricity production and of the feasible methods to include water-energy security when planning future energy systems are required for planning purposes (van Vliet et al., 2016). Therefore, at either the local or the country level, several coupled hydrological-electricity models have already been developed, which include the effects of local or regional water constraints on power supply (Pereira-Cardenal et al., 2014; Hamlet et al., 2010; Koch et al., 2012).
As stated by Pereira-Cardenal et al. (2013), the implementation of these joint models is hard because of differences in their spatio-temporal scales and current management. Firstly, energy systems (including pipeline networks and the power grid) span an entire nation or several nations. Moreover, the power grid does not follow natural boundaries such as river basins and power supply must satisfy demand on a second-by-second basis. In the end, energy can be moved relatively easily. On the other hand, water systems are spatially limited by a catchment area and hydraulically connected. Moreover, the balancing between supply and demand is rather flexible, whereas the inter-basin transfer of water requires significant investments of energy and is not economically feasible for bulk water (WWAP, 2014). Secondly, from the management point of view, these two systems are noticeably different: electricity is commonly traded in a wholesale market, while water is allocated using a wide variety of water rights regimes (Bruns et al., 2005).

The purpose of this thesis is to find a proper method to further improve the modelling of the water-energy nexus in order to analyze the effects of thermal cooling constraints on both thermal and overall energy production, as well as on the entire water-power system. In order to achieve this goal, a spatially detailed representation of this coupled system is required.

At the global scale, about 80% of the energy generation comes from thermoelectric power plants (e.g. fossil fuels and nuclear), which require cooling for efficient and safe operation (International Energy Agency, 2015). As Byers et al. (2014) state, most of this cooling is obtained through water abstractions from, and thermal discharges to, the water network (e.g. rivers, sea).
When planning and managing thermal power stations, the long-term availability of a cooling resource must be considered because: (i) poor performance (due to decreased water availability) could threaten the financial feasibility of a project (EC JRC, 2001; Förster et al., 2009); (ii) the impacts of the sector must be fully taken into account in wider

water resources management, in order to avoid the threatening of other users' long-term water availability (Byers et al., 2014).
For example, in the USA thermoelectric generation represents the largest water user with its 38% of all freshwater withdrawals in 2010, followed by irrigation and public supply (USGS, 2010). In water-stressed areas of the country, power plants will increasingly have to compete with other water users. Thus, tradeoffs will occur and concerns will be raised over which use is more important: water for energy production, growing food or drinking and personal use (Feeley et al., 2008).
Also at the global scale, two factors already caused the shutting down of some thermoelectric power stations because of insufficient cooling water availability: droughts (Mediterranean Water Scarcity and Drought Working Group, 2007; Byers et al., 2014) and heatwaves (Hightower et al., 2008; Byers et al., 2014). For instance, a thermal power plant might withdraw water from a river whose streamflow is too low and/or temperature is too high, putting the continued use of cooling water at risk. This is not necessarily due to physical laws, but because water quality regulations might be violated (Förster et al., 2009). As far as river temperatures are concerned, most of the water withdrawn by the thermal power plants is discharged back into the water body at higher temperatures, thus heating it. This may have consequences for further utilization of the water from other users (Förster et al., 2009).
These examples confirm the vital importance and the complexity of including thermal cooling constraints into a joint water-energy model optimization framework.

1.1 Thesis Objectives

This thesis builds on a previous Ph.D. study conducted by Pereira-Cardenal et al. (2013). It introduces several novelties in the modelling of the water-power system of the case study analyzed (i.e. Iberian Peninsula): (i) the simulated system has not been spatially aggregated, i.e. all the hydropower plants have been modelled; (ii) the power system has been extended by modelling not only the hydropower but also the thermoelectric generators; (iii) the hydro-economic model has been implemented through the deterministic flow path method, thus optimized deterministically; (iv) cooling constraints have been applied to the thermal power plants in the optimization framework; (v) the water temperature of the several rivers has been estimated in order to implement the cooling constraints.

The main purposes of this thesis are to:

- Develop a deterministic method to model the spatial and temporal interactions between water and energy systems, without aggregating any constituent element;
- Improve and expand the power system already implemented by Pereira-Cardenal et al. (2013);

- Assess the impacts of cooling constraints on both thermal and overall energy production, as well as on the entire water-power coupled system;
- Estimate some of the potential effects of climate change on the water-energy model of the Iberian Peninsula (IP). In particular, focus on its consequences on thermal power production, constrained by cooling water requirements.

1.2 Thesis structure

This thesis project is divided into six parts:

- Part I: General introduction to the main topic this study is based on and presentation of four main thesis objectives;
- Part II: State of the art, i.e. literature overview on the main, relevant topics to this thesis study;
- Part III: Presentation of both the case study (i.e. IP) and the main input data;
- Part IV: Assessment of the methods employed to construct and optimize the deterministic model;
- Part V: Discussion of the significant results and overview of the main project simplifications, together with possible further researches to be developed to overcome these limitations;
- Part VI: Conclusions.

Part II

State of the Art

Part II

State of the Art

"The interdisciplinary nature of water resources problems requires the integration of technical, economic, environmental, social and legal aspects into a coherent analytical framework" (Serageldin, 1995). Nowadays, water is more and more considered an economic good because of its competing use resulting in resource scarcity (Briscoe, 2005; Young et al., 2014). Consequently, policy demand for information about the economic value of water together with the economic impacts of water management has increased. The implementation of integrated hydro-economic models needs to capture this complexity of interactions between water and economy in water resources problems. Their purpose is to link relevant hydrological and biogeochemical processes to implicit economic laws of supply and demand in the provision of scarce water services (Brouwer et al., 2008). In the following chapters, a literature overview of preexisting hydro-economic models, mainly focused on water-energy modelling, is presented. A review of the main studies concerning thermal power plants modelling and cooling water requirements is also included.

Chapter 2

Power Market

Electricity is vital for any modern economy (Al-Sunaidy et al., 2006). Traditionally, most countries saw their electricity sectors evolving with mainly vertically integrated geographic monopolies, which were either state or privately owned. These monopolies were subject to price and entry regulation, since utilities industry was (and still is) considered as a natural monopoly[2] (Al-Sunaidy et al., 2006; Joskow, 2006). Single utilities companies were to provide all the primary components of electricity supply (i.e. generation, transmission, distribution and retail supply) in exchange for exclusive franchises to supply electricity to every retail consumer (i.e. residential, commercial and industrial) within a certain geographic area (Joskow, 2006). In this framework, economic efficiency was often only one of the industry's priorities, since governments primarily wanted to provide a larger percentage of the population with modern infrastructure and services, in order to catalyze economic development (Williams et al., 2006).

During the 1980s, many state utilities started experiencing a financial crisis: their revenues were not high enough to cover costs and a strong under-capitalization lead them to suffer from supply shortages and high system losses. Nevertheless, an element external to the power sector was the trigger factor promoting market reform initiatives concerning the electricity supply industry: finance (Williams et al., 2006). Several justifications were mentioned as a support to these reforms. Firstly, it was quoted the willingness to introduce competition in order to: (a) make the power industry more efficient, (b) prices more transparent and (c) transfer more risk from consumers to suppliers. Secondly, lower electricity costs and improved benefits for ultimate consumers were pointed out, both driven by: (a) the ensuing productivity improvements, (b) better rationalization of labor and fuel costs, (c) superior choice of generation technologies, etc. (Sioshansi, 2008).

Thus, a consistent number of countries started to opt for deregulation as a major electricity market reform to improve economic performance (Al-Sunaidy et al., 2006). Several examples and outcomes of this renovation can be found in the most recent electricity market literature country by country (Al-Sunaidy et al., 2006; Williams et al., 2006; Sioshansi, 2008).

[2]Joskow (2006) gives a technological definition of natural monopoly: "A firm producing a single homogeneous product is a natural monopoly when it is less costly to produce any level of output of this product within a single firm than with two or more firms".

According to Al-Sunaidy et al. (2006), deregulation only affects power generation and supply, whereas the transmission and distribution networks in between them remain natural monopolies, and are best regulated. Deregulation may involve: (i) liberalization, allowing companies to enter the market in competition with the incumbents; (ii) restructuring, splitting incumbent companies vertically (e.g. transmission from generation) and/or horizontally (e.g. creating several competing generators); (iii) privatization. In 1982 Chile was the pioneering state of this liberalization process, followed by England and Wales in the early 1990s, which created the first electricity pool in Europe (Conejo et al., 2010).

Electricity trade between consumers and producers is facilitated by two trading arenas that form deregulated power markets: pool market and futures market. Moreover, there might be the possibility of suppliers and consumers signing bilateral contracts[3] and/or the presence of reserve and regulation as additional products in electricity markets (whose main product is energy). The reserve market fills in for temporary equipment failures or sudden demand/supply changes, while the regulation one follows the demand in real-time (Conejo et al., 2010; Pereira-Cardenal et al., 2013). However, these peculiarities are outside the scope of this thesis.

2.1 Pool Market

Pool market is a marketplace where power is exchanged on a short-term basis. Typically, it consists of three elements: (i) a day-ahead market, where the energy traded in the pool is mostly negotiated; (ii) several adjustment markets, used to make adjustments to the energy cleared in the previous market; (iii) balancing (or real-time) markets, which allow last minute energy adjustments, covering the dispatched power that is not produced because of equipment failures or the intermittent nature of some sources (e.g. wind or solar-thermal power plants).

The structure and working principle of this market are shown in Figure 2-1. Producers (i.e. non-dispatchable producers[4] and producers[5]) on one side and consumers[6] and retailers[7] on the other submit production offers and consumption bids respectively to the pool market. In the meantime, the market operator (MO) clears the market, determining prices and traded quantities (Conejo et al., 2010).

[3]A bilateral contract is a free deal between a supplier and a consumer made outside an organized marketplace (Conejo et al., 2010).
[4]Entities generating energy through non-dispatchable sources (e.g. wind or solar-thermal power plants) (Conejo et al., 2010).
[5]Entities owing the electricity production units (Conejo et al., 2010).
[6]End users of the electricity. They may buy it either in the pool or the futures market (Conejo et al., 2010).
[7]Entities purchasing energy to be delivered to their clients, i.e. consumers that do not directly participate in the electricity markets (Conejo et al., 2010).

2.2 Futures Market

Futures market is a marketplace that allows power trading on a medium- or long-term horizon. This means that it permits electricity exchange in the future at today prices, a very useful feature if the power price is highly uncertain in the pool (which is this the case).

The structure and working principle of this market are displayed in Figure 2-2. Producers on one side and consumers and retailers on the other use the futures market to sell and buy electricity at stable prices respectively. Two of the products available in this market are forward contracts[8] and options[9] (Conejo et al., 2010).

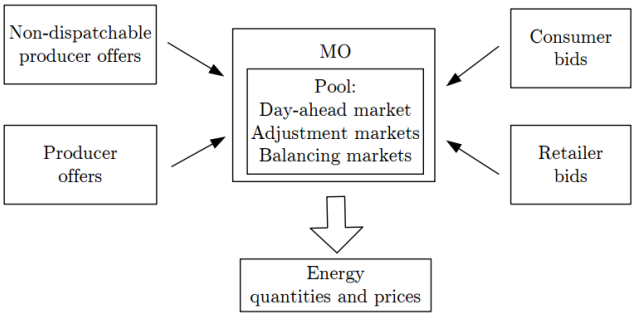

Figure 2-1: Pool market structure and functioning. Thin arrows represent the inputs to the pool market (i.e. offers and bids), whereas the thick arrow shows the market outcomes (Conejo et al., 2010).

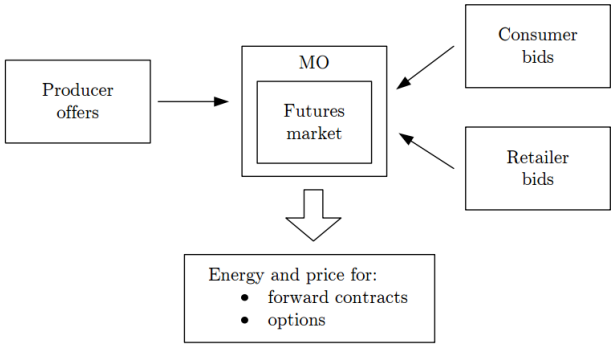

Figure 2-2: Futures market structure and functioning. Thin arrows represent the inputs to the futures market (i.e. offers and bids), whereas the thick arrow shows the market outcomes (Conejo et al., 2010).

[8]Agreement of delivering (consuming) a certain amount of power in the future at a fixed price (Conejo et al., 2010).
[9]Agreement for having the choice of delivering (consuming) a certain amount of power in the future (Conejo et al., 2010).

Chapter 3

Economic Value of Water

> *Water has an economic value in all its competing uses and should be recognized as an economic good. [..] Past failure to recognize the economic value of water has led to wasteful and environmentally damaging uses of the resource. Managing water as an economic good is an important way of achieving efficient and equitable use, and of encouraging conservation and protection of water resources.*
>
> Committee on Education, Principle No. 4 (UN, 1992)

Water is a vital resource used in multiple sectors, including the environment. Thus, its allocation is inherently a political and social process, which will most likely be analyzed more and more as the competition among the different sectors increases, due to socioeconomic development and population growth (Tilmant et al., 2009). Growing conflicts among water users and rapidly rising incremental costs of new supplies (aquifers already heavily exploited, best dam locations taken and other rivers protected) is leading to the need of a wider view in a mature water economy in order to face water scarcity problems (Harou et al., 2009). Under conditions of water scarcity, an economic focus helps water managers to identify efficient water allocations and reduce wasteful practices.

Water is typically allocated according to historical, institutional, political, legal and social traditions and conditions. This is what makes water slow to adapt to environmental or water demand changes. Thus, water managers' idea of water demand has to change from a static one to a demand related to the economic concept of value (Harou et al., 2009).
The former is defined through water rights, priorities and projections of population growth and agricultural and industrial water requirements. In other words, water demand is usually represented as a fixed supply target that has to be satisfied in non-economic system models (Pulido-Velazquez et al., 2008). For example, when crop irrigation is considered, water is often allocated through a system of annual rights to use a fixed volume, which is typically less than farmers' expectations (Young, 2005).
On the other hand, the economic value of water demand implies that water value changes with the quantity and type of use. One of the advantages of monetizing all water uses is an even-handed comparison among several uses (Harou et al., 2009). Moreover, it helps diffuse conflicts by clarifying and revealing the often relatively modest quantities involved (Fisher et al., 2002).

The Committee on Education also mentions this economic concept of water in Principle No. 4 (UN, 1992): "Managing water as an economic good is an important way of achieving efficient and equitable use".

The notion of economic efficiency is usually referred to as Pareto optimality: a given allocation of resources (e.g. water) is said to be economically efficient if and only if no individual could be made better off without making someone else worse off (Howe et al., 1986). However, economic efficiency must be traded off against the economic equity objective when allocating water among competing users.

Equity objectives refer to fairness or justice concepts and aim to redistribute the resource itself or the benefits derived from the use of the resource (Tilmant et al., 2009). In water resources allocation problems, implementing economic equity means redistributing and sharing the benefits rather than the water itself (Sadoff et al., 2002; Fisher et al., 2005). The study conducted by Tilmant et al. (2009) puts this idea into practice. They proposed a two-step approach:

- An optimization model, whose purpose is to maximize basin-wide net benefits, is used to identify economically efficient allocations policies;
- Financial compensations are derived from optimal allocation decisions and marginal water values. They are computed as follows: first, curtailed users receive compensations, which should be at least equal to their forgone benefits. Secondly, the individual contribution of the beneficiary user to compensations is calculated as proportional to its productivity. The expression beneficiary user refers to users who benefit from higher water allocations.

Hydro-economic models are based on the economic concept of water explained above.

Chapter 4

Hydro-Economic Models

Economics and engineering are two disciplines that have always been bounded together and exchanged their fundamental principles throughout the centuries (Lund et al., 2006). The French engineering school of the 1800s set the roots for modern engineering and economics (Hayek, 1950; Langins, 2004). Throughout the 19th and 20th centuries, water engineers continued to incorporate economic principles in systems' analysis through the development of hydro-economic models. In particular, these models can be traced back to the 1960s and 1970s in arid regions (e.g. Israel and the southwestern United States) (Harou et al., 2009). Bear et al. (1964, 1966, 1967, 1970) were among the first researchers to optimize water resource systems using economic water demand curves, establishing the conceptual framework for regional-scale integrated water management models (Gisser et al., 1973; Noel et al., 1980). According to Harou et al. (2009), since then researches have been using different names to refer to the implementation of this hydrologic engineering – economic water modelling approach including: hydrologic-economic (Gisser et al., 1972), hydroeconomic (Noel et al., 1982), economic-hydrologic-agronomic (Lefkoff et al., 1990b), integrated economic-hydrologic (McKinney et al., 1999; Rosegrant et al., 2000), integrated hydrologic-economic (Cai et al., 2003a; Ringler et al., 2004; Pulido-Velazquez et al., 2006) and so on. This thesis will use the term 'hydroeconomic' as defined by Noel et al. (1982) for brevity.

"Hydro-economic models integrate regional hydrologic, engineering, environmental and economic aspects of water resources systems within a single coherent framework, to examine water management for diverse types of economic values" (Medellìn-Azuara et al., 2009). They differ from engineering models, aimed at minimizing financial costs, or economic models (e.g. economy-wide general equilibrium models, cost-benefit analysis, etc.). For example, economy-wide general equilibrium models are distinct from most of the hydroeconomic ones because they represent how water resource policies influence the entire economic system, rather than focusing on the impact of economics on water resource management. Furthermore, they do not typically represent spatially distributed water resource systems (e.g. Mukherjee, 1996).

In hydroeconomic models, water allocation is driven or evaluated by the economic values it generates. Moreover, these models represent all major spatially distributed hydrologic and engineering parts of the system. These elements are usually modelled through a node-link network, where nodes are associated with economic demands and costs (or benefits)

are incurred on links. The network suits both physical and economic spatially distributed systems (Harou et al., 2009).

4.1 Compartment vs Holistic Approach

As far as model formulation and solution approaches are concerned, Braat et al. (1987) classify hydroeconomic models into: (i) models with a compartment or modular approach; (ii) models with a holistic approach. The former allows for an effective transfer of information from one component to the other, whereas the latter is just one integrated model.

In particular, in the modular approach, the hydrological[10] and the economic model are connected, and the output from one model usually provides the input for the other. Theoretically, both parts operate independently of each other and systems of equations are solved exogenously (Brouwer et al., 2008).

As for holistic models, there is one single unit with both components tightly interwoven in a consistent endogenous model. Thus, the exogenous variables of the compartment case are now solved endogenously in a system of equations (Cai et al., 2003a). As McKinney et al. (1999) state, the different components of a holistic model have to be implemented in a simple way, in order to be able to solve the complexity of simultaneous equations.

Some difficulties might occur in both approaches (Cai et al., 2003a): information transfer among the different components of a compartment model is still an obstacle (while it is conducted endogenously in holistic models), while the hydrologic side of holistic models is often too simplified because of model-solving complexities (e.g. Booker et al., 1994).

Regarding solution approaches, combined simulation and optimization techniques can be used in a compartment model, whereas a holistic one must be solved in its entirety (Cai et al., 2003a).

4.2 Optimization Problems

When formulating the water resources allocation problem as a hydropower-irrigation optimization problem, two allocation schemes can be implemented: (i) static, based on the static concept of water rights; (ii) dynamic, built around the economic notion of water.

Within the former allocation framework, irrigation withdrawals do not essentially depend on the status of the water resources system (i.e. the reservoirs' storage levels and the inflows). As long as there is enough water in the system, irrigation water rights are met.

[10]The term hydrological refers to both water quantity flow models and biogeophysical water quality and water allocation models (Brouwer et al., 2008).

Therefore, the allocation problem is scaled down to programming releases from the hydropower reservoirs.

On the other hand, since hydroeconomic models use the economic value of water, they are optimized through a dynamic allocation approach. In this case, both irrigation withdrawals and hydropower releases become decision variables. Thus, they are directly influenced by the status of the system and will be given a value so as to maximize basin-wide net benefits, while satisfying physical and management constraints (Tilmant et al., 2009).

Hydropower is also included in the hydroeconomic model because hydropower reservoirs are a fundamental link between water and power systems, as Pereira-Cardenal et al. (2013) state. For instance, the water can be either directly turbinated to generate electricity or released to meet downstream water demands. Moreover, hydropower reservoirs provide the most effective means of storage. In most recent works, hydroeconomic models have been extended to include thermal power also. Researchers have become more and more interested in assessing the linkage between thermal power plant water demand and water resources management, as well as the impacts of thermal cooling water requirements on this coupled system (Koch et al., 2009) (see Section 4.3).

Several techniques can be used to optimize hydroeconomic models (particularly the hydropower reservoir systems that compose them):

- Linear Programming (LP), one of the most popular optimization methods (Rani et al., 2009);
- Dynamic Programming (DP) (Pereira-Cardenal et al., 2013);
- Stochastic Dynamic Programming (SDP) (e.g. Vedula et al., 1992; Dudley et al., 1993; Pereira-Cardenal et al., 2014), usually applied to solve complex holistic hydroeconomic models (Cai et al., 2003a);
- Stochastic Dual Dynamic Programming (SDDP), a method developed within the electric power community by Pereira et al. (1991).

4.2.1 Linear Programming (LP)

LP flexibility for application to large-scale problems, convergence to global optimal solution and readily available efficient software packages (e.g. CPLEX) is what makes it one of the most implemented optimization techniques (Rani et al., 2009). Rather recent works used this method for different purposes, such as determining optimal operation policies (Crawley et al., 1993), flood control (Needham et al., 2000), etc.

However, LP presents two main disadvantages: restriction of using linear and convex objective functions and linear constraints (Rani et al., 2009). According to Rani et al. (2009), the nonlinearity in some problems (e.g. due to nonlinear benefit or cost functions)

might be overcome by approximation and extension of LP to separable LP (Crawley et al., 1993) and successive LP (Mousavi et al., 2000; Barros et al., 2003). Moreover, binary, integer and mixed integer LP may be able to handle the nonconvexity of the problem (Randall et al., 1997; Tu et al., 2003).

LP and its aforementioned extensions belong to a deterministic class of methods (Rani et al., 2009).

4.2.2 Dynamic Programming (DP)

DP was developed by Bellman (1957) and together with LP, is among the most popular optimization procedures. Its purpose is to solve multistage problems by decomposing them into a series of simple sub-problems, solved recursively one at a time. Furthermore, both nonlinear problems and problems involving stochastic variables can be adapted to this optimization technique (Rani et al., 2009).

Yakowitz (1982) provided an extensive review of DP applications to many water resources problems, whereas Nandalal et al. (2007) presented applicability and limitations of DP. One of its major disadvantages is the so-called curse of dimensionality: the discretization of state variables leads to an exponential growth of memory and computational effort as the number of state variables increases (Pereira-Cardenal et al., 2013). This limitation forces the DP method to work only with systems of three or four reservoirs (Labadie, 2004).

4.2.3 Stochastic Dynamic Programming (SDP)

In addition to the advantages of DP, SDP provides the benefit of explicitly considering streamflow uncertainty in its recursive function (Rani et al., 2009). Braga et al. (1991) state that SDP is an effective optimization procedure for a single reservoir with serially correlated inflows. The working principle of this method is the following: it optimizes a problem by discretizing stochastic variables (e.g. future inflow) as well as state variables (e.g. storage) to obtain optimal policy for each discrete state of a reservoir system (Rani et al., 2009). Thus, SDP can provide optimal releases or storage policies (Labadie, 2004).

Given uncertain future flows, an application of SDP called the water value method (Stage et al., 1961; Wolfgang et al., 2009) can be implemented to obtain rational reservoir operating rules. This procedure consists in using the traditional Bellman formulation in order to compute the full total cost (immediate plus expected future cost) of system operation for each state and stage, and then taking the derivative of such costs with respect to the reservoir level (Pereira-Cardenal et al., 2014). The result is a water value table showing the expected value of a marginal amount of water if it is stored for later use. These values are a function of the storage, inflow state and stage and are later used as

marginal costs of hydropower in a hydrothermal system simulation (e.g. Wolfgang et al., 2009; Pereira-Cardenal et al., 2013).

SDP experiences the same limitation of DP, but worsened: now the stochastic variable (typically the inflow) becomes part of the state vector, thus it has to be discretized (Pereira-Cardenal et al., 2013). Rani et al. (2009) propose several solutions to overcome the curse of dimensionality of SDP: aggregation-disaggregation of reservoirs (e.g. Turgeon et al., 1998; Serrat-Capdevila et al., 2007), one-at-a-time successive decomposition (e.g. Arunkumar et al., 1973) and a combination of the two (e.g. Saad et al., 1996).

4.2.4 Stochastic Dual Dynamic Programming (SDDP)

SDDP extends the traditional SDP to handle a large state space, i.e. a large number of reservoirs and allocation decisions, without facing the curse of dimensionality (Tilmant et al., 2009). As explained by Pereira-Cardenal et al. (2013), SDDP is a combination of DP, which can handle a large number of stages but few states, and Benders decomposition, which in turn can handle a large amount of states but few stages. This method is used to optimize multireservoir systems and iterates between stochastic simulation and optimization until a satisfactory solution is obtained.
In the latest years, SDDP has been increasingly used in the water resources community, typically to optimize multi-purpose reservoir problems (e.g. Kristiansen, 2004; Tilmant et al., 2008; Tilmant et al., 2009; Goor et al., 2011; Pereira-Cardenal, 2014).

According to Pereira-Cardenal et al. (2013), SDDP approximates the cost-to-go function through hyperplanes using linear programming. Thus, although the curse of dimensionality is overcome, some of the advantages of DP methods are lost since linear programming requires the problem to be linear (or convex at least).

4.3 Latest Researches: Incorporation of Thermal Cooling Water

According to the US Energy Information Administration (2011), thermoelectric (i.e. nuclear and fossil-fueled) power plants generate at present 91% and 78% of the total electricity in the United Stated and in Europe respectively. Their power production directly depends on the availability and temperature of water resources used for cooling. For instance, coal-, gas- and nuclear-fueled power plants worldwide withdraw freshwater for cooling (van Vliet et al., 2012). These withdrawals are highest in North America (224 $km^3\ yr^{-1}$), followed by Europe (121 $km^3\ yr^{-1}$), which jointly account for about 86% of the global thermoelectric water withdrawals (Vassolo et al., 2005). In particular, thermal power is responsible for 40% and 43% of total surface water abstractions in the United States (King et al., 2008) and in Europe respectively (van Vliet et al., 2012).

Even if most of this water is returned to its natural source, it may still cause problems to the environment when it is discharged back, because it absorbed excess thermal energy

during the heat exchange. This warming up of the cooling water may lead to an increase in the ambient temperature of the water source, thus damaging the aquatic ecosystem (McDermott et al., 2014). Langford (1990) states that mid-20s °C represents a dangerous threshold for aqueous plants and certain fish species, since water temperatures at or above this limit cause reduced oxygen levels and raised concentrations of ammoniac. This is why many countries adopted environmental laws restricting the maximum allowable water temperature discharge from thermal plants, known as 'thermal pollution' (McDermott et al., 2014).

In this framework, several recent studies have been conducted in order to analyze whether cooling water accessibility constraints thermal power production and quantify its impact. Some works mainly focus on the generic consequences of growing power demand on thermal cooling water consumption (e.g. Feeley et al., 2008), whereas others explicitly incorporate climate change into their analysis and even test adaptation options for thermal plants to a warming climate (e.g. van Vliet et al., 2016). Not only researchers, but also social media started showing an interest in the connection between thermal energy production, water scarcity and climate change. For example, several journalists wrote articles about the heat waves of the last decade and the resulting shutting down of some European (e.g. Gentleman, 2003; Godoy, 2006; Pagnamenta, 2009) and American (Miczek, 2008; Sohn, 2001; Eaton, 2012) thermal stations. All these studies have been grouped and summarized in the Fifth Assessment Report of the Intergovernmental Panel on Climate Change (IPCC, 2014) as follows: "Another problem facing thermal power generation in many regions is the decreasing volume and increasing temperature of water for cooling, leading to reduced power generation, operation at reduced capacity, and even temporary shutdown of power plants". The same topic has been covered thoroughly in the literature, at a local scale also (e.g. Maulbetsch et al., 2006; Kirshen et al., 2008).

Koch et al. (2009) extend their research to an integrated water resources management model. Their aim is to assess the impacts of socio-economic and climate change through a coupled simulation of thermal power plant water demand and water resources management (i.e. water availability). By socio-economic change, the authors mean changes in energy demand, energy prices and technological progress, whereas climate change affects water demand and availability for the thermal stations. However, they do not consider the consequences that water shortages in large regions could have on energy prices.

Förster et al. (2010) narrow down the impacts of climate change on a single hypothetical nuclear plant in Central Europe with a once-through cooling technology (see Section 7.2.1). They calculate annual average load reductions under two scenarios: (i) temperature change scenario (with a maximum reduction of 11.8% and resulting annual average income losses of up to 80 million €); (ii) streamflow and temperature change scenario (with average annual costs of 111 million € in a worst-case scenario).

From a more general point of view, van Vliet et al. (2012) try to assess the effects of climate change on the whole power sector. Depending on the cooling system type and climate scenario for 2031-2060, their simulations give as an output a 6.3-19% and a 4.4-16% reduction in the average summer capacity of thermal stations in Europe and the US, respectively. In conclusion, these researchers state that climate change will affect thermoelectric power production in both continents through a combination of increased water temperatures and reduced river flow, especially during summer. However, they do not model the impacts on electricity prices either.

On the other hand, Colman (2013) assesses that the risk the power sector has to face under a climate change scenario is small, especially given the gradual nature of global temperature changes. For instance, the projections of future temperature changes over the next hundred years are less dramatic than the temperature variation experienced by a thermal plant during a year (or even a day). As it can be noticed, this topic is very controversial.

Finally, McDermott et al. (2014) are the first ones to identify the impact of cooling water availability on electricity prices in Germany. All the contemporaneous and dynamic settings they tested show that electricity prices are driven higher by falling river levels and high river temperatures.

None of the studies mentioned in this section implemented a constraint on the maximum allowable temperature increase in the cooling water discharged back into the water source by thermal power plants. This means that none of them assessed the impacts of this constraint on thermal power generation and, more in general, on the power market of a nation. Therefore, the proposed thesis project will try to explore this topic, modelling the consequences of thermal cooling water constraints in both an historical and a climate change scenario. The case study will be the Iberian Peninsula, presented in the following Part.

Part III

Case Study

Chapter 5

Case Study: The Iberian Peninsula

The case study considered is the whole Iberian Peninsula (IP).

There are several reasons why the IP is a good framework to implement the water-energy nexus (Pereira-Cardenal et al., 2013): (i) its water and energy systems present strong interdependencies; (ii) climate change might affect some of these interdependencies; (iii) the two countries constituting the IP (i.e. Spain and Portugal) share both the hydrological and the power system, with small exchanges with other countries. For instance, they have most of the major river basins in the region in common and their mutual power market (the MIBEL) exchanges less than 2% of total production with other countries. Moreover, the IP presents an impellent need for an integrated water and energy resource planning because (Rio Carrillo et al., 2009): (i) water demand of the thermo-electrical sector has increased more than 1/3 between 2001 and 2006, and it is expected to keep on rising, due to projected increases in energy demands (Spanish National Institute of Statistics, 2008). This will intensify the competition with food production (i.e. the agricultural sector) for limited water resources; (ii) the introduction of local biofuels production, which will worsen the corrivalry with food and electricity production for restricted water resources, especially in regions where water is scarce; (iii) energy and water supply will be limited by more constrained freshwater resources in the future. Although there are enough freshwater resources to meet Spain's water needs now, water availability remains a region-specific problem (International Water Management Institute, 2007).

5.1 Water-Energy Nexus

Hardy et al. (2012) assess the strict interdependency between water and energy systems in the IP. They call this interconnection 'water-energy nexus' because of the bidirectional effects of, among other factors, process efficiency, the amount of resources involved, leaks in the system, poor or good resources management and the choice of technologies. Within the water-energy nexus, they define the 'energy for water' as the energy costs of the water use cycle, i.e. extraction and water treatment, distribution/water use and wastewater treatment. Therefore, power is considered as the main variable cost factor in all stages of water usage (Pereira-Cardenal et al., 2013). On the other side, 'water for energy' accounts for the amount of water required to produce one unit of energy, both outside the power plant to extract the raw material and inside the plant for cooling systems (Hardy et al., 2012).

In Spain, the water sector was responsible for 5.8% of total energy demand in 2008. On the other hand, the energy sector reached 25% of total water withdrawn (without considering the volume of water used by the hydropower sector), even though it accounted for only 3.2% of the total water-related energy usage (Hardy et al., 2012). 96% of this 25% of total water withdrawn was non-consumptive, i.e. it was discharged back into its natural source (Hardy et al., 2010).
Throughout the years, the Spanish water and energy systems have been developing, emphasizing their interdependency even more. This progress can be identified in the following sectors (Hardy et al., 2010): (i) irrigation systems increased their efficiency, causing a much higher electricity consumption; (ii) the European Climate Change Mitigation Policy has been promoting the production of biofuels, which requires a considerable volume of water for irrigation and processing, as well as land. This led to an enhanced competition with traditional crops for soil and water resources; (iii) in dry areas, some renewable energy sources with high potential might face some problems if their water demands cannot be met.

The interconnection and competition between water and power systems might be affected by climate change, which generally involves higher temperatures and lower precipitation (MMA, 2005). The energy sector might be affected as follows (MMA, 2005): (i) lower efficiency of the Rankine cycle, used in thermal power production; (ii) higher environmental impact of cooling water discharged back into its natural source (e.g. river); (iii) smaller transmission capacity. On the other hand, smaller water volumes in the hydrological system (induced by climate change) may have some negative consequences on the water sector (MMA, 2005): (i) reduced hydropower generation; (ii) increased agricultural deficit; (iii) a more regulated hydropower production (thus a reduced power generation) due to the introduction of new policies aimed at satisfying the agricultural demand first (over hydropower); (iv) increased power demand due to new desalinization plants; (v) increased power consumption due to groundwater pumping and conveyance in order to face newly raised water deficits.
Overall, competition among different water resources users (i.e. agriculture, domestic and industry) might be exacerbated under climate change.

Nowadays, in Spain, agricultural use is responsible for 60.9% of total annual freshwater withdrawals on average, domestic use for 17.8% and industrial use for 21.3%, as can be noticed in Figure 5-1a. Industrial use is then split into electricity generation (17% of the total annual freshwater withdrawals) and other industrial use (4.3%) (The World Data Bank, 2016). Portugal presents quite the same percentages as Spain (The World Data Bank, 2016). As far as consumed water is concerned, agricultural demand accounts for 75% of total water consumption, domestic for 17% and industrial for 6% (MMA, 2007), as can be observed in Figure 5-1b.

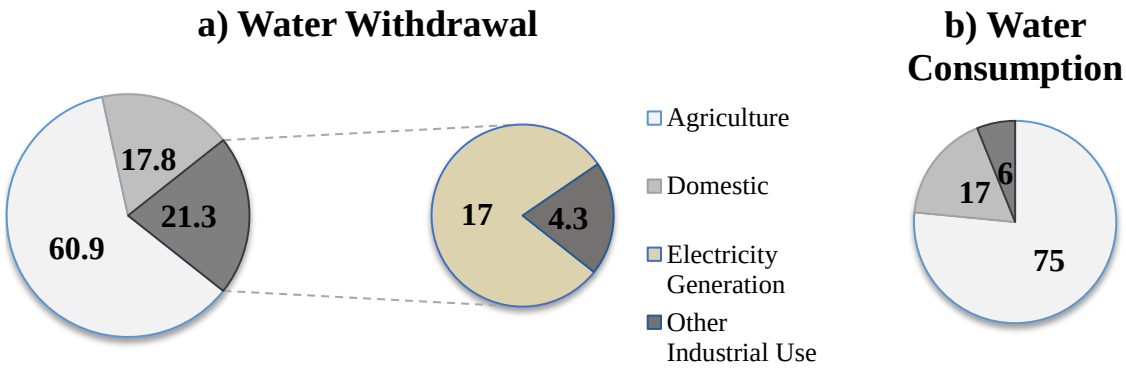

Figure 5-1: Agricultural, industrial and domestic use fractions of a) total freshwater withdrawals and b) total water consumption in Spain. The freshwater withdrawals data are taken from the World Data Bank (2016) and computed as an average of the annual data recorded for 2007, 2012 and 2013. The total water consumption data come from MMA (2007).

In Spain, among the seven river basins the IP is divided into in this study, irrigation demand is generally higher than 75% of total water consumption. Exception is made for Tajo and Miño-Sil, whose agricultural demand is equal to 52% and 17% respectively (MMA, 2007). Since Portugal shares a portion of these river basins, the situation is expected to be the same (Pereira-Cardenal et al., 2013).

In this thesis, the competing water users modelled are narrowed down to irrigation, hydropower and thermal power plants only for simplicity. However, other uses (e.g. residential and ecological) can be easily included in the model as either constraints (i.e. the total or a portion of the demand must be satisfied) or decision variables (through a demand function).

5.2 Modelled Area

The area modelled in this study covers 400 800 km^2, which represents approximately 70% of the entire IP extent. It consists of the seven major river basins in the Peninsula (i.e. Tajo, Ebro, Duero, Guadiana, Guadalquivir, Miño-Sil and Jucar).

Pereira-Cardenal et al. (2013)'s modelled area was obtained by dividing each of the seven major river basins (i.e. catchments) into three sub-catchments (except for the Jucar, which

was split into four sub-catchments). Twenty-two resulting sub-catchments were thus considered. Moreover, they applied a hydropower reservoir aggregation technique in order to reduce the number of state variables, thus face the curse of dimensionality affecting SDP and SDDP methods, employed to optimize their system.

Since the deterministic optimization performed in this study does not suffer from this curse (only one trajectory through the state space is computed), there is no need to aggregate the reservoirs. Therefore, all the 116 hydropower plants already considered by Pereira-Cardenal et al. (2013) are modelled. They account for 85% of total hydropower capacity within the modelled area. Moreover, they belong to the 246 (208 in Spain and 38 in Portugal) situated all over the IP, whose installed capacity is equal to or higher than 10 MW and that account for a total capacity of more than 20 GW (Pereira-Cardenal et al., 2013).

Figure 5-2 displays the case study area and the location of the modelled hydropower reservoirs. As can be observed, in this thesis project the modelled area is computed as the extent of every hydropower watershed, i.e. upslope catchment area contributing flow to each one of the 116 hydropower plants. Seven fictitious reservoirs with zero capacity were added at the outlet point of each of the seven river basins in order to represent the sea. Thus, seven additional watersheds were created, whose purpose was to delineate the most downstream area in each basin that was not included in any actual hydropower watershed. Overall, the modelled area is made up of 116+7 watersheds.

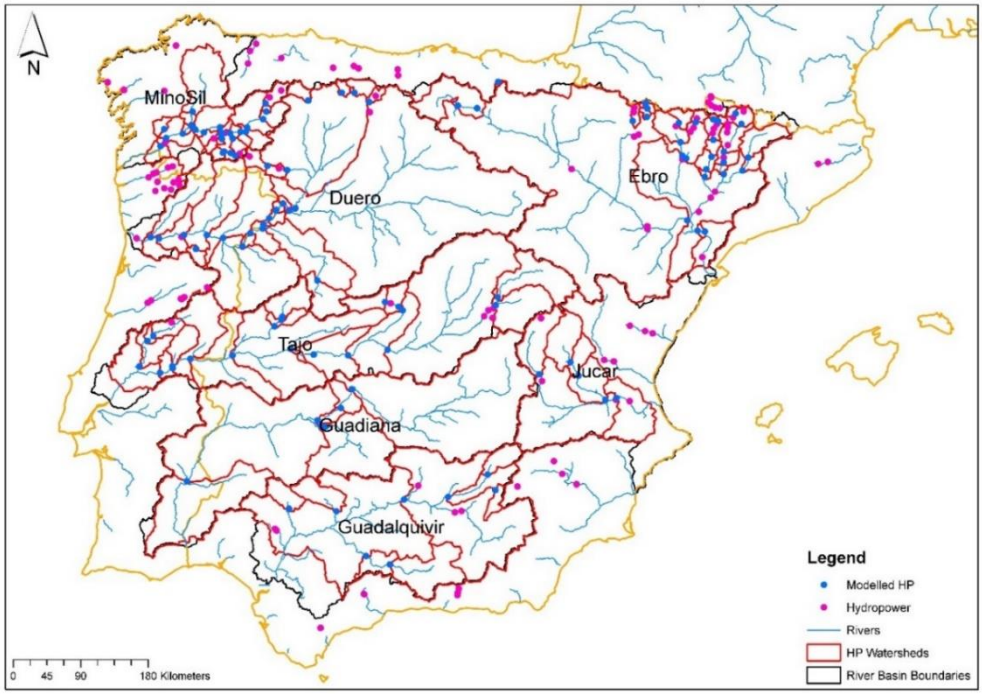

Figure 5-2: Area of the IP modelled in this study and delineated by the red hydropower watersheds. Each watershed represents the catchment area of one modelled hydropower plant in the Peninsula. The pink dots indicate the 246 reservoirs situated all over the IP.

5.2.1 Hydropower Watersheds Delineation

Watersheds are physically delineated by the area upstream of a specified outlet point (i.e. hydropower reservoir in this case).

The 123 hydropower watersheds constituting the study area were digitally delineated from a Digital Elevation Model (DEM) of both Spain and Portugal, using the software ArcGIS 10. This elevation map was downloaded in raster format with a resolution of 1 km x 1 km (EEA, 2012), whereas the stream network and the hydropower plants were already available from Pereira-Cardenal et al. (2013)'s shapefile data.

Firstly, a flow direction grid was computed and then used in the Watershed function. This function uses a raster of flow direction to determine the areas contributing to the flow going into every hydropower reservoir. The pour points (i.e. hydropower plants) method was applied to define the final watersheds. In order to get an insight into the whole, detailed ArcGIS procedure, see Appendix A.1.

The following chapters assess: (i) the hydrological and power systems of the IP; (ii) the expected impacts of climate change on these two systems. The hydrologic data are from year 1961 to 1990; they were derived from Pereira-Cardenal et al. (2013) and averaged or downscaled at a weekly time step. The power system is the current one, with data sources variating from 2006 to 2016.

Chapter 6

The Hydrological System of the IP

The IP covers a 583 254 km^2 area and its topography varies a lot throughout the region. The mountain ranges mainly run from west to east, reaching altitudes of approximately 3000 m a.s.l. (the Peninsula presents the second highest mean altitude (637 m a.s.l.) in Western Europe). These mountains have influenced the hydrological system of the IP (i.e. the river network and the spatial configuration of its seven major river basins) (Lorenzo-Lacruz et al., 2013). The seven major river basins constituting the IP can be divided into the ones of rivers flowing towards the Atlantic Ocean (i.e. Miño-Sil, Duero, Tajo, Guadiana and Guadalquivir basins) and the ones towards the Mediterranean Sea (i.e. Jùcar and Ebro basins), as can be noticed in Figure 6-1.

The annual precipitation is characterized by a southeast to northwest gradient (De-Castro et al., 2005; Gonzàlez-Hidalgo et al., 2011), due to the location and topography of the IP, as well as to large atmospheric circulation patterns (Lòpez-Bustins et al., 2008). This precipitation pattern is shown in the lower right corner of Figure 6-1. 40% of the annual precipitation occurs in winter, and varies from less than 300 mm yr^{-1} in the southeast regions to more than 1500 mm yr^{-1} in the northwest ones (Lorenzo-Lacruz et al., 2013). The precipitation gradient is also reflected by the mean annual streamflows of the seven river basins in the IP. For instance, river basins in the northern sector of the Atlantic watershed produce abundant yields, with mean annual flows ranging from 10 570 Hm^3 yr^{-1} for the Miño-Sil to 12 350 Hm^3 yr^{-1} for the Tajo river[11]. On the contrary, the Guadiana and Guadalquivir rivers (in the southern sector of the Atlantic watershed) present modest mean annual streamflows of 4039 Hm^3 yr^{-1} and 3780 Hm^3 yr^{-1} respectively. As for the Mediterranean watershed (the Jùcar and Ebro basins), the streamflows are generally low, except for the Ebro, whose flow is abundant (12 279 Hm^3 yr^{-1}) because it is generated in the Cantabrian Range and the Pyrenees (Lorenzo-Lacruz et al., 2013).

[11]The mean annual flows have been measured at the most downstream streamflow gauges (Lorenzo-Lacruz et al., 2013).

Thus, the IP presents an uneven distribution of water resources, which, together with a rising demand for water, resulted in conflicts among users and regions (Quiroga et al., 2011). In order to optimize the use of available resources and compensate the differences in the temporal distribution of precipitation, a complex network of dams have been built (Lorenzo-Lacruz et al., 2013). During the 20th century, a large number of major reservoirs has been constructed, which together account for a total storage capacity of 56 500 Hm^3 (Berga-Casafont, 2003). This stored volume is approximately equal to the mean annual streamflow of the eight main rivers of the IP (55 850 $Hm^3\ yr^{-1}$) (Lorenzo-Lacruz et al., 2013). 40% of the natural annual flows in Spain alone is thus regulated (Berga-Casafont, 2003).

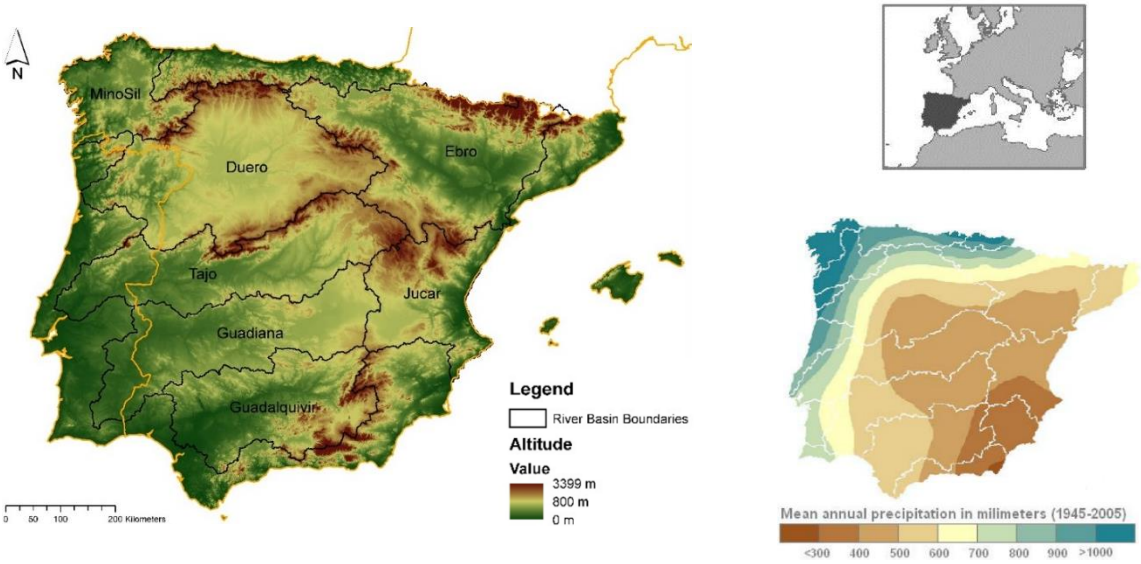

Figure 6-1: On the left: topography of the IP. The seven major river basins modelled in this study are also displayed. Upper right corner: IP location map (Lorenzo-Lacruz et al., 2013). Lower right corner: distribution of the mean annual precipitation (1945-2005) over the IP (Lorenzo-Lacruz et al., 2013).

6.1 Rainfall-Runoff Model

A rainfall-runoff model was setup by Pereira-Cardenal et al. (2013) in order to calculate a daily runoff time series [m^3/sec] for each one of their 22 simulation sub-catchments, from 1961 to 1990 (see Section 5.2). This time series was used in this study as well, after adapting it to the modelled area. For instance, it was downscaled proportionally to the area of the 123 modelled watersheds, in order to obtain a runoff time series per watershed. This downscaling procedure is summarized in Appendix B.1.

The portion of runoff in the 116 actual watersheds is implemented as a controlled water volume entirely flowing into the hydropower reservoir that delineates that particular watershed. On the other hand, the portion of uncontrolled flow is the one in the seven

downstream fictitious watersheds only, as it goes directly into the sea without being able to be stored/turbinated by any hydropower plant.

6.2 Air-River Water Temperature

River water temperature is fundamental to evaluate the river's thermal capacity, which will be constraining the thermal discharge of thermal power plants across the IP (inequality constraint 5; see Section 9.2.3). An air-water temperature sigmoid function from Mohseni et al. (1998) was implemented in order to convert Pereira-Cardenal et al. (2013)'s weekly air temperature data per sub-catchment into river water temperatures. The procedure employed to estimate the parameters of the S-shaped function and water temperature time series afterwards is summarized in Appendix B.2.

The adopted water temperature modelling procedure is not dynamic, i.e. the temperature increase in the river downstream due to thermal cooling discharge is not considered, as it would result in nonlinear constraints. In order to deal with this issue, nearby thermal power plants were aggregated (see Section 7.2.2).

As stated in Section 7.2.1, the maximum legal river water temperature increase due to 'thermal pollution' is 3 °C. Moreover, water temperature cannot exceed 28 °C, according to the European legislation. Therefore, the available thermal increase dT in each river (employed in inequality constraint 5; see Section 9.2.3) was evaluated as follows:

$$dT = max(0, min(3, 28 - T_r)) \quad (6\text{-}1)$$

where T_r is the river water temperature in a certain river basin. This equation implies that up to 25 °C, the maximum river temperature increase allowed is 3 °C, whereas the delta becomes smaller and smaller over 25 °C. If the 28 °C upper limit is reached, no more heat can be discharged.

6.3 Hydropower Reservoirs

The 116 modelled-hydropower plant data were obtained from Pereira-Cardenal et al. (2013)'s dataset. The main parameters needed are:

- **Local energy equivalent *y*** [KWh/m^3] of a single hydropower reservoir. It corresponds to the amount of energy production per turbinated water and is proportional to the reservoir head. Reservoir heads were assumed constant at maximum level (Pereira-Cardenal et al., 2013). For instance, a considerable variation in the energy production rates *y*, due to a varying reservoir's level *h*, would result in a non-linear *y = f(h)* function;
- **Installed capacity** [MW] of a single hydropower reservoir. This parameter was converted into maximum turbinated flow [Hm^3/week];
- **Maximum and minimum storage** [Hm^3] of a single hydropower reservoir.

The detailed description of how these three parameters were computed is presented in Appendix B.3.

6.4 Irrigation Demand

Beside the consumptive cooling water demand of a certain thermal power plant (equality constraint 3; see Section 9.2.3), the only water demand considered in this study is the agricultural demand, as in Pereira-Cardenal et al. (2013). The term 'agricultural demand' refers to irrigation water demand, which was computed as follows:

$$IWD = CWD - P_i, \text{ where } P_i = P * A_{irr} \quad (6\text{-}2)$$

where *IWD*[12] is irrigation water demand and *CWD*[13] crop water demand. P_i corresponds to the precipitation P on the irrigated area A_{irr}.

In the model, *CWD* was assumed equal to crop potential evapotranspiration for simplicity. Its values were taken from Wriedt et al. (2009)'s dataset for Europe, computed according to a 10 x 10 km^2 grid raster format.
The yearly *CWD* values for the whole IP were downscaled to the constituent elements of the model, i.e. each watershed, through the software ArcGIS 10. The systematic procedure is presented in Appendix A.2. The annual demand was then distributed over the months of the year proportionally to observed monthly requirements in the Ebro river basin (Pereira-Cardenal et al., 2013). Thus, it was assumed that this percentage distribution could be indifferently applied to all the basins in the IP, i.e. it was supposed that all the basins had the same temporal irrigation pattern. The monthly demand was equally split into weeks. The Ebro distribution is displayed in Figure 6-2.
As can be observed, the trend in the data follows a sort of bell-shaped curve, with a peak at about 27%, occurring during the summer months. Most of the *CWD* is required at this time of the year, since it is usually both the warmest and the driest period. For instance, more evapotranspiration (due to high air temperatures) together with less precipitation occur, leading to an increase in crop water demand. On the other hand, in winter the percentage is close to zero, since the few crops surviving during these months are mostly fed by high precipitation.

According to the definition given above, *CWD* is the sum of irrigation water demand and precipitation over the irrigated land. In order to obtain irrigation water demand from 1961 to 1990, precipitation estimates had to be subtracted from the total water demand. This was achieved through a four-steps procedure, described in Appendix B.4. Mean annual irrigation water demand at the IP level is represented in Figure 6-3.

[12]Wriedt et al. (2009) refer to it as follows: "the amount of water that has to be applied in addition to rainfall to serve crop water requirements".
[13]According to Wriedt et al. (2009), *CWD* is "the total amount of water required for transpiration by a well-managed crop grown under optimum growth conditions without water- and nutrient stress".

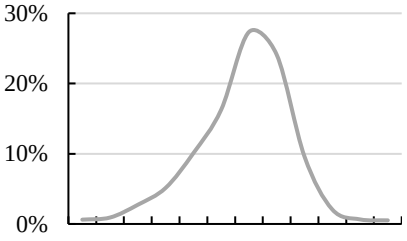

Figure 6-2: Monthly percentage of yearly crop water demand in the Ebro river basin (Pereira-Cardenal et al., 2013).

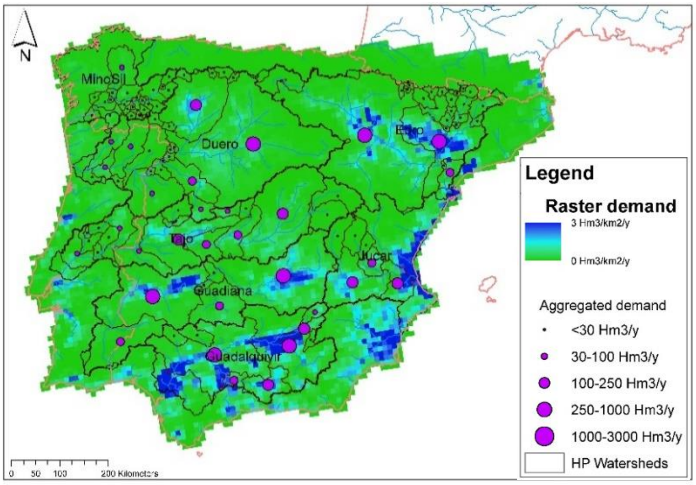

Figure 6-3: Mean annual irrigation demand ($Hm^3/km^2/yr$). The purple dots show the sum of the irrigation demands (Hm^3/yr) per watershed (source: Wriedt et al., 2009).

As can be noticed, agriculture is spread all over the Peninsula, with particular focus on the flat areas of the Andalusia region (southern Spain), which accounts for about 24% of total irrigation demand (Instituto Nacional de Estadistica, 2008). This region is mostly included in the Guadalquivir river basin, whose irrigation water demand equals to 31% of the total in the modelled area of this study. Nevertheless, the Guadalquivir basin only represents 13% of the total modelled area. Moreover, the irrigation demand has an opposite trend compared to the precipitation distribution in Figure 6-1: it is higher where the mean annual precipitation is lower (e.g. Guadalquivir river basin).

At the Peninsula level, the irrigation demand is met by 80% of surface water and 20% of groundwater (Instituto Nacional de Estadistica, 2008). However, in this thesis irrigation was modelled as a surface water user only, even if its groundwater abstractions are significant in many river basins. For instance, groundwater abstractions are expected to eventually result in river discharge reductions. This assumption does not take two elements into account: (i) water abstractions from aquifers that are not connected to surface water; (ii) over-abstraction, i.e. abstractions exceeding recharge. Moreover, only the consumptive use of irrigation has been considered, because of the coarse spatial scale of the model this study is based on. At last, return flows were ignored, as the portion of the abstractions for both leaching of salts and compensation of application efficiency will eventually return to the system. Pereira-Cardenal et al. (2013) made the same assumptions.

Chapter 7

The Power System of the IP

On July 1st 2007, the two separated Iberian electricity systems (i.e. Spanish and Portuguese) were merged into a single, combined electrical network, the so-called Iberian Electricity Market (MIBEL) (MIBEL, 2016). The MIBEL is an example of a deregulated power market, embodying all the characteristic features described in Chapter 2.

As can be noticed in the following figures, the power production curve of the MIBEL follows the hourly, daily and monthly trend of a typical power supply curve. Bilateral contracts are not counted in the total amount of energy produced and displayed in the graphs below.
The **hourly** electricity production and price data have been collected for the time window September 21st – 27th 2015 and the respective curves are presented in Figure 7-1a. The prices follow approximately the same pattern of the power production. For instance, they both reach their lowest peaks between 02:00 and 05:00 every day. Since demand is very small during this time slot, only the cheapest power plants are active and manage to cover the entire power demand themselves, causing the electricity price to be very low. On the other hand, when the demand rises during peak hours, the price increases consequently, since the more expensive power plants have to go on line and produce power.

As far as the **daily** electricity production and prices are concerned, the entire month of September 2015 is taken as a sample time window. The respective curves are shown in Figure 7-1b. The power supply curve presents the same pattern as the hourly one, but at a bigger scale. The only difference between them is that the daily electricity production reaches its lowest peak during the weekends. Once the economic activities restart on Monday, the production increases again. The price curve still follows approximately the same pattern of the power production. Sometimes there are some less clear variations in the price, which might be due to climatic factors (e.g. temperature, humidity) or data aggregation. For example, the price reaches its lowest peaks on September 13th and 16th 2015, a Sunday and a Wednesday respectively. The low value on the former date might reflect the correspondent low demand of the weekend, whereas the one on the latter date has to be explained by another reason. For instance, on September 16th, there was an unexpectedly high special regime production equal to 561 GWh/day, 48% more on average than the special regime production throughout the whole month of September. This renewable energy production peak can be noticed in Figure 7-1c.

In the end, the **monthly** electricity production and price data have been collected for the time window January 2008 – December 2014 and the respective curves are presented in Figure 7-1d. It can be noticed that the power generation always increases during winter in order to satisfy the relatively high winter demand. Even so, its pattern is not very clear because of the economic crisis in Spain and Portugal that caused a considerable power demand reduction (thus, a noticeable electricity generation decline) (Pereira-Cardenal et al., 2013). As for the price, some low peaks can be observed. The first decrease is due to low oil prices throughout 2009, whereas an unexpectedly high wind and hydropower generation (REE, 2014) might have caused the last one, occurred during February 2014.
Moreover, the monthly electricity production has been averaged throughout the years 2008 - 2014 and divided per generation technology. The results can be observed in Figure 7-1e. It can be noticed that the special regime production is quite constant throughout the months, whereas the hydropower varies from winter (when it is higher, because of more water availability) to summer months (when it lowers, due to less water available). The percentage of electricity produced by each technology, contributing to the annual average power production, is summarized in Table 7-1.

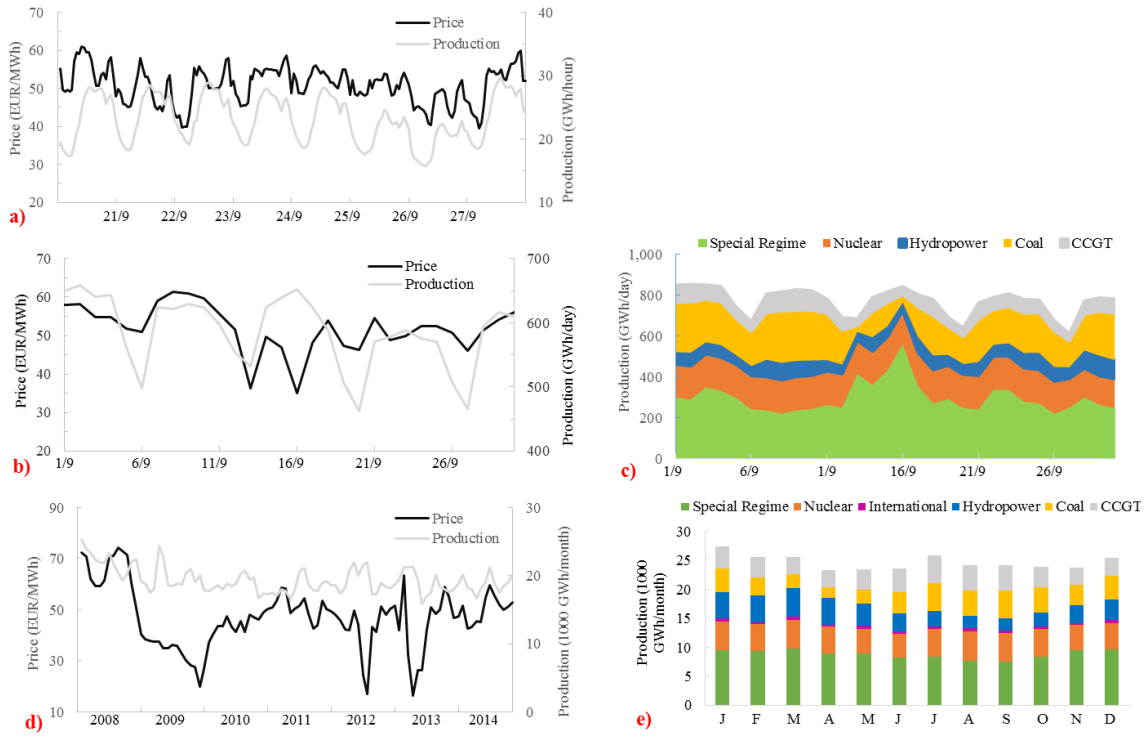

Figure 7-1: Hourly (a), daily (b) and monthly (d) power production and electricity price curves in the MIBEL. Daily (c) and average monthly (e) power production divided per generation technology in the MIBEL. Data source: OMIE (2016).

Table 7-1: Contribution (%) of each power generation technology to the annual average electricity production (OMIE, 2016).

	Special Regime	Nuclear	International	Hydropower	Coal	CCGT
% of Total Electricity Production	35.7%	18.9%	1.8%	14.0%	14.7%	14.9%

In conclusion, the MIBEL is managed as a competitive power market, whose aim is to find an equilibrium point between power supply and demand. Thus, using appropriate power supply and demand functions together with a market equilibrium model, the final price of electricity and its traded amount can be estimated (Pereira-Cardenal et al., 2014).

The following sections discuss how the power demand and supply were implemented in the model.

7.1 Power Demand

Power demand data was taken from Pereira-Cardenal et al. (2013)'s dataset. They assumed power demand to be inelastic and calculated it through the heating and cooling degree-day approach developed by Valor et al. (2001). In particular, this method employs linear regressions to estimate daily power demand, based on population and mean daily temperature data. The former dataset was obtained from LandScan (Bright et al., 2008), the latter from E-Obs' gridded product (Haylock et al., 2008). Electricity demand was acquired from OMIE (2016). More details about this computation procedure can be found in Pereira-Cardenal et al. (2014).

Furthermore, special regime production was subtracted from the overall power demand, since it is always cleared regardless of market conditions. As for pumped-storage, it was not considered because its net production is close to zero when aggregated at a weekly time scale (Pereira-Cardenal et al., 2014).

In the end, a weekly power demand time series was generated for the control period 1961-1990. This approach neglects the elasticity in the demand corresponding to fluctuating energy prices; this fluctuation is anyway assumed to be small at a weekly time step.

7.2 Thermal Power Supply

According to the structure of the model implemented, power demand has to be met at any time step by the different power suppliers. The energy producers consist of hydropower, thermal power plants and remaining power production, which embodies the producers not modelled individually. A unit energy production cost is associated with every producer (see Section 9.2.3). Hydropower has already been presented in Section 6.3, thus the

following sub-sections will focus on thermal power suppliers only (i.e. thermal power plants and residual thermal power).

7.2.1 Thermal Power Plants

In the IP, there are 32 thermal power plants (TPP) located inside the modelled hydropower plants' watersheds, as displayed in Figure 7-2. They represent approximately 50% of total thermal power generation capacity of the entire Peninsula (refer to Table 7-2) and are the ones directly modelled in this thesis. However, most of the TPPs situated outside the model area are located at the sea, thus probably use sea water for cooling purposes. Therefore, even if half of the TPPs are modelled, most of the freshwater requirements for thermal cooling are represented. The remaining 50% of thermal power capacity is represented through a residual thermal supply curve, addressed in Section 7.2.3.

In reality, the number of modelled thermal generators was lowered down to 15, after aggregating the ones located in the same watershed into a single thermal generator (see Section 7.2.2).

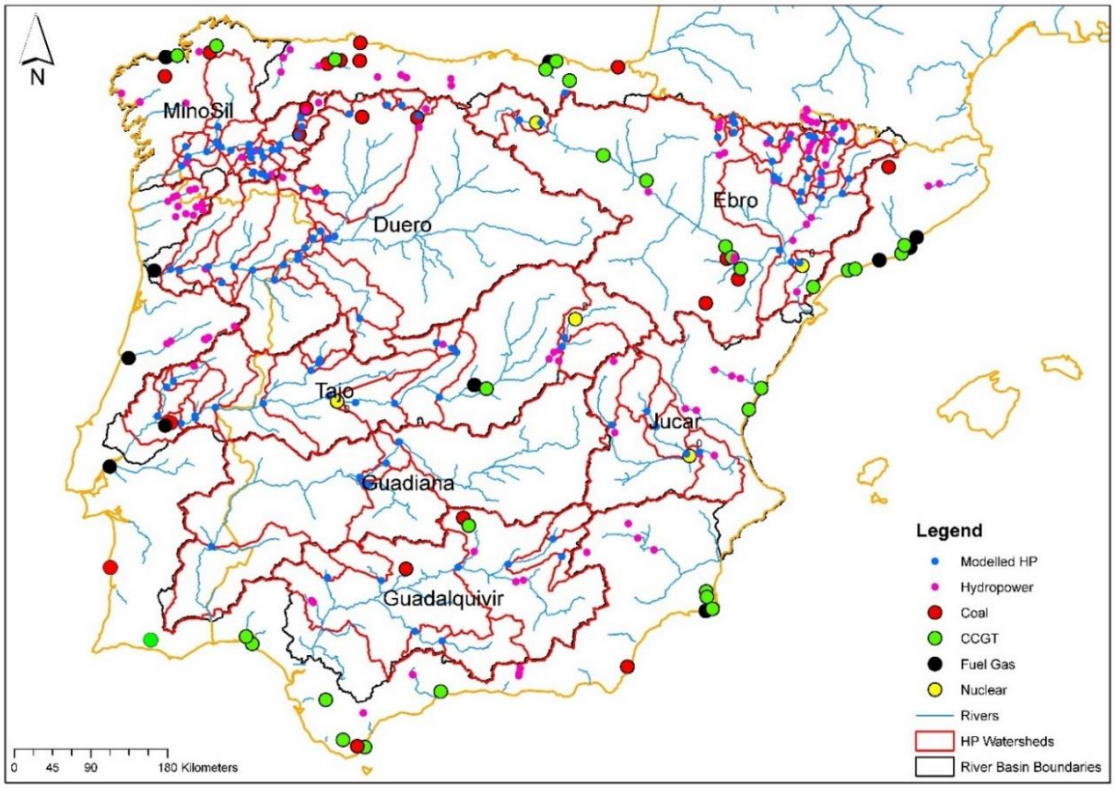

Figure 7-2: Location of all the hydropower and thermal power plants in the IP. The blue dots represent the hydropower reservoirs modelled in this study (116 in total), whereas the red lines delineate their watersheds. As for thermal power, all the active generators of the IP are displayed. Nevertheless, the only generators modelled are the ones located inside each watershed (32 in total, 15 after aggregating them).

Table 7-2: Modelled vs Total thermal power production throughout the IP. A percentage of modelled thermal power plants production over total one was computed. An average percentage over the three reference years was calculated, too. Modelled thermal power production data come from Global Energy Observatory (2016), whereas total production data come from OMIE (2016).

Thermal Power Production Year	Modelled TPP Production (GWh/yr)	Total TPP Production* (GWh/yr)	Modelling Percentage (%)
2006	91 377	152 970	60
2007	89 070	193 944	46
2008	90 284	211 914	43
TOTAL	***270 731***	***558 828***	***49***

*Total thermal power production was computed as total energy produced throughout the IP minus hydropower and special regime production.

In the following sections, several aspects concerning the modelled thermal power plants are addressed: (i) their working principle and a description of different thermal cooling technologies; (ii) legal limitations on river water temperature increase due to cooling water discharges; (iii) their main parameters, needed as input data to the model.

Working Principle

Thermal power generators are power plants in which heat energy is converted into electric power. They differ according to the type of heat source they use: fossil (e.g. coal, natural gas or petroleum), nuclear, geothermal, biomass combustion or solar thermal electric. Despite this distinction, most of them are steam driven: the water is heated, thus it turns into steam and spins a steam turbine, which drives an electric generator. After going through the turbine, the steam is condensed in a condenser and recycled to where it was heated first (i.e. Rankine cycle) (TEPCO, 2010). In Figure 7-3, the working principle of a thermal power plant burning fossil fuels (natural gas) is displayed as an example.

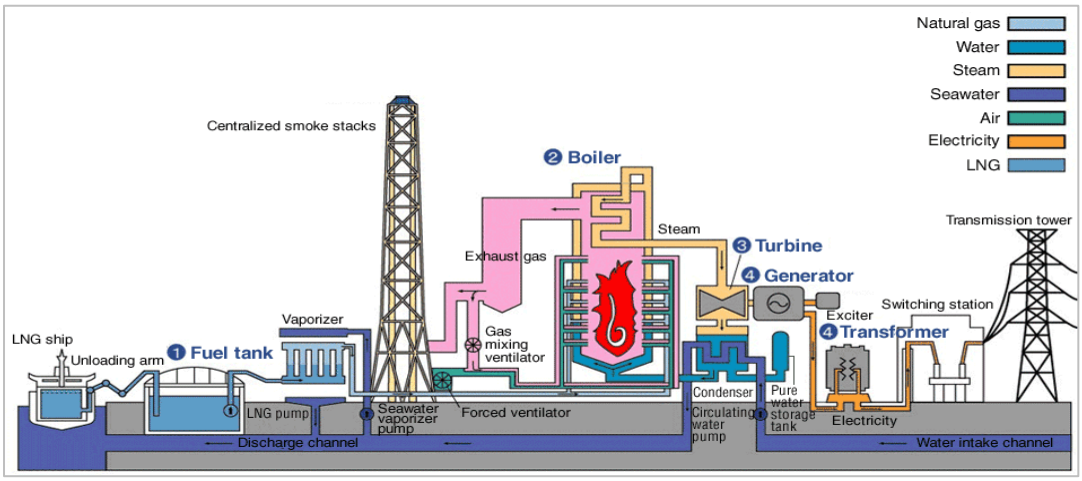

Figure 7-3: Electricity generation process of an ordinary thermal power plant (liquefied natural gas (LNG)-fired) (TEPCO, 2010).

Here the fossil fuels (LNG) contained in a fuel tank (1) are burnt, the water is converted into steam in a boiler (2) and a steam turbine is activated to generate electricity (3 & 4 Generator). Meanwhile, the temperature and pressure of the steam decrease, until the steam is converted back to water in the condenser. The newly condensed water starts a new loop, passing through the boiler, the turbine and the generator once again. The electricity produced goes through a transformer (4 Transformer) and is finally transmitted to the power grid through a transmission tower (TEPCO, 2010).

Cooling water is required during the steam condensing phase as a cooling medium to condense the steam and convert it back to water (Macknick et al., 2012). The majority of water withdrawn by thermal power plants is used during this cooling process. It is necessary to explain how the dissipation of waste heat occurs in power plants according to their cooling system, in order to understand their use of water (Koch et al., 2009).

Cooling System

According to Koch et al. (2013), the cooling systems of thermal power plants can be broadly classified into wet and dry systems. They differ from the way the waste heat is discharged: the former conducts it away by water, the latter discharges it directly into the atmosphere.

Three main types of wet cooling systems exist (Koch et al., 2013), outlined in Figure 7-4:

a. Once-through cooling: the water withdrawn from the natural source is used for cooling in the condenser and subsequently discharged back in its entirety into the body of water. Most of the waste heat is dissipated by the cooling water and transported to the natural water source. As a result, the amount of water needed is considerable, as well as heat loads in surface waters. Therefore, this cooling system is generally used in large power plants where sufficient cooling water is available (Koch et al., 2009);
b. Once-through cooling with cooling tower: in order to avoid high heat loads in water bodies, once-through systems are often equipped with a cooling tower (Koch et al., 2009). The potential stress on the surface water body is reduced because now the water is cooled in a cooling tower before it is discharged back to its natural environment. This tower cools the water down by putting it into contact with an air stream before it is returned to its natural source. Most of the waste heat is dissipated by the air stream and not into the receiving surface water. Since evaporation losses occur during this cooling process, the amount of water discharged back is smaller than the volume of water withdrawn (Koch et al., 2009);

c. Closed-circuit cooling: the water heated in the condenser is cooled in a cooling tower and subsequently recirculated to the condenser. This way the volume of water withdrawn is minimum and high heat loads are avoided. A downside of this cooling type is that, compared to the once-through without a cooling tower, the water in the cooling system reaches higher temperatures, leading to lower power plant efficiencies. Moreover, the evaporation losses are higher and more water is lost than in the once-through system (Koch et al., 2009).

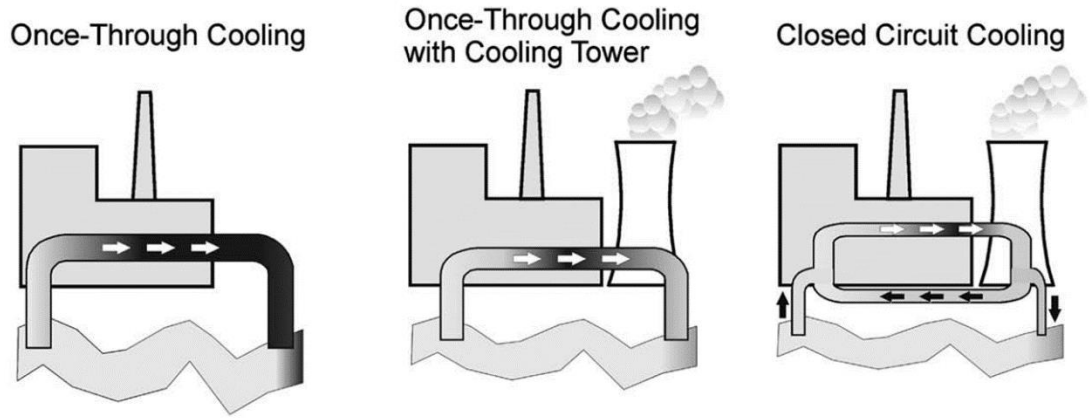

Figure 7-4: Three main types of wet cooling systems thermal power plants might be equipped with (Koch et al., 2009). The cooling water natural source may be a river, the sea or an artificial pond built next to the power plant (Macknick et al., 2012).

In once-through cooling systems, water temperature is particularly relevant as a limiting factor on waste heat discharges. On the other hand, when the power plant is equipped with a cooling tower, the cooling water demand and the amount of evaporated water depend more on the local climate conditions (i.e. air temperature and humidity in particular) (Koch et al., 2009).

In addition to the type of wet cooling system used, the volume of cooling water required by the power plant depends also on the amount of waste head produced. The quantity of heat to be dissipated is mainly determined by plant-specific factors (e.g. degree of fuel utilization and electricity capacity generation of the plant) and is computed as the share of energy input that is not transformed into electricity by a thermal power plant (Koch et al., 2013). The residual percentage of energy input turned into power by a thermal generator is called thermal efficiency.

In this thesis, the volume of water required by a thermal power plant is restricted only to cooling purposes, since the amount of water needed for other scopes can be considered negligible (Koch et al., 2013).

As far as dry cooling is concerned, the heat is removed by air circulation via fans and radiators, allowing this system to operate without water (Byers et al., 2014). Thus, thermal power plants equipped with this cooling technology are not relevant in this study.

Legislation on Thermal Pollution in the IP

Regardless of the type of wet cooling system applied, the natural source of cooling water undergoes stress because of the so-called "thermal pollution" effects (see Section 4.3). Its impacts are either increased water temperatures (once-through cooling) or large evaporation losses (from cooling towers). Thus, when analyzing the water use in thermoelectric power plants, environmental conditions and legal regulations on thermal pollution must be also taken into account (Koch et al., 2013).

The European Directive 2006/44/EC states that:

I. "The temperature measured downstream of a point of thermal discharge (at the edge of the mixing zone) must not exceed the unaffected temperature by more than 3 °C in cyprinid waters";
II. "Thermal discharges must not cause the temperature downstream of the point of thermal discharge (at the edge of the mixing zone) to exceed the 28 °C in cyprinid waters".

Thus, the thermal power plants in the IP must respect this legislation.

Main Input Parameters

General information about the thermal power plants (e.g. location, type of combustible, cooling technology, installed capacity, etc.) were found either on Global Energy Observatory (2016) or on the website of a single producer/power plant (e.g. Endesa Educa, 2014). Regardless of the source, the main parameters to be collected are:

- **Thermal efficiency** [%] of a single thermal power plant. Sometimes, efficiency data are available for some individual thermal power plants, but they are still few and represent an exception. Commercial or private database exists (e.g. Platts's World Electric Power Plants Database; STE database (Koch et al., 2013)); nonetheless, they are not open access. Thus, average thermal efficiency data divided per technology were used for both Spain and Portugal (IEA, 2008).
  Average thermal efficiencies of thermal power plants in the IP are presented in Table 7-3 below, divided by fuel type and country. Their computation procedure is summarized in Appendix B.5.

Table 7-3: Average thermal efficiencies of thermal power plants in Spain and Portugal, divided by fuel type. They were calculated using data from the 2001-2005 time period (IEA, 2008).

	Coal	Natural Gas	Oil
Spain	37.8%	50.4%	34.6%
Portugal	39.5%	54.1%	38.1%

As can be noticed, the efficiency of natural gas power plants is higher than both the coal and oil one. For instance, in a CCGT plant, the steam turbine cycle roughly produces one third of the power, whereas the gas one generates two thirds of the

power output. Moreover, there is less combustible (i.e. gas) consumption since gas is burnt only during the warming up phase of the gas cycle. Less combustible used means a higher thermal efficiency of the power plant (Electrical Engineering Portal, 2012).

As far as nuclear thermal power plants are concerned, a world nuclear database was used to extract the data necessary to calculate the individual thermal efficiencies of the different nuclear generators (i.e. design and thermal capacities) (World Nuclear Association, 2016). The average nuclear thermal efficiency in the IP was found to be approximately equal to 34%;

- **Design Capacity** [MW] of a single thermal power plant. It is also called Gross Capacity and represents the maximum electric output an electricity generator can produce under specific conditions (US Energy Information Administration, 2016). This electric output is measured at the outlet of the main transformers, i.e. it includes the amount of electricity used in the plant auxiliaries and in the transformers (Eurostat Statistics Explained, 2012).

  Design Capacities were collected from different sources according to the thermal power plant considered (e.g. Global Energy Observatory, 2016) and were transformed into [GWh/week];
- **Beta Factor (β)** [-] of a single thermal power plant. It is defined as the share of waste heat lost through the cooling tower. This factor is discussed in detail in Section 9.2.2.

7.2.2 Thermal Power Plants Aggregation

Among the 32 thermal power plants located inside the modelled area of the IP, some are actually different generator units situated at the same place and constituting one single power plant. Sometimes, they are built with different cooling technologies and are run by different companies.

Since the waste heat discharged into the river by one thermal generator is assumed not to affect (i.e. increase) the river temperature downstream, all the power plants can take advantage of the full thermal capacity of the river itself. This would lead to an overestimation of the thermal capacity of the natural source, thus of the possible thermal production (i.e. inequality constraint 5 would be overestimated; see Section 9.2.3). In reality, thermal power plants located close to each other have to share the thermal capacity of the stream they all discharge into.

Therefore, all the thermal generators situated inside the same watershed are aggregated into one production unit. This is achieved by performing a weighted average of their main characteristics (i.e. efficiency and β), using their design capacities as weights. As for the gross capacities, they are summed up. However, two units equipped with different fuel types and whose production costs are different (e.g. nuclear and coal-fired) cannot be

merged together. For instance, their aggregated average production cost would change the optimization framework and not be representative for the actual costs.

In the end, 15 thermal power plants have been modelled in this thesis study. Their main characteristics are summarized in Table B-2 (see Appendix B.6).

7.2.3 Residual Thermal Power Supply Curve

Wangensteen's (2012) merit order approach is the concept standing behind the construction of the residual thermal supply curve in the model. Generally, this method assumes generators to have constant marginal costs and schedules them from cheapest to most expensive until the power demand is fully satisfied. As Pereira-Cardenal et al. (2014) state, producers' variable efficiency rates, transmission and security constraints and intertemporal ties (e.g. generators' start-up costs) are neglected this way.

The supply function of residual power represents the quantity of electricity supplied as a function of the market price. Its building process is the same followed by Pereira-Cardenal et al. (2014) and is presented in Appendix B.7.

In the end, 10 generation levels of 250 GWh each were created and associated with a different constant marginal cost. This cost represents the average price of a residual thermal generator and was computed by averaging the prices falling into each 250 GWh slot. The resulting ten generators and the corresponding marginal costs are summarized in Table C-3 (see Appendix C.2).

This methodology assumes that neither water shortages nor restricting high water temperatures ever affect the residual thermal producers. This is thought to be reasonable since most of the remaining thermal power plants are located along the shoreline. Thus, they use seawater as a cooling source, which is never affected by temperature increase constraints.

7.3 Power Grid

Once the electricity is produced, it has to be transmitted through a power grid in order to be distributed and to reach its final users (Wangensteen, 2012).

In the IP, transmission lines tend to develop along the river network of the region, since power generators and cities (i.e. the main centers of power demand and consumption) are located next to water bodies. For instance, hydropower plants have to be situated in mountains and river valleys that provide sufficient head, whereas thermal generators along rivers, lakes (natural or artificial ponds) and the sea in order to have a secure source of cooling water guaranteed (Pereira-Cardenal et al., 2013).

Chapter 8

Climate Change

In order to assess the possible impacts of climate change on the IP water-power system and in particular the subsequent effects of cooling constraints on thermal production, a climate change scenario has been developed for the time frame 2036-2065.

Three Regional Climate Models (RCM) from the ENSEMBLES Project (van der Linen et al., 2012) were employed in the model as feasible climate change scenarios, thus used to derive precipitation and temperature time series under climate change. They all refer to the A1B emission scenario, which is based on the following assumptions applied at a global scale: (i) very rapid economic growth; (ii) population peak by 2050; (iii) quick spread of new and efficient technologies; (iv) balanced emphasis on energy sources (Nakiâcenoviâc, 2000).

The same three RCMs used by Pereira-Cardenal et al. (2013) and that best perform over the IP (Herrera et al., 2010) were considered in this thesis. They are listed in Table 8-1.

Table 8-1: Three Regional Climate Models employed as feasible climate change scenarios in the model. They were used to derive precipitation and temperature time series under climate change scenario.

RCM	Institution	Reference
CLM	Swiss Institute of Technology (ETHZ)	Jaeger et al. (2008)
M-REMO	Max Planck Institute for Meteorology (MPI)	Jacob et al. (2001)
RACMO	Koninklijk Nederlands Meteorologisch Instituut (KNMI)	van Meijgaard et al. (2008)

A set of monthly change factors (CF) was computed for each one of the three RCMs in order to generate precipitation and temperature time series for the future scenario. The resulting three sets of CFs were averaged to create a fourth scenario, named ‘meanRCM’. The monthly precipitation and temperature CFs over the IP are displayed in Figure B-3 and Figure B-4 respectively (see Appendix B.8).

In particular, precipitation and temperature time series have been produced through the *delta-change* method (Pereira-Cardenal et al., 2013; Fowler et al., 2007). Since the optimization algorithm runs with a weekly time step (see Section 9.2.3), it would average out extreme values obtained through more sophisticated procedures. This method applies the four sets of monthly CFs to observed precipitation and temperature series (1961-1990) to generate forcing input data to the rainfall-runoff model under three climate change

scenarios (plus the average one). CFs are multiplicative for precipitation and additive for temperature. The resulting temperature dataset was employed to estimate reference evapotranspiration time series (Pereira-Cardenal et al., 2014).

Runoff

The estimated annual average runoffs aggregated at the Peninsula level for both the control (1961-1990) and the four climate change scenarios (2036-2065) are compared in Figure 8-1a.

As can be observed, the simulated runoff for the control period is higher during most of the weeks in the average year, as already expected. The only exception is represented by the last two weeks of February, when the RACMO and REMO climate models present a peak in the runoff. This is due to a corresponding peak in the precipitation estimates, which has been recorded during the same time frame. The CLM model presents the lowest runoff values among all the four RCMs considered and throughout the entire average year. For instance, it is the climate model that estimates the lowest precipitation values among the four considered.

Overall, the yearly average volume of total runoff over the IP is higher in the control period than under climate change scenario. Pereira-Cardenal et al. (2013) reached the same conclusions.

River Water Temperature

The logistic function equation and its estimated parameters presented in Appendix B.2 were used to estimate future river water temperature time series. The air temperature dataset needed as input to the S-shaped curve is the one estimated through the aforementioned *delta-change* method.

The estimated annual mean water temperatures averaged over the Peninsula for both the control and the four climate change scenarios are compared in Figure 8-1b.

As can be observed, the estimated water temperature for the four climate models is higher during all the weeks in the average year, as already expected. This is due to higher air temperatures under climate change. Even if control and climate change scenarios are characterized by different absolute water temperature values, they both present the same trend: water temperature is higher during the summer months (with a peak around end of July/beginning of August) and lower in winter. The four RCMs curves mostly overlap.

Irrigation Water Demand

Future irrigation water demand (*IWD*) was generated by applying monthly CFs in estimated evapotranspiration to *CWD*, thus subtracting climate change precipitation series.

The estimated annual average *IWDs* aggregated at the Peninsula level for both the control and the four climate change scenarios are compared in Figure 8-1c.

As can be observed, the total *IWD* aggregated at the Peninsula level is higher under climate change scenario than in the control period throughout the whole average reference year displayed. This was expected, since evapotranspiration is likely to increase and precipitation to decrease under climate change. Even if control and climate change scenarios are characterized by different absolute *IWD* values, they both present the same trend: irrigation water demand is higher during the summer months (with a peak in July) and lower/null in winter. This pattern is due to high evapotranspiration and very low precipitation in summer, vice-versa for winter. The four RCMs curves mostly overlap.

Overall, the yearly average amount of total *IWD* over the IP is lower in the control period than under climate change scenario. Once again, Pereira-Cardenal et al. (2013) reached the same conclusions.

Power Demand

Changes in seasonal temperature patterns will have an impact on power demand trends, since power demand is estimated from the corresponding mean daily temperature data (see Section 7.1). For instance, higher temperatures will likely decrease (increase) winter (summer) electricity demand.

In particular, power demand data were updated using the climate change temperature series and applying the same procedure presented in Section 7.1. The estimated annual average power demands at the Peninsula level for both the control and the four climate change scenarios are compared in Figure 8-1d.

As can be observed, and as already expected, power demand under climate change scenario is higher during the summer months and lower during winter, compared to the control period. This is due to higher temperatures predicted for the future, which will shift the peak in power demand from winter to summer.

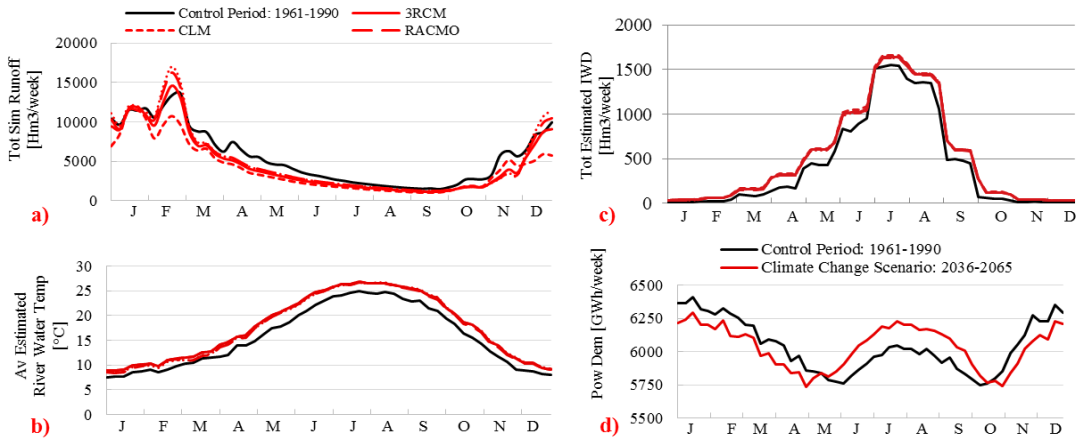

Figure 8-1: Total simulated runoff (a), total estimated river water temperature (b) and total estimated irrigation water demand (c) aggregated at the Peninsula level and averaged throughout the 30-year control (1961-1990) and climate change (2036-2065) scenarios. The former is identified by the black line, whereas the latter is represented through the four different RCMs (red lines). Total estimated power demand (d) is characterized by one time series for climate change scenario in general (red line).

In the following Part, the methods applied to model the water system, the power system and their coupling are described. The purpose is to generate a coupled model of these two systems in order to assess and quantify the interconnections between them.

Part IV

Models and Methods

Chapter 9

Model Formulation

In this study, a deterministic, single objective, resource allocation problem optimized through a linear programming solver is proposed to assess the linkages between the water and power systems in the IP, with special regard to the impacts of water cooling constraints on the entire model. In particular, the single objective consists in minimizing the net costs of the system. The optimal values for each decision variable provided by the solved optimization problem over the planning horizon are considered 'optimal' with respect to this performance criterion. Since it is an economic criterion, the optimization of the water-energy system is referred to as economic optimization.

The following sections address: (i) the conceptual model of the system; (ii) the formulation of the joint water-power optimization problem; (iii) a sensitivity analysis of the model to several input parameters.

9.1 Conceptual Model

Each constitutive element of the system (i.e. watershed) was simplified as in the conceptual model displayed in Figure 9-1, in order to be able to feasibly represent it during the implementation procedure of the optimization model. All the 123 watersheds constituting the system were implemented according to this model outline.

As can be observed, each watershed is characterized by a hydropower plant, an inflow value and an irrigation water demand. In particular, this single demand volume results from the aggregation of different agricultural demands, spread over the watershed. Moreover, some watersheds present a thermal power plant.

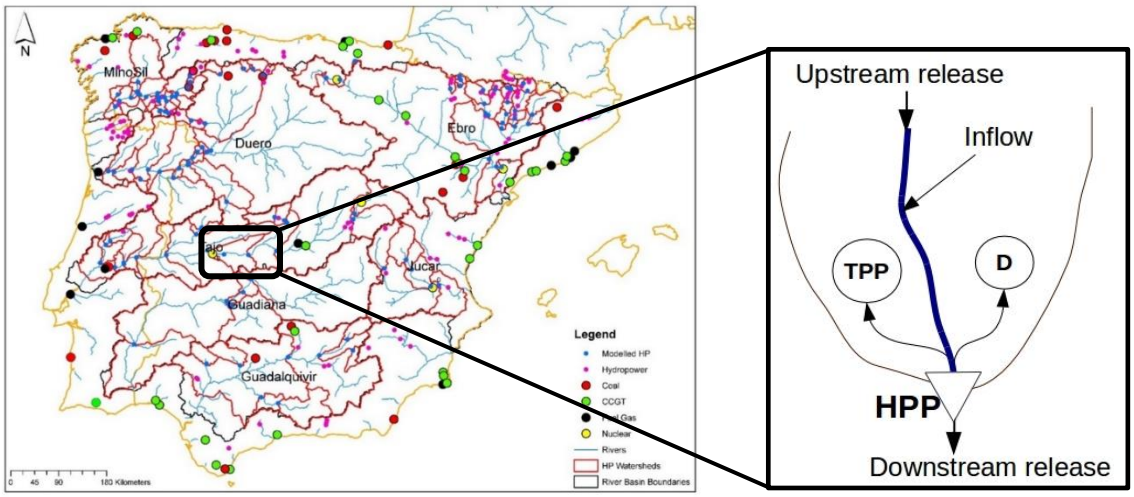

Figure 9-1: Conceptual model of each constitutive element of the system implemented (i.e. watershed, represented by the black thin line). HPP identifies the hydropower reservoir delineating the watershed, TPP a given thermal power plant and D the agricultural demand. 'Upstream release' refers to the water released from the hydropower reservoir directly upstream, whereas 'Downstream release' represents the water volume released from the HPP displayed.

9.2 Joint Water-Power Optimization Modelling

Figure 9-2 shows the summary scheme of the joint water-energy model of the IP, its key components and its optimization framework.

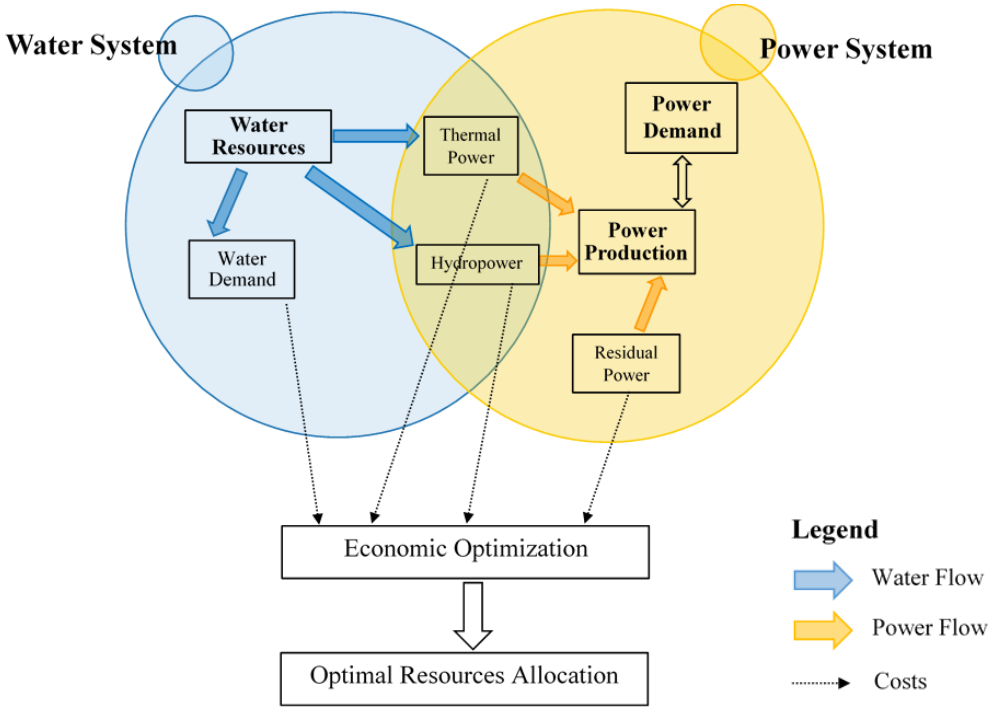

Figure 9-2: Joint modelling framework of the water-energy systems in the Iberian Peninsula. The blue circle represents the water system, the orange denotes the power system, while their overlapping includes the elements responsible for the interaction between these two systems.

The modelling approach displayed and adopted in this study works as follows: Water Resources, which can be allocated to Water Demand (i.e. agriculture), Thermal Power and Hydropower in a flow path-based modelling approach, constitute the Water System. Hydropower is also able to store water and make it available for the 'Water Resources' category again. The Water System is connected to the Power System through Thermal and Hydropower, which both contribute to power production (together with Residual Thermal Power) and require water to produce electricity. Total energy production has to fully meet power demand on a second-by-second basis (i.e. the double-sided black arrow in Figure 9-2 above). Costs are associated to power and water flows, while optimal resource allocation is reached through the optimization (minimization in particular) of global costs. All the elements just described enter the economic optimization framework as either decision variables, i.e. part of the objective function (e.g. thermal power), or constraints (e.g. power demand).
The Water System is based on a flow path representation, while linear programming rules both the flows (i.e. water allocation and power production) and economic optimization. Moreover, the power system implemented is the one existing in the IP nowadays.

The following sub-sections present the modelling technique applied to the water-energy system in the IP in detail.

9.2.1 Flow Path-Based Representation of the Water System

In this study, the water distribution network in the IP has been modelled according to a simplified version of the deterministic flow path-based (network) model proposed by Cheng et al. (2009). The following simplifications have been applied to their model: (i) there is no need to keep track of the water delivery relationship between suppliers and receivers. For instance, this thesis assumes water as a single commodity, i.e. multiple water titles are not considered (Cheng et al., 2009); (ii) loops and two-way pipes are not included in the flow path model, since only water distribution through natural rivers (gravity driven and unidirectional) is taken into account. As for the constraints, most of Cheng et al. (2009)'s are kept in this model. Some additional constraints have been added in order to represent the power market properly.

Theoretical Framework
Cheng et al. (2009) propose a deterministic flow path model that provides a general methodology to implement water distribution systems. Their model uses all possible flow paths in the network in order to predefine the physical distribution scheme. Within this predefined physical delivery system, all water delivery actions can be considered as water-moving activities from one location (i.e. source node) to another (i.e. associated demand or sink node).

A source node is a node connecting only the tails of the emitting arcs, whereas a sink node (i.e. receiving node) links only the arrow heads of the confluent arc. The former and the latter identify the physical location of the available water resource (e.g. river source or reservoir) and of the collecting point of the delivered water (e.g. demand node, reservoir or ocean) respectively. The scheme of a hypothetical water distribution system modelled through the flow path method is displayed in Figure 9-3. Here, for example, node 1 is a source node, while node 4 is a receiving node.

A flow path is a possible water delivery route. It stars from a source node, passes through the physical distribution network along the direction of non-repeated arcs, and finally ends at a sink node. Arc 1 → Arc 6 represents one of the several flow paths in Figure 9-3.
Special reference needs to be made to storage nodes (e.g. reservoir), which are not only source but also sink nodes, since they all can supply and receive water. Thus, in the flow path model a storage node (e.g. reservoir R_1) is represented by a source (I_3) and a sink node (S_3) simultaneously, as shown in Figure 9-4. Here, the dotted black arrow means that the water delivered to the receiving node S_3 at time *t* becomes a source at the source node I_3 at time $t + 1$. This linkage is called carryover storage for a reservoir.

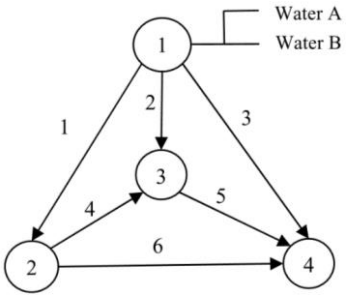

Figure 9-3: Structure of a flow path-based model of a hypothetical water distribution system. Arrows are referred to as arcs (Cheng et al., 2009).

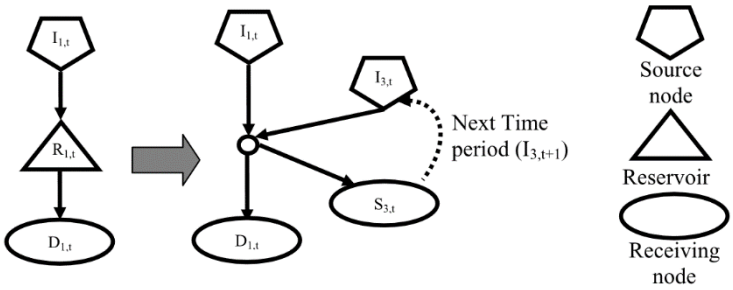

Figure 9-4: Example of how a storage node (i.e. reservoir) is implemented in a hypothetical flow path-based model (Cheng et al., 2009).

In the following, the adaptation of Cheng et al. (2009)'s model to this thesis project is discussed.

Sources and Sinks

In this study, all five categories of elements characterizing each watershed were considered as nodes in the network representation. In particular, they were implemented as either a source or a sink node, as discussed in the following:

- **Hydropower plant**: modelled as both a source and a sink node, since it can release and receive water. Thus, two nodes were employed to represent it and linked through a carryover storage, as in Cheng et al. (2009). Moreover, each hydropower reservoir can supply water to the users in both the watershed it defines (in order to

represent the local storage capacities and avoid "fictive curtailments" in the most upstream watersheds) and the downstream ones;

- **Inflow**: corresponds to the runoff in each watershed. It was modelled as an inflow going directly into the reservoir delimiting the watershed, instead of being implemented as a node. This allows to reduce the number of state variables in the system (i.e. the number of flow paths), without modifying its structure and operating principle;
- **Basin outlet**: is a fictitious reservoir with zero capacity, added in order to delineate the watershed located downstream the last hydropower plant in each basin. It was modelled as both a source and a sink, not linked through the carryover storage. The former node is only needed in order to take the watershed inflow into account, the latter represents the water flowing to the sea (or outside the model area);
- **Water demand**: only refers to irrigation water demand. It was implemented as one sink node per watershed;
- **Thermal power plant**: is a sink, representing the thermal cooling water use of the power plant(s) in a given watershed.

Flow paths

All the possible connections between sources and sinks are computed and called 'flow paths'. The method required that there was only one possible flow path between a source and a sink, thus no loops were allowed in the system. The model also assumed that water was able to flow from any source to any sink connected by a flow path within a single time step.

More detailed information about the network and flow path matrix construction can be found in Appendix C.1. An explanatory example of how the implemented flow path model works was also included.

9.2.2 Cooling Constraints Implementation

As already explained in Section 7.2.1, thermal power plants generate waste heat when they produce electricity. For a given electricity production P [GWh/week], the waste heat H_w [GWh/week] released by a thermal generator was formulated as follows:

$$H_w = \frac{1-e_{th}}{e_n} * P \tag{9-1}$$

where e_{th} and e_n are thermal and net efficiency of the power plant respectively. e_{th} mainly depends on the combustible type (e.g. coal, natural gas, etc.) and design characteristics (e.g. cooling technology) of the power plant. However, it may also depend on time-varying factors, such as air temperature or production rate (Koch et al., 2013). In the implemented

model, e_{th} was assumed to be constant for a certain thermal plant. e_n also takes into account the generator own electricity consumption.

Cooling water is needed to dissipate the amount of waste heat produced by a certain power plant. A heat balance can be employed to compute these water requirements, similarly to Koch and Vögele (2013). It requires waste heat to be divided into: (i) an amount H_w^e absorbed by water evaporating in the cooling tower, which generates consumptive use; (ii) an amount H_w^w transferred by cooling water increasing its temperature, which is discharged back into the natural source (e.g. river) and generates non-consumptive water requirements. These two factors were computed as follows:

$$H_w^e = H_w * \beta \tag{9-2}$$

$$H_w^w = H_w * (1 - \beta) \tag{9-3}$$

where β represents the fraction of waste heat lost through the cooling tower, i.e. evaporated.

Equations (9-2) and (9-3) assume that all the waste heat is absorbed by the cooling system. However, since a small share of it is lost through other parts of the system, this assumption leads to a slight overestimate of the actual waste heat that needs to be discharged via cooling medium.

Starting from equation (9-3), waste energy discharged into the natural source (H_w^w) can be computed as follows (adapted from Koch et al., 2013):

$$H_w^w = H_w * (1 - \beta) = V * \rho * c_P * dT \tag{9-4}$$

where V is the amount of non-consumptive cooling water needed by a thermal plant to discharge part of its waste heat (i.e. $(1 - \beta) * H_w$) into, dT the temperature increase in the natural source, c_P the calorific capacity of water and ρ the density of liquid water.
The maximum temperature increase regulation is on the downstream water. Therefore, assuming total mixing, V is the amount of water flowing in the river downstream of a given thermal power plant and including the volume of cooling water discharged back. dT represents the maximum legal temperature increase in the river.

Equation (9-4) also applies to cooling water actually withdrawn by a thermal generator, where dT is called DT and refers to the temperature increase in this volume of cooling water withdrawn (refer to equation (9-7)).

On the other hand, equation (9-2) leads to the following waste energy discharged in water evaporated through a cooling tower (H_w^e) (adapted from Koch et al., 2013):

$$H_w^e = H_w * \beta = V_c * \rho * L_e^* , \quad with \quad L_e^* = (L_e + c_P * DT^*) \tag{9-5}$$

where V_c is the water consumed (evaporated) and L_e^* the latent plus sensible evaporation heat of water, which takes the energy for both temperature increase and phase change into account. L_e is the latent evaporation heat of water and DT^* the average water temperature increase up to its boiling point, which is estimated to be around 80 °C.

The total amount of water $Vtot$ needed in the river upstream of a certain thermal power plant - in order to satisfy its consumptive and non-consumptive water requirements - was calculated as follows:

$$V_{TOT} = V + V_C = H_w * \left(\frac{\beta}{\rho * L_e^*} + \frac{1-\beta}{\rho * c_P * dT}\right) \quad (9\text{-}6)$$

Equation (9-6) was employed as a constraint in thermal power production (see Section 9.2.3).

Since very few plant-specific water consumption measurements could be detected, typical water consumption and withdrawal volumes were used and derived from Macknick et al. (2012), as it seemed the most complete study on the topic. Table 9-1 summarizes Macknick et al. (2012)'s dataset (employed in this thesis) as well as results from other researches conducted on the same subject.

Table 9-1: Water withdrawal (WW) and consumption (WC) data [m^3/MWh] according to three different studies. Macknick et al. (2012) appeared to be the most complete work, thus their results were also employed in this thesis. Thermal power plants are divided per fuel type (i.e. nuclear, CCGT, coal) and cooling technology (i.e. once-through (OT), cooling tower (CT)). The last two columns display the values of β estimated by using Macknick et al. (2012)'s and NETL (2011)'s water volumes respectively.

Fuel Type	**Cooling Tech.**	**Macknick et al. (2012)**		**NETL (2011)**		**EPRI (2002)**		**Macknick et al. (2012)**	**NETL (2011)**
		WW	WC	WW	WC	WW	WC	Estim. β [-]	Estim. β [-]
Nuclear	OT	167.9	1.0	123.6	0.5	160.9	1.5	0.27	0.19
	CT	4.2	2.5	4.9	2.2	3.6	2.7	0.99	0.98
CCGT	OT	43.1	0.4	26.9	0.0	54.9	0.4	0.35	0.03
	CT	1.0	0.7	0.7	0.5	0.9	0.7	1.00	0.99
Coal	OT	94.6	0.4	83.3	0.0	-	-	0.21	0.01
	CT	2.0	1.8	2.0	1.5	1.4	0.8	1.00	0.99

As can be noticed, water withdrawal and consumption values are different according to the thermal power plant fuel type (i.e. nuclear, CCGT, coal) and cooling technology installed (once-through (OT), cooling tower (CT)). Moreover, no differentiation between

cooling towers with or without closed circuit is made, thus they were not separated in the model.

Using Macknick et al. (2012)'s water volumes, one β per thermal power plant type was estimated (Table 9-1). For instance, β is related to water withdrawal and consumption volumes through equations (9-4) and (9-5), which were employed to derive the following relation:

$$\beta = \frac{\gamma}{\frac{WW}{WC}+\gamma-1}\ ,\ \ with\ \ \gamma = \frac{Le^*}{c_p * DT} \tag{9-7}$$

where WW is the water withdrawn, WC the water consumed and DT the temperature increase in the cooling water discharged back into the river (which is different from dT, the temperature increase in the downstream river). DT was assumed to be equal to 10°C on average (EPRI, 2002). However, its value influences significantly the resulting β showed in Table 9-1. β was also influenced by the choice to use Macknick et al. (2012) as reference data. If NETL (2012)'s water volumes were employed, the corresponding estimated value of β would be between 20 and 30% lower for Coal and CCGT power plants respectively (Table 9-1).

Equation (9-7) assumes that water consumption is for cooling purposes only, which is reasonable as long as no carbon capture system (CCS) is implemented (Byers et al., 2014). This is most likely the case in Macknick et al. (2012)'s dataset, since CCS is a recent, expensive and little extended technology. As a result, once-through (OT) systems present non-zero water consumption volumes, thus a positive β value, even though they are not equipped with a cooling tower.

The proposed flow path-based model of the water distribution system, together with the implemented power system, can be used to formulate a generalized optimization model for the regional water-power system of the IP. Because of several advantages of linear programming, a flow path-based linear programming model for water-power system optimization is formulated in this study and presented in the following sub-section.

9.2.3 Linear Programming

Theoretical Framework

Linear Optimization or Linear Program (LP) refers to a class of constrained optimization, whose purpose is to maximize or minimize a linear objective function. This objective is expressed in terms of the decision variables of the problem, which are required to satisfy a system of linear constraints, i.e. linear equations or inequalities. The constraints must be expressed in terms of the decision variables as well and represent known relationships and dependencies in the problem (Gale, 2007).

Mikosch et al. (2006) provide the general, standard form for an LP, reported below.

$$\min_{\boldsymbol{x}} \phi = \boldsymbol{c}^T \boldsymbol{x}$$

$$s.t. \quad A\boldsymbol{x} \leq \boldsymbol{b} \qquad (9\text{-}8)$$
$$D\boldsymbol{x} = \boldsymbol{e}$$
$$\boldsymbol{x} \geq 0$$

Equation (9-8) represents the matrix formulation, where the letters in bold identify vectors. ϕ is the objective function to be minimized by selecting optimal values for the decision variables **x**, whereas **c** are the coefficients of the objective function. A and D are *m x n* and *q x n* matrices representing the inequality and equality constraints, whose right hand side is represented by **b** and **e** respectively. Finally, *n* represents the number of decision variables, while *m* and *q* symbolize the number of inequality and equality constraints.

In Figure 9-5, the identification process of the feasible region (i.e. the yellow quadrilateral) for a 2-dimensional LP with 2 decision variables (i.e. x1 and x2) is displayed. In this case, the feasible region is bounded. Nevertheless, it could also be an unbounded polytope in a more general framework. In both cases, it always has vertices where the constraints intersect. As for the optimal solution, if it exists, it also lies at the intersection point of the constraints (i.e. the green circle). For a feasible problem, if multiple vertices end up in the same objective function value, a unique solution may not always exist (Loucks et al., 2005).

In order to solve an LP problem and obtain optimal values for its unknown decision variables, two main methods can be applied: (i) interiorpoint; (ii) simplex algorithm. Since the latter is considered one of the oldest and most widely used algorithm to solve LPs, it is also employed in this study.

The simplex algorithm was invented by George Dantzig in 1947 and relies on a fundamental fact: if an LP has a bounded optimal solution, then its optimal value is obtained at a BFS, i.e. at a vertex (or so-called 'extreme point') of the polytope including all the feasible points. This feasible polytope is also referred to as 'simplex', which is where the algorithm gets its name (Weber, 2010). Today multiple forms of this algorithm exist, e.g. the revised simplex and the dual simplex. Regardless of the variant considered, the simplex algorithm starts at one of the BFS (Phase I) and iteratively pivot from one vertex to the other along the direction of decline of the objective function, until no further decrease is possible (Phase II) (Mikosch et al., 2006). Its working principle is shown in Figure 9-6.
According to the type of simplex solver, the selection of the starting point changes (Mikosch et al., 2006). As far as the simplex algorithm performance is concerned, Weber (2010) states that in practical problems, typically only *O(m)* steps are needed to solve a LP problem with *m* constraints. Unfortunately, there is no known way to guarantee that the algorithm takes the shortest path.

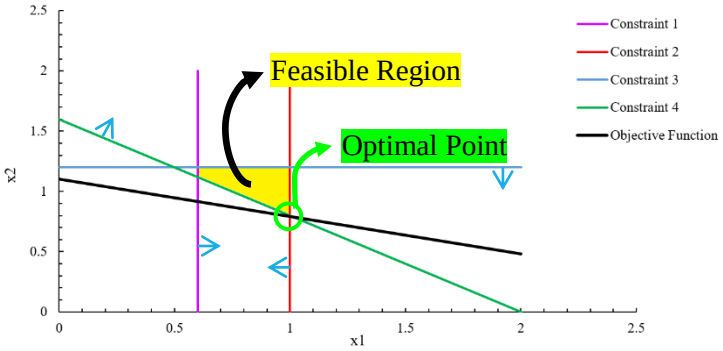

Figure 9-5: Feasible region and optimal point for an LP with 4 constraints and 2 decision variables (x1 and x2). Adapted from: Loucks et al., 2005.

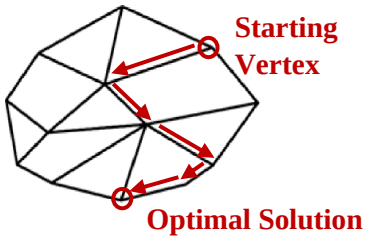

Figure 9-6: Consecutive iterations of the simplex algorithm in a 3D problem (i.e. 3 decision variables). The starting point is one of the BFS, while the end is at the optimal solution vertex. Adapted from: Wikipedia, 2016.

According to Loucks et al. (2005), the large availability of computer programs that can solve linear programming problems made LP one of the most implemented optimization algorithm (e.g. Cheng et al., 2009). Another reason why LP is one of the most popular optimization methods is that many models of complex water resources systems are (or can be transformed into) linear. Regardless of its power and popularity, LP is best viewed as a preliminary screening tool, whose main purpose is mostly to reduce the number of alternatives for further more detailed simulations, rather than finding the best decision. Nonetheless, it can provide initial designs and operating policy information required by simulation models in order for these models to simulate them.

Time Step

Koch et al. (2013) demonstrate that a smaller time step (e.g. daily) is more accurate than a bigger one (e.g. monthly) when modelling a hydrological-energy system. For instance, in the latter case, extreme events (e.g. days characterized by a very high river water temperature) are levelled out by the averaging of daily values over the month.

On the other hand, if a modeler wishes to use extended time series in order to consider different climatic phenomena, the time step cannot be excessively small. If it were, the model would become too computationally intensive. Moreover, certain input data (e.g. irrigation requirements) are difficult to obtain on a daily basis. At last, the flow path-based model implemented in this study assumes that the water flows from a specific source to all its potential sinks in one time step (see Section 9.2.1). This is not realistic when a river basin scale and a daily modelling time step are considered jointly.

For all these reasons, a weekly time step was assumed reasonable to implement the water-energy system of the IP. This choice appears to be a good compromise because it is small enough to represent both warm and dry periods but large enough to allow the model to run for several years and provide representative results.

Based on the available precipitation and temperature data, the optimization scheme is run for the control period (1961-1990) and for the climate change scenario (2036-2065), both resulting in T = 1560 simulation weeks each.

The following sub-sections explain how objective function, marginal costs, decision variables and equality and inequality constraints were implemented.

Objective Function

Since an economic optimization (i.e. costs minimization) is performed, a cost has to be associated with each decision variable appearing in the objective function.

Within the discussed modelling framework, the objective function ϕ is implemented as follows:

$$\min_{\{x_i\}_{i=1}^{n}} \phi = FPC * FP + IDCC * IDdef + TFC * TF + THwC * TPP + RC * RPP \quad (9\text{-}9)$$

ϕ has to be minimized by selecting optimal values for **x,** where **x** is the vector of decision variables consisting of: FP (water allocation, i.e. flow path), IDdef (irrigation water demand deficit), TF (hydropower plant turbinated flow), TPP (thermal power waste heat production) and RPP (residual power production). The five marginal costs assigned to the different decision variables are presented in the following sub-section.

Marginal Costs

The marginal costs represent the multiplication factors of the decision variables in the objective function and indicate how much the whole system gains (benefits) or loses (costs), depending on the optimum values assigned to the decision variables. They include:

a. **FPC**: Flowpath cost, which represents the cost of each water delivery. It is assigned zero value, since it is assumed not to influence water allocation decisions;
b. **IDCC**: Irrigation curtailment cost. The cost associated to deficit in irrigation water demand (i.e. curtailment cost) corresponds to the marginal benefit (MB) of the marginal user (Pereira-Cardenal et al., 2013).
   MMA (2007) provides annual irrigation water demands (Hm^3/yr) for ranges of net benefits in each river basin in Spain. A weighted average of these demands was performed in order to obtain only one net benefit per river basin, assuming a constant willingness to pay for all water allocations. Since only net benefits data are available, they were employed as a proxy for marginal benefits, thus for irrigation curtailment costs. Seven constant IDCC were used, one per modelled river basin;
c. **TFC**: Hydropower plant turbinated flow cost, which corresponds to the marginal cost of hydropower production. According to CNE (2008), a cost of 3 €/MWh has been attributed to it, i.e. to hydropower plants turbinating a certain flow.

Since the focus of the model is mainly on the difference between thermal power and hydropower variable costs, rather than on their single numerical values, the hydropower one has been approximated with 0 €/MWh;

d. **THwC**: Thermal power waste heat production cost. It refers to the marginal cost of a thermal power plant's associated electricity production.
   Thermal power generation was simulated as three different technologies (i.e. Nuclear, Coal and CCGT) with a constant marginal cost[14] obtained from CNE (2008).
   Marginal costs of coal and CCGT are very close but different (58 and 57 €/MWh respectively). Thus, in the model, they have been assumed to be equal and set to 57 €/MWh, in order to avoid creating an artificial difference between these two generation technologies.
   For instance, if no cooling constraint was active and two different costs were considered, the implemented model would prefer to let all the CCGT power plants in the IP produce, before using the coal ones. This occurs because the purpose of the optimization model is to minimize net costs, therefore the cheaper electricity generators (i.e. nuclear and CCGT) will be all used first at full capacity (but constrained by water availability). This case is not representative of reality, where different power plants, belonging to the same generation technology, may have very different marginal costs;
e. **RC**: Residual power production cost, which denotes the marginal power production cost of the producers not explicitly represented in the model.
   Residual power production cost was inferred from the residual thermal power supply curve and consisted of ten different constant marginal costs, one per every synthetic generator of 250 GWh/week established.

The numerical values of the costs multiplying the decision variables in the objective function and employed in the model are reported in Appendix C.2.

Decision Variables

The decision variables embody water and energy management strategies, are subject to constraints and optimized by the objective function. Five categories of decision variables are implemented in the model:

a. **FP**: Water allocation (i.e. flow path, $FP_{i,j}^{t}$). Similar to Cheng et al. (2009)'s flow path-based model, the water allocated to each sink *j* in the network from its corresponding source *i* at each time step *t* is considered as a decision variable;

[14]Marginal costs correspond to 'variable costs', since fixed costs do not depend on the quantity of energy produced.

b. **IDdef**: Irrigation water demand deficit ($IDdef_p^t$). It represents the share of irrigation water demand that is not met due to a smaller amount of water allocated to that irrigation sink *p* at time *t*;
c. **TF**: Hydropower plant turbinated flow (TF_p^t). It denotes the amount of water flowing through a certain hydropower plant *p* at a given time step *t* and thus used to produce electricity;
d. **TPP**: Thermal power waste heat production (TPP_{pp}^t). It corresponds to the amount of waste heat (Hw) generated by the electricity production process of a certain thermal power plant *pp* at a given time step *t*;
e. **RPP**: Residual power production (RPP_k^t). It embodies the quantity of remaining thermal power produced by a synthetic generator *k* at a given time step *t*, i.e. the amount of power generated by the producers not explicitly represented in the model.

The standard LP formulation constraining all the decision variables to be non-negative is applied in the model.

Equality Constraints – Aeq Matrix

Equality constraints are implemented in the equality constraints matrix Aeq and represent mass balance relations at the different nodes in the system. They limit both water and power allocations. The Aeq matrix is made up of four equality constraints:

1) **Water Mass Balance** (∀p ∈ HP s.t. j ∈ HP and Downstream Nodes & i ∈ HP and Upstream Nodes):

$$\sum_j FP_{p,j}^t - \sum_i FP_{i,p}^{t-1} = InWatershed_p^t \quad (9\text{-}10)$$

It ensures that the sum of all allocations ($\sum_j FP_{p,j}^t$) from a given source node *p* (i.e. reservoir) is equal to the amount of water available at time step *t*. This quantity consists of the volume of water flowing into that same source at time *t* ($InWatershed_p^t$) and the carry over storage from a previous time step ($\sum_i FP_{i,p}^{t-1}$). At time *t=0* (i.e. the beginning of the optimization procedure), there is no carry over storage from previous time steps into a given reservoir. Instead, an initial reservoir storage is summed to *InWatershed* in order to represent the whole water availability at the first time step.

2) **Irrigation Water Demand** (∀d ∈ Irrigation Demand Sink Node s.t. i ∈ Upstream Nodes):

$$IDdef_d^t = ID_d^t - \sum_i FP_{i,d}^t \quad (9\text{-}11)$$

It defines irrigation water demand deficit ($IDdef_d^t$) as the difference between estimated irrigation water demand (ID_d^t) and water allocated to that demand sink ($\sum_i FP_{i,d}^t$) at time *t*.

3) **Thermal Cooling Water Consumption** (∀pp ∈ TPP s.t. i ∈ Upstream Nodes):

$$\sum_i FP_{i,pp}^t - \frac{\beta * H_{w,pp}^t}{\rho * (L_e + c_P * DT^*)} = 0 \quad (9\text{-}12)$$

It makes water allocation to a given TPP *pp* ($\sum_i FP_{i,pp}^t$) depend on both the waste heat generation decision variable ($H_{w,pp}^t$) and the power plant's parameter β, through equation (9-5).

4) **Power Market Equilibrium** (∀k ∈ River Basin & z ∈ Residual Power Supply Curve Step):

$$\sum_k TF_k^t + \sum_k TP_k^t + \sum_z RPP_z^t = PDem^t \quad (9\text{-}13)$$

It links the seven basins together and ensures that power demand ($PDem^t$) is met by the overall power production at each time step *t*. Total production is computed as the sum of hydropower ($\sum_k TF_k^t$), thermal power ($\sum_k TP_k^t$) and residual thermal power production ($\sum_z RPP_z^t$) at time *t*.

Inequality Constraints – A Matrix

Inequality constraints are implemented in the inequality constraints matrix A and represent physical limitations in the system. They limit both water and power allocations. The A matrix is made up of five inequality constraints:

1) **Hydropower Maximum Storage** (∀p ∈ HP s.t. i ∈ HP and Upstream Nodes):

$$\sum_i FP_{i,p}^t < HPCap_p \quad (9\text{-}14)$$

It limits the volume of water stored in a given HPP *p* ($\sum_i FP_{i,p}^t$) to its maximum capacity ($HPCap_p$) at each time step *t*.

2) **Hydropower Available Flow** (∀p ∈ HP s.t. i ∈ HP and Upstream Nodes & j ∈ Downstream Nodes):

$$TF_p^t < \sum_{i,j} FP_{i,j}^t \quad (9\text{-}15)$$

It limits the amount of water turbinated by a certain HPP *p* (TF_p^t) to the volume of water available ($\sum_{i,j} FP_{i,j}^t$), i.e. the amount of water flowing through the hydropower plant at a given time step *t*.

3) **Hydropower Maximum Turbinated Flow** (∀p ∈ HP):

$$TF_p^t < HPTCap_p \quad (9\text{-}16)$$

It limits the amount of water turbinated by a certain HPP *p* (TF_p^t) at a given time step *t* to the maximum capacity of its turbines ($HPTCap_p$).

4) **Maximum Waste Heat Production** (pp ∈ TPP):

$$H_{w,pp}^{t} < TPcap_{pp} * (1 - e_{pp})/e_{pp} \quad (9\text{-}17)$$

The waste heat produced by a given TPP *pp* at time step *t* ($H_{w,pp}^{t}$) is constrained by maximum waste heat release ($TPcap_{pp} * (1 - e_{pp})/e_{pp}$). This release corresponds to design capacity ($TPcap_{pp}$) transformed into maximum waste heat release through the multiplication factor $(1 - e_{pp})/e_{pp}$, where e_{pp} is the thermal efficiency of the TPP. This constraint limits the maximum power production of a TPP to its design capacity.

5) **Thermal Cooling Water Constraint** (pp ∈ TPP; j ∈ TPP and Downstream Nodes; i ∈ Upstream Nodes):

$$H_{w,pp}^{t} * \left(\frac{\beta}{\rho * L_e^*} + \frac{1-\beta}{\rho * c_P * DT}\right) < \sum_{i,j} FP_{i,j}^{t} \quad (9\text{-}18)$$

It comes from equation (9-6) and limits upstream cooling water requirement of a certain TPP *pp* at time step *t* ($H_{w,pp}^{t} * \left(\frac{\beta}{\rho * L_e^*} + \frac{1-\beta}{\rho * c_P * DT}\right)$) to the upstream water flow ($\sum_{i,j} FP_{i,j}^{t}$). This cooling water requirement does not correspond to the TPP's withdrawn water, as dT indicates the temperature increase in the entire downstream river after mixing.

This constraint applies to thermal power plants located on main rivers only. Since affluents are usually situated at higher altitudes than main rivers, they always present temperatures lower than 25°C. Thus, the maximum available temperature increase in their waters (dT) is assumed to be 3 °C at any time of the year.

Moreover, this cooling constraint considers water withdrawal capacity of a given TPP as theoretically 'infinite', which would be incorrect in case of both high river water temperatures and large water availability. However, it is a reasonable assumption since high temperatures are always and only associated with water scarcity periods in the model implemented.

Building procedures examples of Aeq and A matrices can be found in Appendix C.2, where their aggregation over several river basins and time steps is also presented.

9.2.4 Solving Process: CPLEX Solver

The global LP problem is solved once for the whole management period considered (i.e. 30 years, from 1961 to 1990) and once for the climate change scenario (i.e. 30 years, from 2036 to 2065). Because of its computational speed, CPLEX® V12.4 for Matlab, an optimization toolbox developed by IBM to solve LP problems, was employed in this study.

The result of this optimization procedure is a column vector of decision variables, reflecting the optimal management strategy for the water-power system of the IP

modelled. Since the LP model implemented is deterministic, it operates under a 'perfect forecast', which means that the hydrologic conditions of future time steps are known in advance. Thus, they can be anticipated in the optimal management strategy.

Within the optimization framework, the LP presents per time step (i.e. one week):

a. 1 911 decision variables with:
b. 778 constraints, of which:
c. 262 equality constraints, and:
d. 516 inequality constraints.

Table 9-2 summarizes the whole optimization model setup and the units employed, together with several data sources.

9.3 Sensitivity Analysis

A sensitivity analysis was performed in order to evaluate the dependency of several model outputs on some input parameters. In particular, the model was re-optimized for each small change in several input parameters values, in order to test the robustness of the cost function to these small variations. Four main parameters were considered: (i) inflow; (ii) temperature; (iii) thermal marginal costs; (iv) thermal efficiency.

The impact on the model is mainly expressed in terms of % increase/decrease in total costs per % increase/decrease in the reference value of each input parameter tested. Reference values are the ones employed in the optimization over the control period; they were increased up to 110% and decreased down to 90% their initial value.

Table 9-2: Summary of the different variables/elements constituting the entire optimization model, together with their amounts and units specification.

	Variable	Description	Amount	Unit	Source
Indices	*t*	Current time step		[week]	
	T	Total length of the optimization scenario	1 560	[week]	
	Nyr	Number of years in the optimization scenario	30	[yr]	
	i, j	Indices for: upstream node (source) and downstream node (sink)		[-]	
	p, pp, d, z, k	Indices for: hydropower reservoir/watershed, thermal power plant, irrigation demand (sink), generator in the residual power supply curve and river basin		[-]	
	sb	Index for Pereira-Cardenal et al. (2013)'s sub-basins	22	[-]	
OBJECTIVE FUNCTION					
Marginal Costs	*FPC*	Flowpath cost (cost of each water delivery)	0	[€/m^3]	
	IDCC	Irrigation curtailment cost	7	[€/m^3]	MMA (2007)* [a]
	TFC	Hydropower plant turbinated flow cost	0	[€/MWh]	CNE (2008)
	THwC	Thermal power waste heat production cost	3 → 15 [b]	[M€/GWh]	CNE (2008)
	RC	Residual power production cost	10	[M€/GWh]	OMIE (2016)* [a]

Decision Variables	$FP_{i,j}^{t}$	Water allocation decision from source *i* to sink *j* at time *t*	1 647*T	[Hm^3]	
	$IDdef_{p}^{t}$	Agriculture water deficit of watershed *p* at time *t*	123*T	[Hm^3]	
	TF_{p}^{t}	Hydropower turbinated flow by hydropower plant *p* at time *t*	116*T	[Hm^3]	
	TPP_{pp}^{t}	Waste heat release from thermal power plant *pp* at time *t*	15*T	[GWh]	
	RPP_{k}^{t}	Residual thermal power production of generator *k* at time *t*	10*T	[GWh]	OMIE (2016)* [a]
	Ndv	Total number of decision variables	1 911*T	[-]/[week]	
		MODEL INPUTS			
Hydrology	$InWatershed_{p}^{t}$	Inflow to watershed *p* at time *t*	123*T	[Hm^3]	P*
	$Prec_{p}^{t}$	Precipitation on irrigated area of watershed *p* at time *t*	123*T	[Hm^3]	P* ; Wriedt et al. (2009)*
	DT_{sb}^{t}	Maximum river temperature increase according to the law in sub-basin *sb* at time *t*	22*T	[°C]	P*
Demand	ID_p	Yearly agricultural water demand of watershed *p*	123	[Hm^3]	Wriedt et al. (2009)* [a]
	Distrib	Weekly distribution of yearly demand in the Ebro	52	[%]/[week]	P
	$PDem^{t}$	Power demand at time *t*	T	[GWh]	P
	$SPReg^{t}$	Special regime production at time *t*	T	[GWh]	P

Hydropower Plant	y_p	Energy equivalent of hydropower *p*	116	[GWh/Hm^3]	P
	$MaxTF_p$	Maximum turbinated flow of hydropower plant *p* per time step	116	[Hm^3/week]	P
	$SCap_p$	Storage capacity of hydropower plant *p*	116	[Hm^3/week]	P
Thermal Power Plant	e_{pp}	Average thermal efficiency of thermal power plant *pp*, according to fuel type	3 → 15 [b]	[%]	IEA (2008)
	$TCap_{pp}$	Design capacity of thermal power plant *pp*	15	[GWh/week]	Global Energy Observatory (2016)
	β_{pp}	Share of waste heat lost through the cooling tower, according to the thermal power plant's fuel type and cooling system	6 → 15 [c]	[%]	Macknick et al. (2012)*
	MR_{pp}	Index for the location of thermal power plant *pp* (main river or not)	1 or 0	[-]	
		MODEL OUTPUTS			
	HPS_p^t	Reservoir storage of hydropower plant *p* at time *t*	123*T	[Hm^3] ; [%]	
	$THPP^t$	Total hydropower production at time *t*	T	[GWh]	
	$TTPP^t$	Total thermal power production at time *t*	T	[GWh]	
	$TTPPC^t$	Total thermal power production cost at time *t*	T	[M€]	
	$TRPP^t$	Total residual power production at time *t*	T	[GWh]	
	$TRPPC^t$	Total residual thermal power	T	[M€]	

		production cost at time *t*		
	$TACC^t$	Total agriculture curtailment cost at time *t*	T	[M€]
	TC	Total cost of the entire optimization process	1	[M€]

P: Pereira-Cardenal et al. (2013).

**: Data source was modified by own calculations; otherwise, raw data were employed.*

[a]: Pereira- Cardenal et al. (2013) used the same data source.

[b]: One different value per fuel type (3 fuel types) and 15 aggregated thermal power plants.

[c]: One different value per fuel type (3 fuel types) and cooling technology (2 cooling technologies) and 15 aggregated thermal power plants.

Part V

Results and Discussion

Chapter 10

Results and Discussion

The main findings of this thesis project are presented and discussed in the following chapters. The first section concerns the validation of the implemented model, performed by comparing its main outputs with Pereira-Cardenal et al. (2013)'s corresponding results together with some related literature researches outcomes. The following sections summarize the leading findings of this thesis and investigate the temporal and spatial variations of shadow prices of several equality and inequality constraints (e.g. water availability, cooling constraint). Moreover, the four climate change scenarios are analyzed and compared with the control period findings discussed earlier. The last section assesses the robustness of the model through a sensitivity analysis, achieved by changing the values of the most important input parameters and looking at the resulting outputs.

Overall, the primary outcome to be discussed is the impacts and strictness of cooling constraints on the entire water-power system of the IP, in particular on: (i) thermal power and hydropower production; (ii) agriculture deficit; (iii) total costs. This is achieved by comparing the outputs of the model implemented with and without cooling constraints, both in the control and climate change scenario. Another effect to be further examined is the climate change one on the water-energy nexus in the Peninsula, with particular focus on its consequences on cooling constraints, thus on the modelled power system.

The last chapter is devoted to the discussion of the limitations and further improvements that could be applied to this thesis project.

10.1 Validity of the Model

In order to assess the reliability of the model implemented, its results can be compared with the corresponding outputs of both some literature researches and Pereira-Cardenal et al. (2013)'s study.

Water Balance

The water balance consists of four elements, which were all averaged at a yearly temporal scale and aggregated at the Peninsula level. Three out of four components (i.e. agriculture allocation, cooling water consumption and flow into the sea) were taken with a negative sign, since they all represent water allocations to different 'users' (i.e. sinks) in the model. The water balance coming from the optimization of the model over the control period (1961-1990) and the literature reference values are summarized in Table 10-1.

Table 10-1: Water balance [Hm^3/yr] computed for the control period (1961-1990) and compared with AQUASTAT website (FAO, 2016) and Rio Carrillo et al. (2009)'s research outputs. All the values refer to a yearly average.

Model Water Balance [Hm^3/yr]	Control Period (1961-1990)	AQUASTAT[a]
Inflow	176 708	188 900
Agriculture Allocation	19 172	16 076
Cooling Water Consumption	175	340[b]
Flow at the Outlet Point	157 361	172 484*
Balance	0	0

*Value calculated by setting the overall water balance to zero.

[a]Three out of four components of the water balance were derived from AQUASTAT website (FAO, 2016). Their values are the result of summing both Spain and Portugal data.

[b]The reference cooling water consumption volume used to compare and validate the model implemented was derived from Rio Carrillo et al. (2009). It refers to the observed one in Spain only in 2005.

Some observations can be made:

a. The amount of inflow recorded is higher in AQUASTAT than in the implemented model. The most likely explanation is that this study covers 70% of the entire IP extension, thus some areas (coastal areas in particular) are not contributing to the overall inflow modelled.
b. The reason behind the two different agriculture allocation values lies in the distinct data sources employed to compute irrigation water demand.
c. Cooling water consumption volume is higher in Rio Carrillo et al. (2009)'s study, since they use the total amount of water consumed by the different thermal power plants. 'Total' means that they consider the quantity consumed for both cooling purposes and maintenance processes (e.g. cleaning) of a thermal generator. Instead, the model implemented takes into account the water consumption for cooling purposes only. Moreover, the literature value was recorded for 2005 only, therefore it cannot be used as a very representative number for yearly averages.
d. The flow at the outlet point is lower in this thesis project since the AQUASTAT one was computed by setting the overall water balance to zero (i.e. it was not observed).

Share of Electricity Production

The total electricity production was averaged at a yearly temporal scale and divided by generation source type (i.e. hydropower, nuclear and other thermal). 'Other thermal' consists of coal, CCGT and residual thermal generation, which is not represented by individual power plants directly implemented in the model. Figure 10-1 displays the comparison between the observed share of electricity production (OMIE, 2016) and the one calculated by the optimization of the model over the control period (1961-1990).

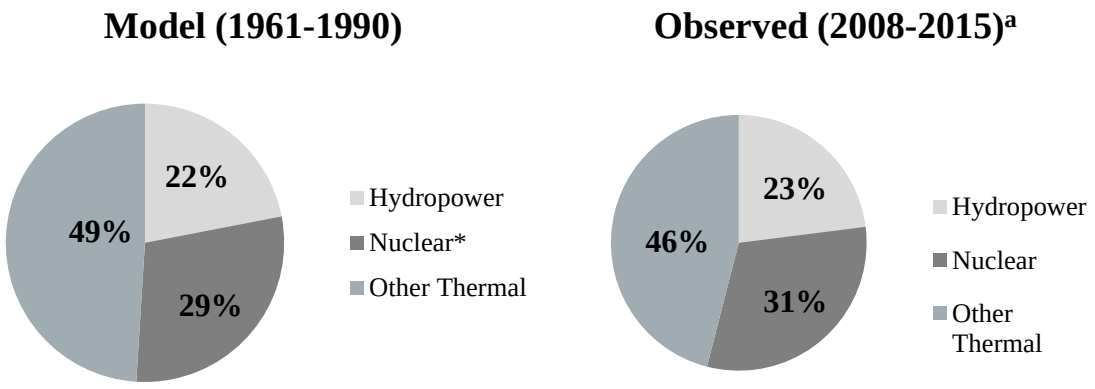

*The nuclear production share obtained as an output of the implemented model was updated by adding the yearly average production of the nuclear power plant along the sea that was not directly modelled (i.e. Trillo) (OMIE, 2016).

[a]The average share of the power production of the different technologies was computed using OMIE (2016) recorded power production values.

Figure 10-1: On the left, the share of the yearly average modelled electricity production is represented. On the right, the share of the observed one is illustrated (OMIE, 2016). Both productions have been divided by generation source type (i.e. hydropower, nuclear and other thermal).

As can be noticed, the model presents a slightly higher coal and CCGT energy production (49% against the observed 46%), whereas the hydropower and nuclear are lower (22% and 29% compared to the recorded 23% and 31% respectively). These slight differences might be due to the different time periods that are compared: even if the power system is the current one in both cases, the hydrological conditions might vary. For instance, the model has been optimized over the period 1961-1990, employing its corresponding hydrological system, whereas the observed production values refer to the years 2008-2015, characterized by likely dissimilar hydrological data.
However, the share of energy production per generation type varies through the years, thus the model output can be considered as a rather good fit to the observed values.

Thermal Power Plants' Water Withdrawal

The yearly mean water withdrawal volumes that were simulated can be compared with the observed ones for the year 2003 (MMA, 2007), both at the river basin and single thermal power plant scale. These two comparisons are summarized in Table 10-2 and Table 10-3 respectively.

Table 10-2: Thermal power plants' water withdrawal volumes [Hm^3/yr] averaged at a yearly temporal scale and aggregated at the river basin level. The comparison is between the withdrawn amounts coming from the optimization of the model over the control period (1961-1990) and the MMA (2007) recorded data for 2003 only.

	Yearly Average Thermal Power Plants Water Withdrawals [Hm^3/yr]*	
River Basin	**Model (1961-1990)**	**Observed (2003)[a]**
Tajo	1 921	1 397
Ebro	565	3 340
Duero	41	33
Guadalquivir	292	0
Guadiana	0	5
Jucar	42	35
MinoSil	48	97
TOTAL	2 910 (3 510[b])	4 907

*The total water withdrawal volume was computed by summing the amount of cooling water both consumed and discharged back into the river by the thermal power plants.

[a]The reference water withdrawal volumes were derived from MMA (2007), which employed observed values of Spanish thermal power production/water withdrawals in 2003 only.

[b]The value in parenthesis was computed by dividing the total water consumption volume by 5%, since thermal power plants consume on average 5% of the total water that they withdraw to produce energy (Rio Carrillo et al., 2009).

As can be noticed, there are quite some noticeable differences between the model outputs and the observed data, both in some river basins (e.g. Ebro) and at the Peninsula level. Several likely reasons can be addressed:

i. MMA (2007) recorded withdrawal volumes for the year 2003 and Spain only, thus they cannot be considered representative enough for yearly average values at the IP scale;
ii. The modelled water withdrawal volumes were computed assuming a temperature increase DT=10 °C in cooling water. This parameter is supposed to vary between 5 and 15 °C, leading to corresponding water withdrawals of 6200 and 2100 Hm^3/yr respectively. It can be noticed that the theoretical withdrawn volume is therefore highly dependent on the arbitrary choice of the DT value. Nevertheless, this decision does not affect the system implemented, since the modelled river thermal capacity is the only limiting factor for the amount of waste heat a thermal generator can discharge into the natural source;

iii. Rio Carrillo et al. (2009) state that Spanish thermal power plants consume on average 5% of the total water that they withdraw to produce energy. Thus, the total consumed volume (175 Hm^3/yr, refer to Table 10-6) can be divided by 5% in order to obtain the total water withdrawn by the thermal generators (3510 Hm^3/yr). This value gets a little bit closer to the MMA (2007) observed one, but it is still lower. For instance, Rio Carrillo et al. (2009)'s 5% takes into account the water volume consumed for both cooling and maintenance processes of the thermal power plant. Thus, a lower water consumption percentage should be employed if only cooling was considered, leading to a higher total water withdrawal.
This technique cannot be applied at the river basin scale; otherwise, the different cooling technologies of the thermal generators in each basin would not weight differently in the calculation of the water withdrawn volume.

At the basin level, observed and simulated withdrawals of individual thermal power plants explain the differences highlighted in Table 10-2. They are summarized in Table 10-3 for four thermal generators.

Table 10-3: Individual thermal power plants' water withdrawal volumes [Hm^3/yr] averaged at a yearly temporal scale. The comparison is between the withdrawn amounts coming from the optimization of the model over the control period (1961-1990) and the MMA (2007) recorded data for 2003 only.

	Yearly Average Thermal Power Plants Water Withdrawals [Hm^3/yr]	
Thermal Power Plant	**Model (1961-1990)**	**Observed (2003)[a]**
Aceca	6	554
Almaraz	1 844	583
Asco	76	2 270
Santa Maria de Garona	207	766

[a]The reference water withdrawal volumes were derived from MMA (2007), which employed observed values of Spanish thermal power production/water withdrawals in 2003 only.

The main findings are that the Almaraz power plant in the Tajo and the Asco power plant in the Ebro have much higher and much lower withdrawal volumes than the observed ones respectively. This leads to a higher modelled withdrawal in the Tajo and a lower one in the Ebro (refer to Table 10-2).

On the other hand, some explanations for the differences between the observed and simulated withdrawals in Table 10-3 are: (i) the non-representativeness of MMA data; (ii) different cooling technologies considered. For example, Aceca and Asco power plants have been modelled with a cooling tower (Global Energy Observatory, 2016), while MMA lists them as once-through. This is why MMA observations are much higher; (iii) the

average thermal efficiencies, marginal costs and water consumption factors may not be representative at the individual thermal power plant level.

Relative Hydropower Storage

Pereira-Cardenal et al. (2013)'s relative storage and the modelled one can be compared. One relative storage curve per river basin was obtained by aggregating all the hydropower reservoirs in a certain basin into an equivalent one.

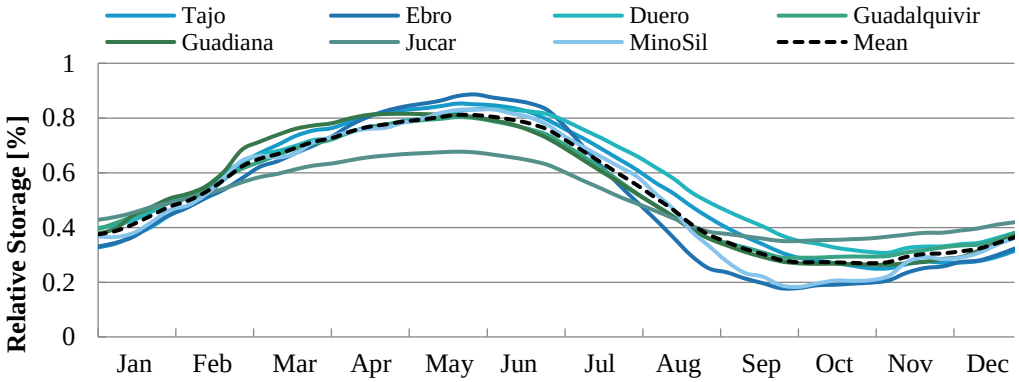

Figure 10-2: Modelled relative storage curves, averaged at a yearly time scale. Each river basin is represented by a different color and has its own curve. The dashed black line represents the mean relative storage, computed by averaging the weekly relative storages of all the seven basins. The mean weekly relative storage (%) was computed as follows: $(S_t - \underline{SCap})/(\overline{SCap} - \underline{SCap})$, where $\overline{SCap}$ and $\underline{SCap}$ are the maximum and minimum storage capacity respectively.

In both Figure 10-3 and Figure 10-2, the different basins show similar relative storage policy patterns: they all store more water in the hydropower reservoirs before the irrigation season starts (i.e. summer), in order to release it from June on when it is most needed.

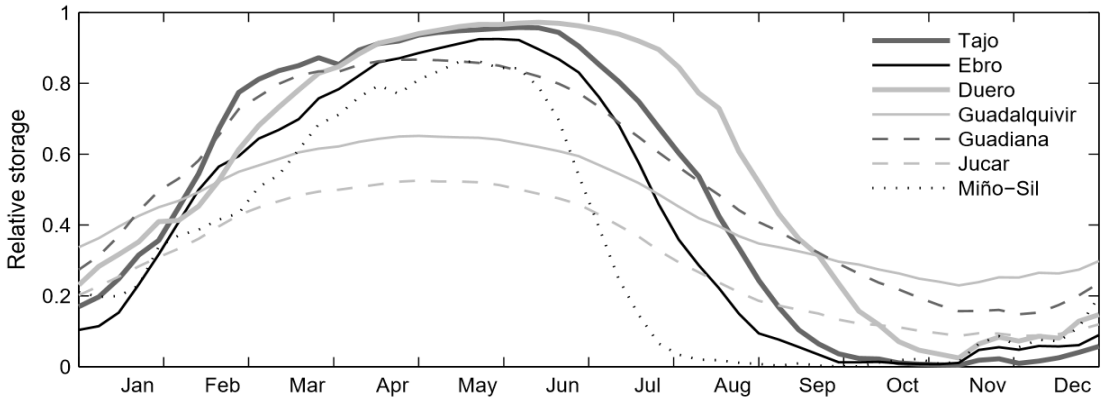

Figure 10-3: Pereira-Cardenal et al. (2013)'s relative storage curves, averaged at a yearly time scale. Each river basin is represented by a different color and has its own curve. The mean weekly relative storage (%) was computed as follows: $(E_t - \underline{E})/(\overline{E} - \underline{E})$, where $\overline{E}$ and $\underline{E}$ are the maximum and minimum energy storage capacity respectively. For instance, they considered hydropower storages as energy storages.

Comparing the modelled and the reference relative storage curves, the basins storing more water before summer (i.e. with a higher storage peak) are the Tajo and the Ebro in both cases. They also belong to the ones with the largest number of power plants.
On the other hand, two of Pereira-Cardenal et al. (2013)'s curves (i.e. Guadalquivir and Jucar) reach a lower peak than the corresponding modelled ones. A likely explanation might lie in the percentage of regulated and unregulated flow that they consider in their study. For example, the Guadalquivir presents at least 90% of unregulated flows for each one of its three sub-catchments. Thus, the water available to be stored in the hydropower reservoirs is less than 10% of the runoff in each catchment. Instead, this thesis project assumes that the only unregulated flow is the fraction flowing into the most downstream watershed (delineated by the sea fictitious reservoir) in each basin. In the Guadalquivir, the modelled unregulated fraction is 3% of total runoff in the basin. Therefore, most of the inflow entirely flows into each reservoir, leading to a higher modelled reservoir storage.

However, the main reason why the simulated and reference storage curves do not match perfectly lies in the procedure employed to model the entire system. For instance, Pereira-Cardenal et al. (2013) considered energy equivalent relative storages, whereas this thesis project used water storages. Thus, upstream storage was characterized by a larger weight than the downstream one in the reference study, which might explain some of the differences.

10.2 Control Period Optimal Policy

The optimization of the model implemented over the control period (1961-1990) results in an optimal policy, which consists of minimum costs achievable and optimal decision variables values at each weekly time step.
Several decision variables, together with their corresponding costs, have been analyzed and correlated. The optimal decisions are always presented as weekly values averaged across the 30 reference years, whereas the optimal costs as a yearly mean. Furthermore, temporal and spatial variations of the most relevant shadow prices have been investigated.

Costs and Decisions
The global costs and the ones associated with two groups of decision variables (i.e. agriculture deficit and thermal power production) are summarized in Table 10-4, both at the river basin and the IP scale.

Table 10-4: Total costs and costs divided per decision variable group [M€/yr]. All the costs are optimal and refer to a yearly average value.

	Costs [M€/yr]			
River Basin	**Total Costs**	**Agriculture Curtailment Cost**	**Thermal Power Production Cost**	**Residual Power Production Cost**
Tajo	1 319	0	1 319	-
Ebro	1 889	46	1 843	-
Duero	123	1	122	-
Guadalquivir	766	445	320	-
Guadiana	141	141	0	-
Jucar	267	94	173	-
MinoSil	74	0	74	-
TOTAL	7 157	726.5	3852	2 579

As can be noticed, the Tajo and Ebro river basins present the highest total costs in the IP, mainly because of a high thermal power production cost. For instance, these are the two basins producing more thermal power at an average yearly scale (41 536 and 45 862 GWh/yr respectively), since the largest number of thermal power plants is located here.

This can also be observed in Figure 10-4, where the thermal generators in the Tajo and Ebro present the highest yearly average production in the IP.

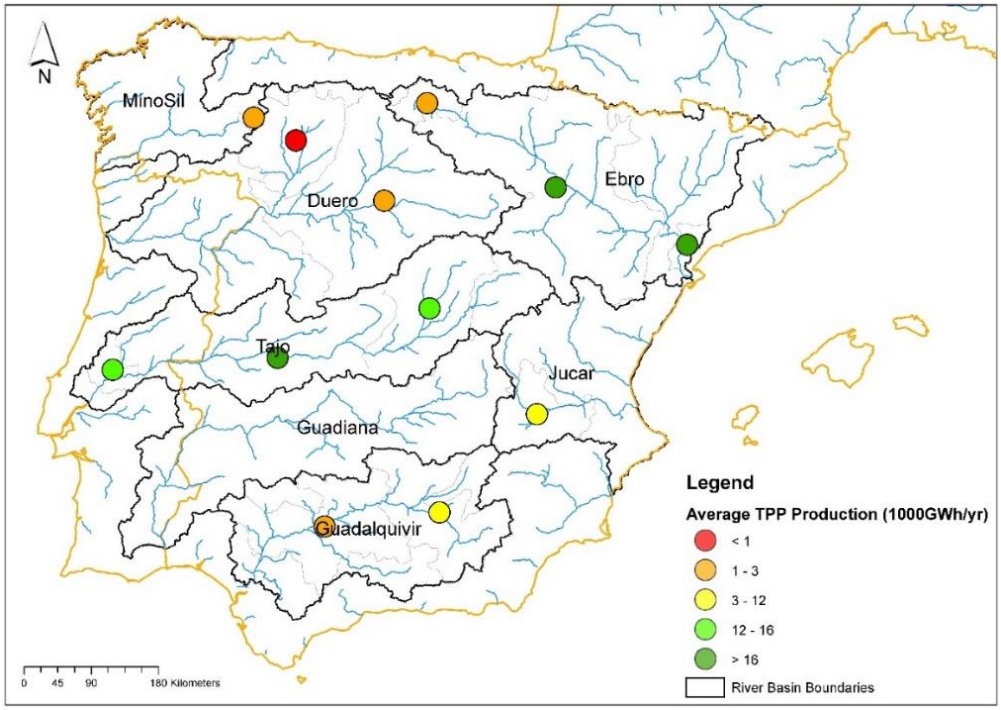

Figure 10-4: Yearly average thermal power production of individual thermal power plants (1000GWh/yr). Each dot represents a different thermal generator. Power plants in the same watershed have been aggregated into one single circle.

A temporal variation of power production at the Peninsula level was also analyzed. Its pattern, together with the power demand curve, can be observed in Figure 10-5.

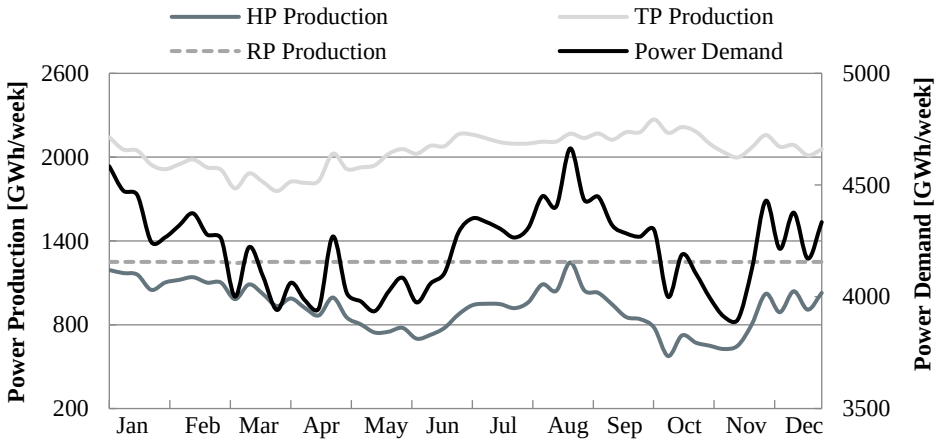

Figure 10-5: Weekly power production and power demand averaged across the 30 years and aggregated at the Peninsula level (GWh/week). Power production has been divided into hydropower (HP), thermal (TP) and residual power (RP) production. **Carefully note** that there is a primary and a secondary axis on the graph, with two different scales.

As can be noticed, hydropower and thermal power productions follow the trend of power demand week by week. In particular, hydropower production can be related to the total hydropower storage curve, displayed in Figure 10-6.

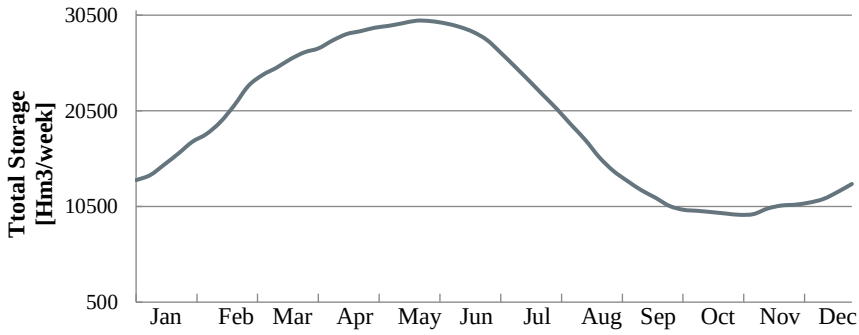

Figure 10-6: Total volume of water stored each week (Hm^3/week) in the hydropower reservoirs aggregated at the Peninsula level.

Hydropower production increases as soon as the reservoirs start releasing water (i.e. end of June). However, the peak in the production in December cannot be related to the storage curve but to the high inflows recorded during winter (refer to Figure 10-8).

Residual power represents the only exception, since it is always constant across the weeks of the average year. This is due to the residual power supply curve that was modelled. The model finds it optimal to produce electricity by following the supply curve up to the fifth step (53.17 €/MWh, see Appendix C.2). Afterwards, it fills the gap between power demand and production by generating the remaining power with coal and CCGT power

plants directly implemented. For instance, their marginal cost is fixed (57 €/MWh) and is lower than the sixth step one in the supply curve (58.10 €/MWh). This can also be deduced by looking at the shadow price of the power demand equality constraint, which stays constant throughout an average year and equal to 57 €/MWh.

In Table 10-4, it can also be noticed that agriculture curtailment cost: (a) represents 10% of the yearly average total costs; (b) is higher in the Guadalquivir, Guadiana and Jucar river basins (refer to Figure 10-22). The corresponding agriculture deficit is summarized in Table 10-5 (yearly average) and displayed in Figure 10-7 (weekly values), together with the weekly irrigation water demand.

Table 10-5: Percentage of yearly average agriculture deficit, both per river basin and aggregated at the Peninsula level.

River Basin	Agriculture Deficit
Tajo	0%
Ebro	4.1%
Duero	0.15%
Guadalquivir	28.1%
Guadiana	11.6%
Jucar	17.9%
MinoSil	0.05%
TOTAL	12.6%

As expected, the agriculture deficit is higher in the Guadalquivir, Guadiana and Jucar river basins. Moreover, irrigation water demand and agriculture deficit present the same pattern, which is opposite to the inflow trend shown in Figure 10-8.

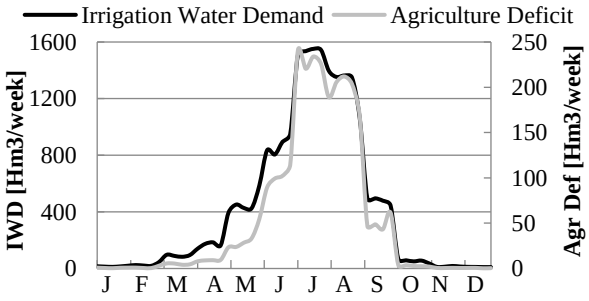

Figure 10-7: Weekly irrigation water demand and agriculture deficit (Hm^3/week) averaged across the 30 years and aggregated at the IP scale.

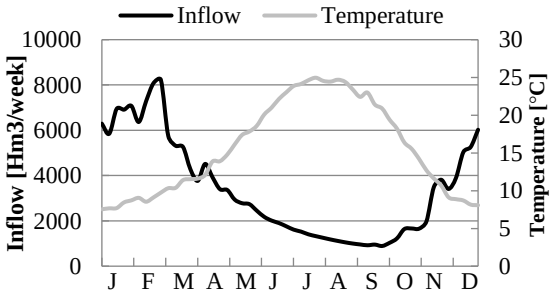

Figure 10-8: Weekly inflow (Hm^3/week) and river water temperature (°C) averaged across the 30 years and aggregated at the IP scale.

Irrigation water demand has a peak in summer, when the inflow reaches its minimum values. Thus, agriculture deficit (and therefore agriculture curtailment cost) increases during this time slot. Less inflow during the summer months means less water available

in the rivers. As a consequence, thermal power plants are forced to withdraw less and consume more water from the river (Figure 10-9) because of: (i) less water availability; (ii) higher river temperatures. These two factors directly influence the strictness of thermal cooling constraints. For instance, they are more likely to be binding if less water is available in the river and its water temperature exceeds 25°C (e.g. some weeks in July and August, refer to Figure 10-8).

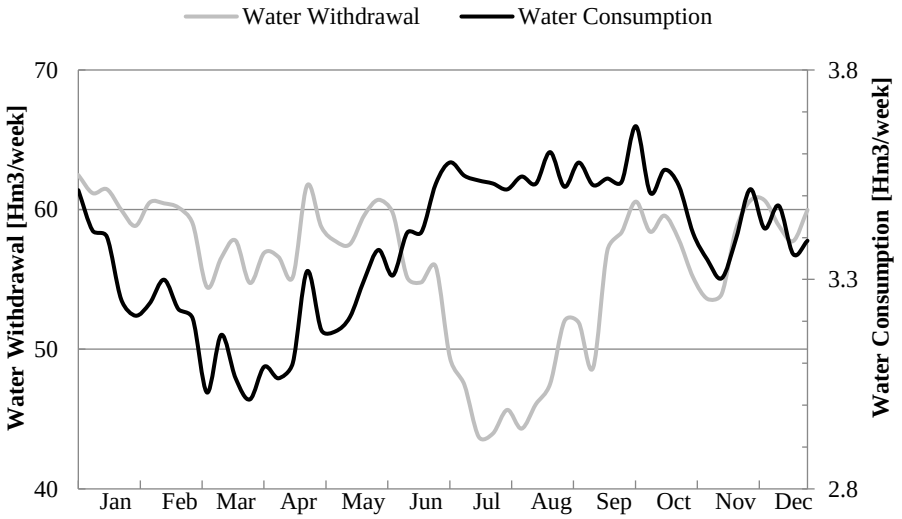

Figure 10-9: Weekly water withdrawal and consumption volumes (Hm^3/week) averaged across the 30 years and aggregated at the IP scale.

Especially during the months characterized by these adverse hydrological conditions, thermal cooling and agriculture can be considered as competing users. Their trade-off can be assessed by analyzing the shadow prices, as performed in the following section.

Shadow Prices and Trade-Off

Firstly, the spatial variation of the water availability shadow price was examined in order to assess the trade-offs among the different users located in the 123 watersheds of the IP. The shadow price was averaged at a yearly time scale and represented graphically in Figure 10-10.

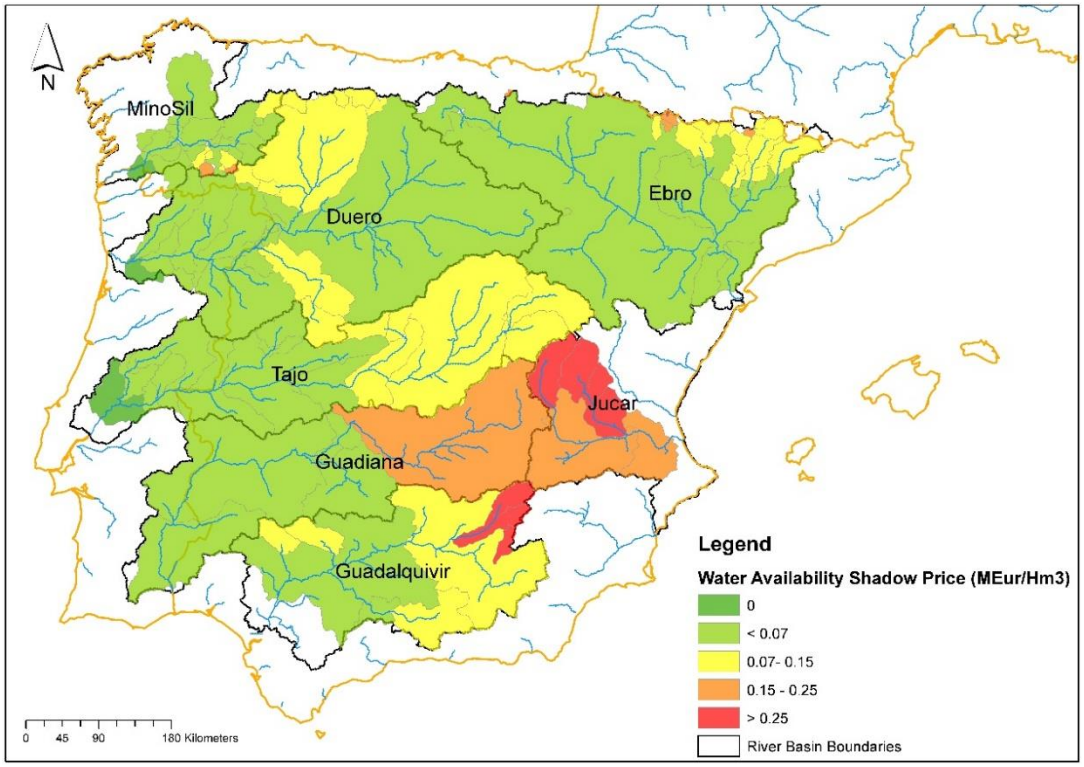

Figure 10-10: Spatial variation of water availability shadow price (M€/Hm^3), averaged at a yearly scale.

Each watershed has a water availability shadow price associated to it. Its value can be compared with the agriculture marginal cost of the river basin the watershed belongs to. As a result, it can be noticed that only the red watersheds present a shadow price that is higher than the agriculture marginal cost of the corresponding Guadalquivir and Jucar basins (0.25 and 0.36 M€/Hm^3 respectively). This means that in these watersheds irrigation is curtailed in favor of the downstream users at a yearly average scale. In all the other watersheds, agriculture can be sometimes curtailed during certain weeks of the average year.

Moreover, agriculture drives the total shadow price in the downstream watershed where all the users (i.e. agriculture, thermal and hydropower) are located simultaneously. This can be observed in Figure 10-11.

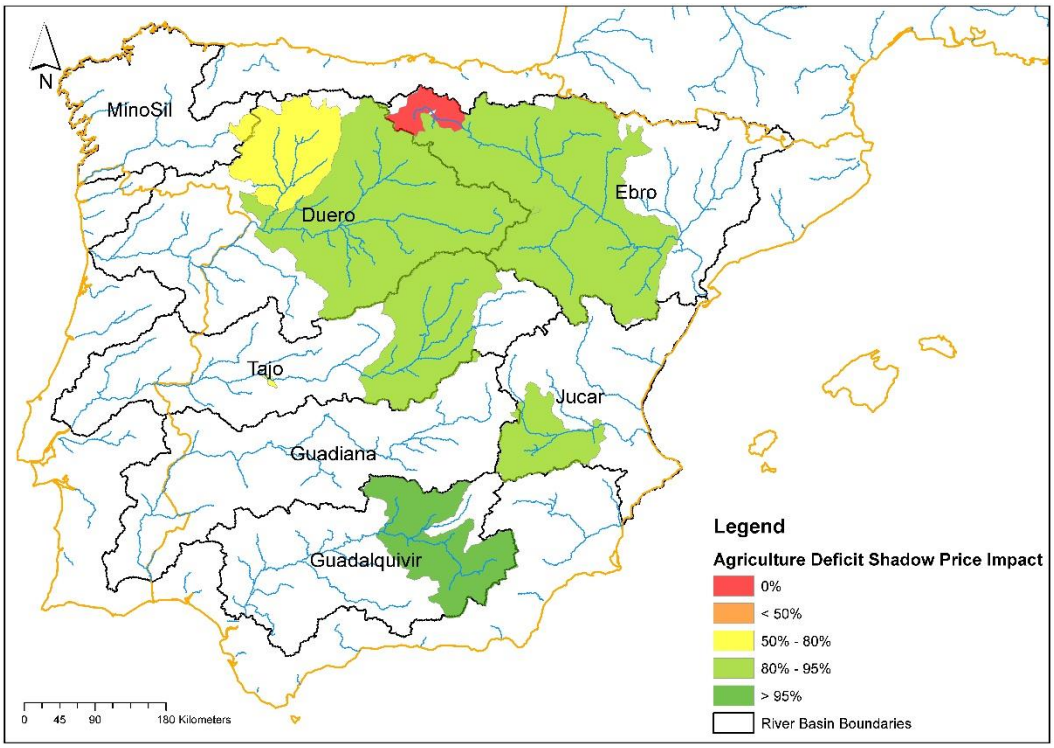

Figure 10-11: Percentage contribution of the agriculture deficit shadow price to the total water availability one in each watershed. The watersheds considered are the ones where all the users (i.e. agriculture, thermal and hydropower) are located simultaneously. The agriculture deficit shadow price was calculated in the watersheds upstream of the highlighted ones.

The percentage displayed shows the contribution of the agriculture deficit shadow price to the total water availability one per watershed. The former shadow price was computed in the watersheds upstream of the highlighted ones. For instance, if the upstream irrigation is served, water will not be available for the downstream users anymore. As can be noticed, agriculture is responsible for about 85% of the total shadow price in each downstream watershed, where it is thus prioritized compared to thermal and hydropower users.

A temporal variation of the water availability shadow price was also investigated, as shown in Figure 10-12.

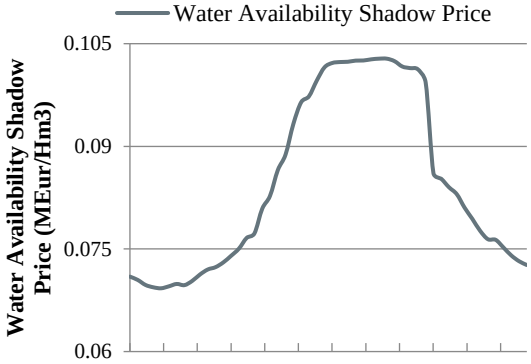

Figure 10-12: Temporal variation of weekly water availability shadow price [M€/Hm^3] averaged across the 30 years. It has been aggregated at the Peninsula level.

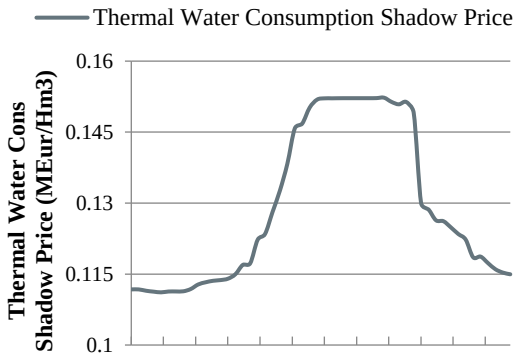

Figure 10-13: Temporal variation of weekly cooling water consumption shadow price [M€/Hm^3] averaged across the 30 years. It has been aggregated at the Peninsula level.

The water availability shadow price presents the same pattern of the cooling water consumption one. For instance, the former increases in summer, since there are both a higher water demand and less inflow, thus less water available in the rivers. As a consequence, the latter peaks in the same period, as displayed in Figure 10-13.

At last, the temporal variation of the thermal cooling constraint shadow price is represented, both in [M€/Hm^3] and [M€/°C] (Figure 10-14). The latter was computed by deriving the volume of non-consumptive cooling water needed by a thermal plant (i.e. $H_w * (1-\beta)/(\rho * c_P * dT)$) with respect to dT (i.e. temperature increase in the river), then multiplying it by the cooling constraint shadow price in [M€/Hm^3].

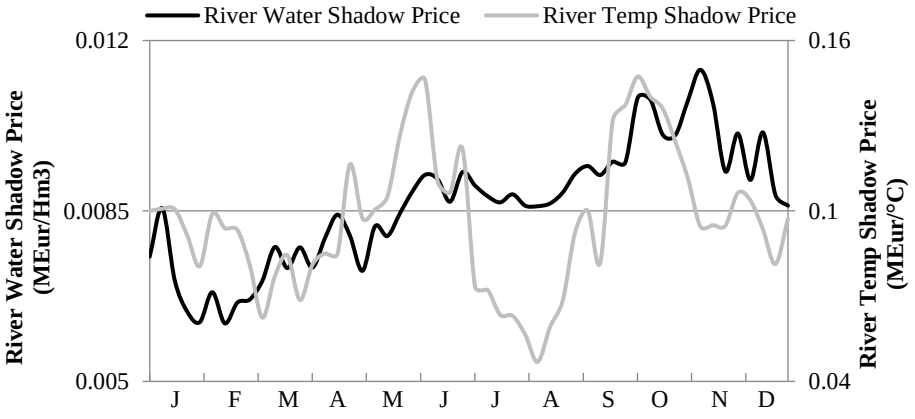

Figure 10-14: Temporal variation of weekly river water [M€/Hm^3] and river temperature [M€/°C] shadow prices. They have been averaged across the 30 years and aggregated at the Peninsula level.

The river water shadow price follows an increasing trend throughout the average year, except for the summer months when it stays quite constant. This flattening is due to the balancing between: (a) power demand increase (Figure 10-5) and water availability decrease (Figure 10-8) on one side, which are both expected to determine the shadow price rise; (b) river temperature increase (Figure 10-8) on the other, which is supposed to drive the shadow price reduction. For instance, when the water temperature approaches the legal upper bound of 28°C, thermal generators cannot discharge any more waste heat into the natural source (they are not allowed to produce electricity anymore). Since the power plants do not gain any more added benefit by having 1 Hm^3 more available in the river, the cooling constraint shadow price decreases. As for the river temperature shadow price, it presents a minimum peak during the summer months. As already observed in Figure 10-9, thermal power plants consume more water in this time frame, which means that the production shifts to the ones with a cooling tower. These generators can generally produce regardless of the river temperature (as long as it is less than 28°C), thus their shadow price is very low.

10.3 Thermal Cooling Constraints Impacts

The impacts of thermal cooling constraints on the water-energy system of the IP were assessed by comparing some relevant outputs of the model, implemented both with and without these constraints.

Firstly, relevant costs and decisions of the two optimal policies can be analyzed. They are presented in Table 10-6.

Table 10-6: Comparison between the main outputs of the model implemented with and without cooling constraints. The values of the costs and decision variables are optimal, have been averaged at a yearly time scale and aggregated at the Peninsula level. They are all outputs of the model optimization over the control period 1961-1990. The column 'Cooling Constraints Impacts' shows the percentage increase/decrease in several model outcomes when the cooling constraints are active.

		Active Cooling Constraints	No Cooling Constraints	Cooling Constraints Impacts
Costs [M€/yr]	Total Costs	7 157	6 969	+3%
	Agriculture Curtailment Costs	726.5	718.5	+1%
	Thermal Power Production Costs	3 852	3 672	+5%
	Residual Thermal Power Production Costs	2 579	2 579	0%
Power Production [1000GWh/yr]	Hydropower	48	48	0%
	Thermal Power	106	106	0%
	Residual Thermal Power	65	65	0%
Cooling Water [Hm^3/yr]	Consumptive Volume	175	175	0%
	Non-Consumptive Volume	2 735	3 324*	-18%

*This water volume is not taken into account in the model.

As can be noticed, the cooling constraints do not have a very significant impact on the model outcomes. The only noticeable differences are in the costs and in the volume of non-consumptive cooling water needed by the thermal power plants.

When the cooling constraints are active, the irrigation deficit is 2% higher (from 12.4% without to 12.6% with thermal cooling), thus the agriculture curtailment cost increases by 1%. Practically, irrigation is not curtailed more than in the case without any cooling constraints. This outcome was expected, since earlier it has been assessed that at a yearly average temporal scale agriculture is usually prioritized. Therefore, it should not be affected by thermal cooling constraints.

As for total costs, they experience a 3% increase in the case with active cooling constraints, which is mainly due to higher thermal power production costs (5% more). For instance, the only thermal generators that are significantly affected by cooling constraints are two nuclear ones (Almaraz and Santa Maria de Garona, whose marginal cost is 18

€/MWh), as can be deduced from Figure 10-15. They present the highest river water temperature shadow prices among all the power plants in the IP (1.11 and 0.33 M€/°C respectively, refer to the two red circles in Figure 10-15) and are constrained 59% and 91% of the weeks in the average year. This is also reflected by reality, since Santa Maria de Garona generator was shut down in 2012 because of cooling constraints reasons. It was also accused by NGOs to not respect the legal river water temperature increase (Pùblico, 2011).

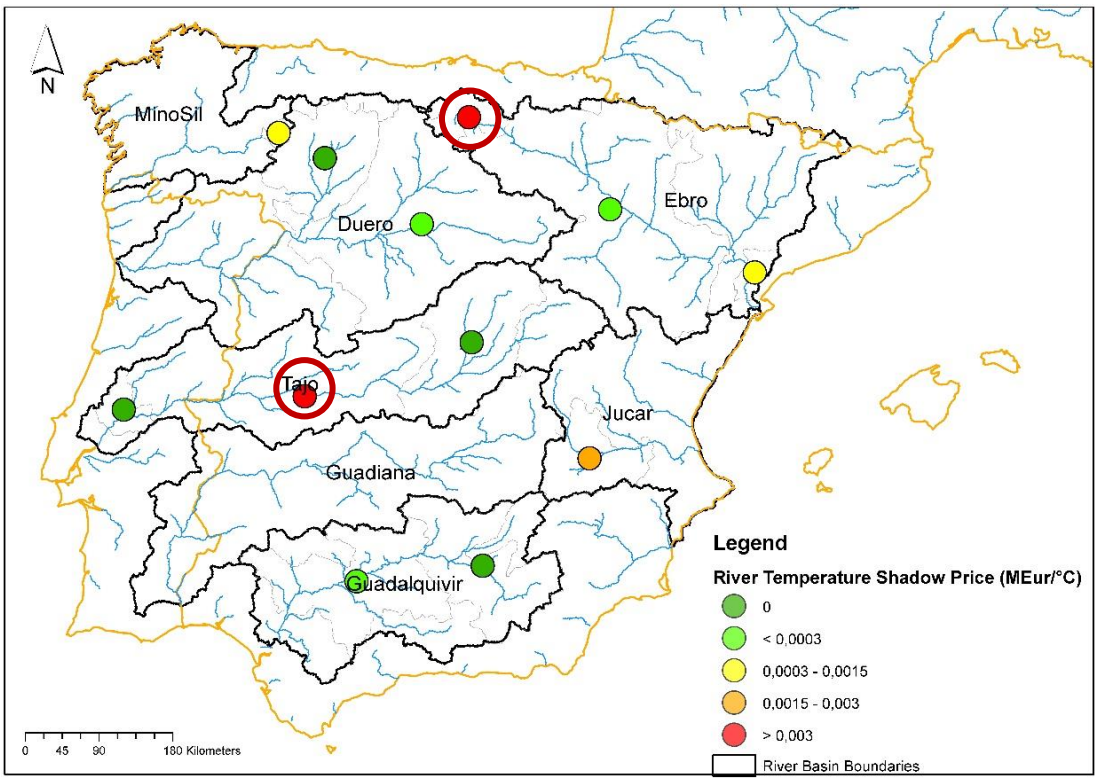

Figure 10-15: River water shadow price [M€/°C] of the modelled thermal power plants, averaged at a yearly scale. Cooling constraints are active.

Since their production is limited, power demand has to be met by producing electricity with alternative coal and CCGT power plants, which are more expensive (57 €/MWh). This is reflected by the thermal production rate (%), displayed in Figure 10-16 for active cooling constraints and Figure 10-17 for the opposite case. The red circles highlight the Almaraz and Santa Maria de Garona nuclear power plants in both maps.

When the cooling constraints are not active, these two generators produce at full capacity (100%, Figure 10-17), at the expenses of coal and CCGT plants (e.g. Pego and Puertollano, the two red dots in Figure 10-17) that generate less power. This leads to a substantial decrease in the total thermal production costs, since nuclear is the cheapest generation technology. Moreover, Almaraz and Santa Maria de Garona are both equipped with a once-through cooling technology, which is not limited by cooling constraints anymore. Thus, they need much more non-consumptive than consumptive water in order to produce more electricity. This is the reason why the no cooling constraints scenario presents a theoretically bigger non-consumptive water volume (18% more, Table 10-6) compared to the opposite case.

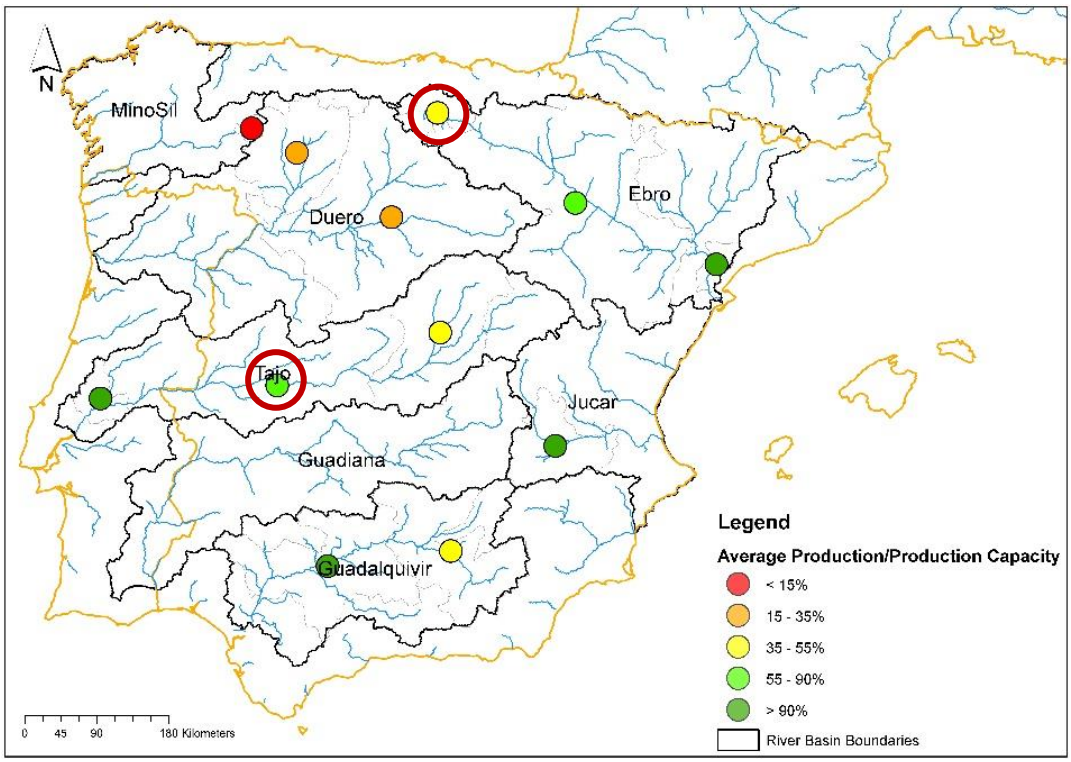

Figure 10-16: Production rate (%) of the modelled thermal power plants, averaged at a yearly scale. This percentage was computed as average production over production capacity of a single generator. Cooling constraints are active.

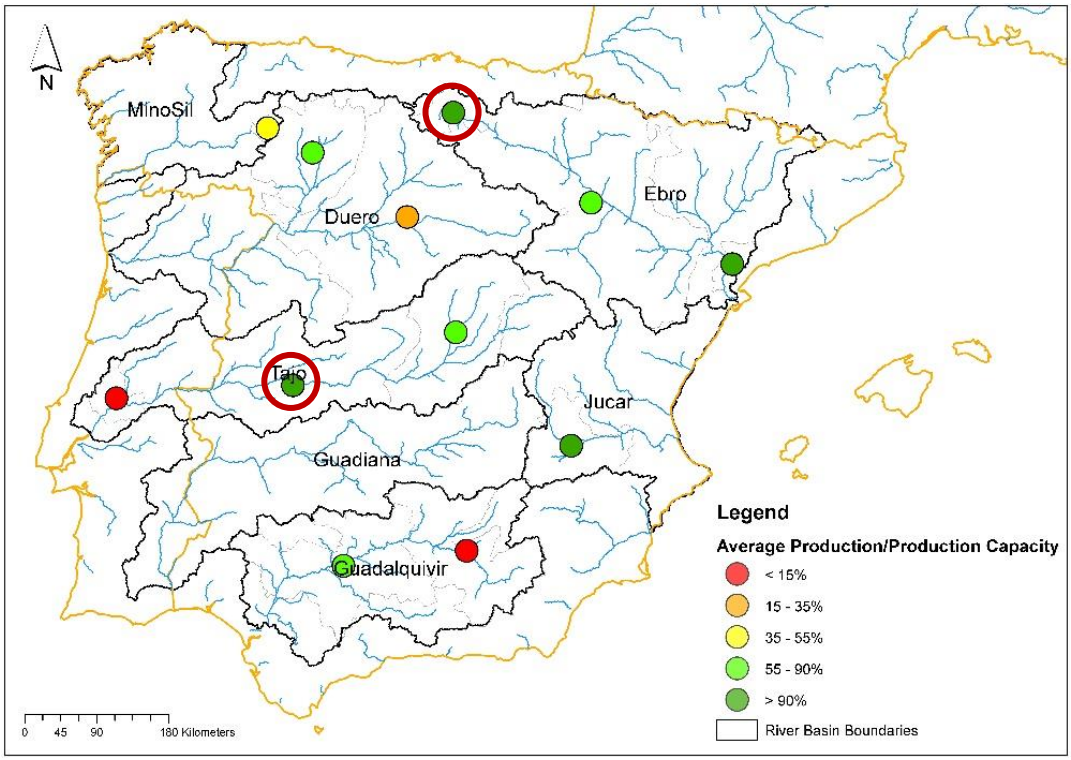

Figure 10-17: Production rate (%) of the modelled thermal power plants, averaged at a yearly scale. This percentage was computed as average production over production capacity of a single generator. Cooling constraints are not active.

The increased nuclear production in the no cooling constraints scenario is also reflected in the share of yearly average electricity generation among different source types (Figure 10-18).

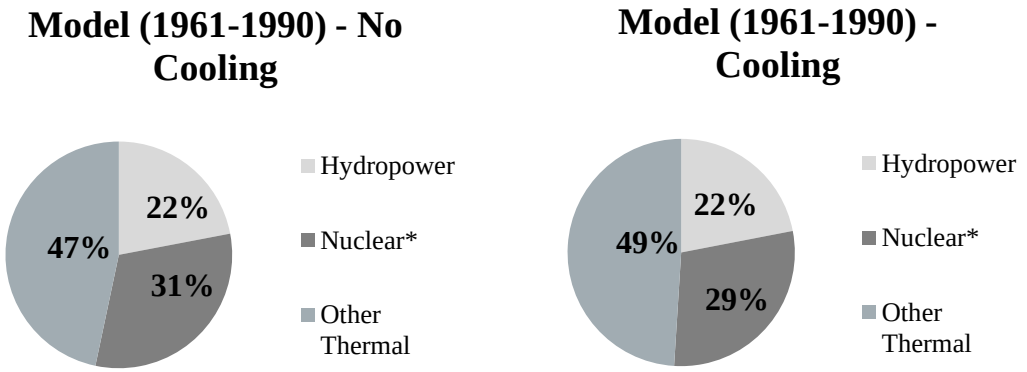

*The nuclear production share obtained as an output of the implemented model was updated by adding the yearly average production of the nuclear power plant along the sea that was not directly modelled (i.e. Trillo) (OMIE, 2016).

Figure 10-18: Both figures illustrate the share of the yearly average modelled electricity production among three generation source types (i.e. hydropower, nuclear and other thermal). On the left, the no cooling constraints scenario is represented. On the right, the opposite case.

As can be observed, hydropower production is always constant (22% of the total), thus it is not affected by thermal cooling constraints. Nevertheless, the difference between the two scenarios in relative hydropower storage of three relevant river basins can be analyzed. The corresponding curves are displayed and compared in Figure 10-19.

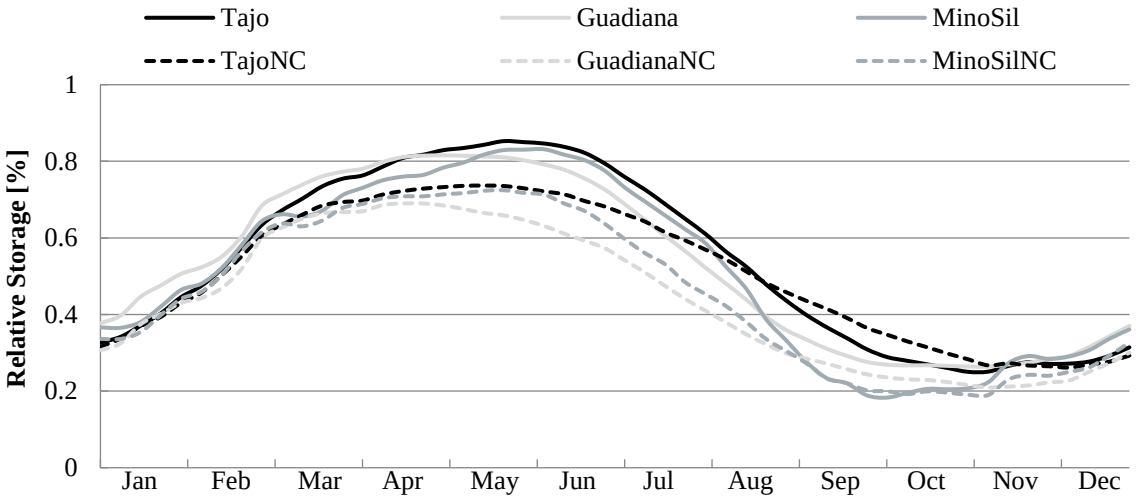

Figure 10-19: Modelled relative storage curves, averaged at a yearly time scale. Each river basin is represented by a different color and has its own curve. The dashed lines represent the no cooling constraints case, whereas the thick ones refer to the opposite case.

When the cooling constraints are not active, the relative reservoir storages are kept lower in all the three basins considered. As already discussed, within this scenario once-through thermal generators (i.e. Almaraz and Santa Maria de Garona) produce more, while the ones equipped with a cooling tower (i.e. Pego and Puertollano) generate less electricity. This means that less (more) consumptive (non-consumptive) water volumes are required, thus more water is left available in the river for other users. This holds particularly true in summer, when consumptive cooling water requirements were significantly higher due to active cooling constraints (Figure 10-9 and Figure 10-13). In conclusion, if cooling constraints are not active, there is no more need to store significant amounts of water in the reservoirs before June in order to fulfill high thermal consumptive demands in summer.

This is perfectly reflected in the difference between the two relative storage curves of the Tajo, since it is the river basin where Almaraz and Pego power plants are located. Its water availability increases, which can also be deduced from a decrease of the corresponding

shadow price within the non-active cooling constraints case, as can be observed in Figure 10-20 (compare to Figure 10-10).

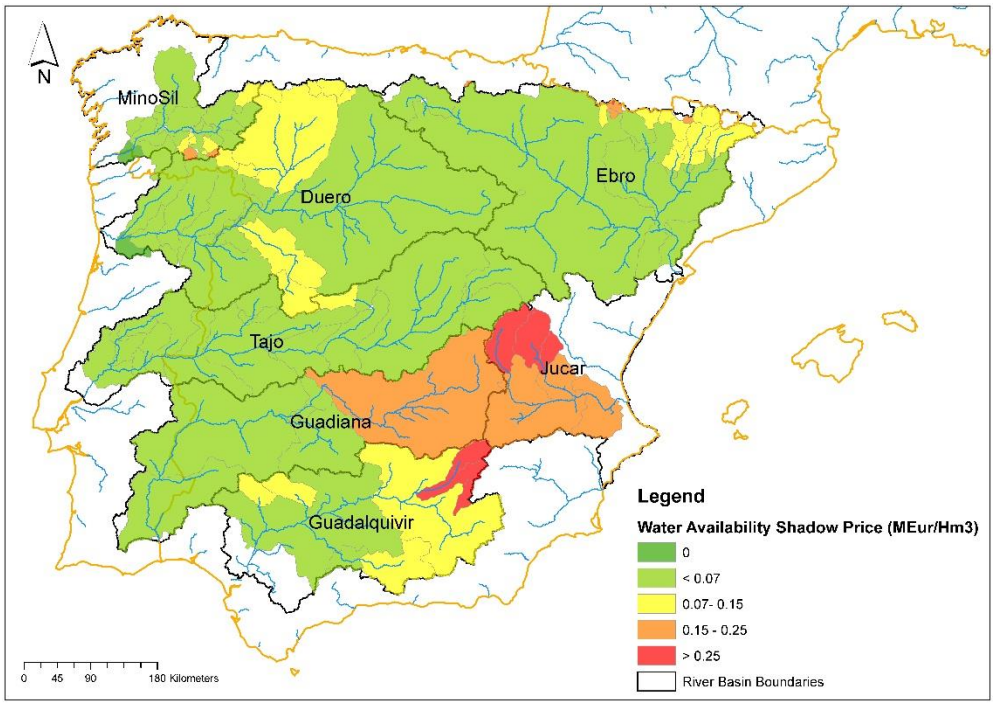

Figure 10-20: Spatial variation of water availability shadow price (M€/Hm^3), averaged at a yearly scale. No cooling constraints scenario.

Water availability increases also at the Peninsula scale, especially during summer. This can be deduced from a lower peak in the temporal variation curve of water availability shadow price, displayed in Figure 10-21 (compare to Figure 10-12).

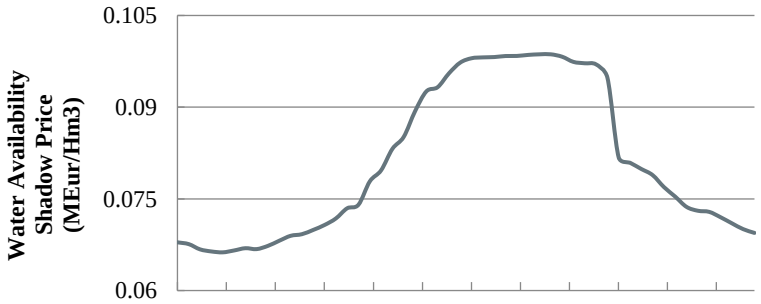

Figure 10-21: Temporal variation of weekly water availability shadow price [M€/Hm^3] averaged across the 30 years. It has been aggregated at the Peninsula level and refers to the non-active cooling constraints case.

10.4 Climate Change Impacts

The impacts of climate change on the water-energy system of the IP were assessed by comparing some relevant outputs of the model, optimized over both the control period and

climate change scenario. The climate change outputs that will be discussed in this section refer to the average climate model 3RCM. The minimum and maximum values obtained among the four CMs have been written in parenthesis next to the reference 3RCM main outcomes. It was observed that the results vary considerably depending on the scenario: usually, CLM presents the highest values (biggest impacts), while RACMO the lowest (smallest impacts). For instance, the CLM model is characterized by the most severe precipitation reductions and temperature increases, which drive the resulting highest agriculture curtailment, lowest hydropower and highest thermal power productions. The graphical results of all the other three CMs not presented here (i.e. CLM, RACMO, REMO) are summarized in Appendix D.1.

Despite the four RCMs present different results, the model outputs can still be considered robust under climate change. For instance, the sign and the order of magnitude of the change in the main elements of the system are constant among the scenarios.

Costs and Decisions

From a broad perspective, the consequences of climate change become more evident when the costs and decisions in the two optimal policies (control and climate change optimization) are compared, as in Table 10-7.

Table 10-7: Comparison between the main outputs of the model optimized over the control period and climate change scenario. The values of the costs and decision variables are optimal, have been averaged at a yearly time scale and aggregated at the Peninsula level. The column 'Climate Change Impacts' shows the percentage increase/decrease in several model outcomes when the model is optimized over the 2036-2065 time frame.

		Control Period (1961-1990)	Climate Change Scenario (2036-2065)	Climate Change Impacts	Lehner et al. (2005)[a]
Costs [M€/yr]	**Total Costs**	7 157	9 197 (8 762 – 9967)	+28% (+22% - +39%)	
	Agriculture Curtailment Costs	726.5	2 063 (1 778 – 2543)	+184% (+145% - +250%)	
	Thermal Power Production Costs	3 852	4 439 (4 334 – 4616)	+15% (+13% - +20%)	
	Residual Thermal Power Production Costs	2 579	2 695 (2 647 – 2808)	+5% (+3% - +9%)	
Power Production [1000GWh/yr]	**Hydropower**	48	38.5 (34.4 – 40.5)	**-20%** (-29% - 16%)	**-19%**
	Thermal Power	106	114 (112 – 116)	+7% (+6% - +9%)	
	Residual Thermal Power	65	67 (66 – 69)	+3% (+2% - +6%)	
Cooling Water [Hm^3/yr]	**Consumptive Volume**	175	194 (190 – 202)	+11% (+9% - +15%)	
	Non-Consumptive Volume	2 910	2 600 (2 493 – 2654)	-11% (-14% - -9%)	

[a]In their study, they refer to developed hydropower potential (i.e. mean supplied electricity proportional to the installed capacity of a power plant) by the 2020s, in both Spain and Portugal.

Climate change affects significantly most of the model outcomes. The most evident impact is on the total costs of the system, which increase by 28% when future climate is considered. The main factor driving this growth is the agriculture curtailment cost, which rises up to 184% its initial value of the control period optimal policy. The higher irrigation cost is due to a significant increase in the agriculture deficit under climate change, at both the river basin and the Peninsula scale. The yearly average percentage growth of the deficit is summarized in Table 10-8, whereas the spatial variation of agriculture curtailment is displayed in Figure 10-22 for control period and Figure 10-23 for climate change.

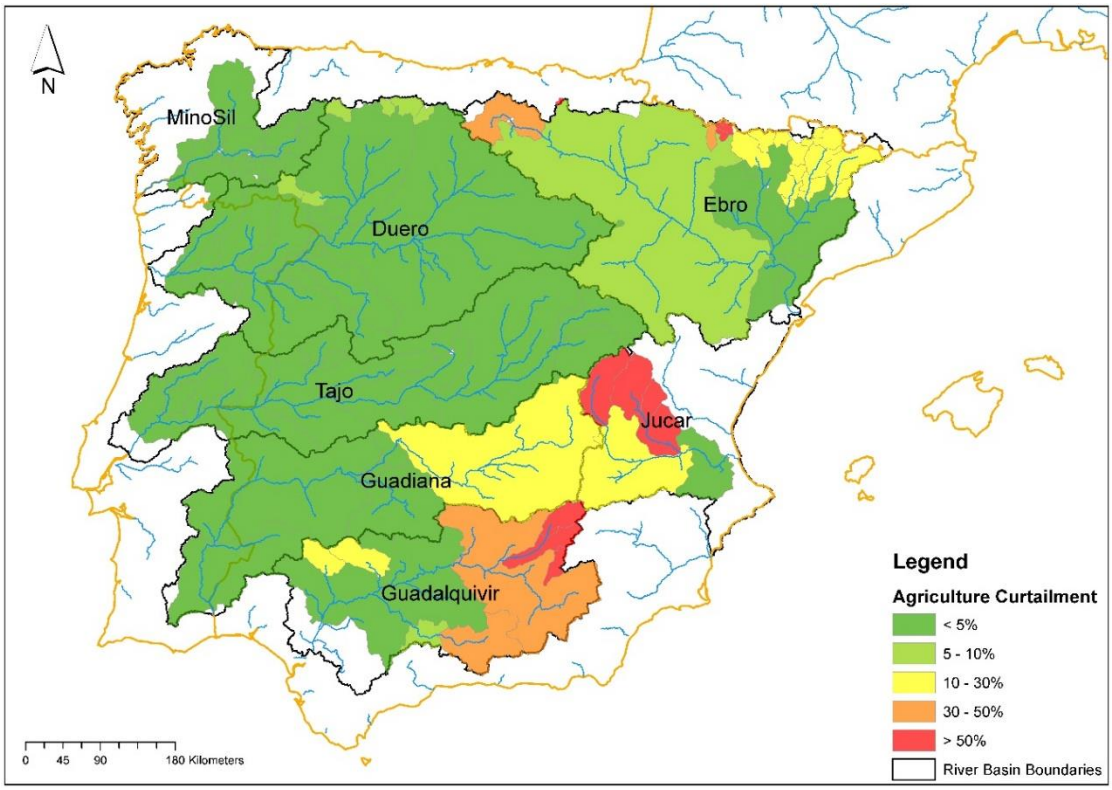

Figure 10-22: Agriculture curtailment (%) per watershed. It was computed as the ratio between agriculture deficit and demand, averaged at a yearly scale. This map refers to the control period optimization.

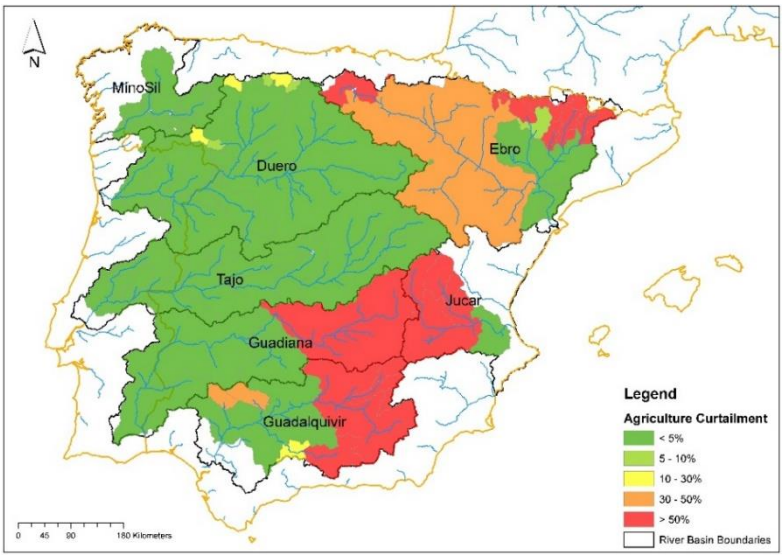

Figure 10-23: Agriculture curtailment (%) per watershed. This map refers to the climate change optimization.

Table 10-8: Agriculture deficit percentage increase under climate change, at both the river basin and the IP scale.

River Basin	Agriculture Deficit Increase
Tajo	0%
Ebro	+687%
Duero	+255%
Guadalquivir	+51%
Guadiana	+139%
Jucar	+166%
MinoSil	0%
TOTAL	**+132%**

As can be noticed, the situation worsens mainly in the basins that have already been curtailed in the control period (i.e. Guadalquivir, Guadiana and Jucar). Higher deficit is due to both lower inflows (thus less water available, especially in the southern basins) and more irrigation water demand during summer under climate change (see Chapter 8).

Climate change does not influence water availability and agricultural demand only, but also river water temperature and power demand, which both increase substantially, especially during the summer months (see Chapter 8). Less water flowing in the rivers and higher water temperatures force thermal power plants to withdraw even less (-11%) and consume even more water (+11%) than in the control period, as displayed in Figure 10-24 (compare to Figure 10-9). For instance, these two hydrological factors influence the strictness of thermal cooling constraints, which are likely to be more binding under climate change (refer to Figure 10-28).

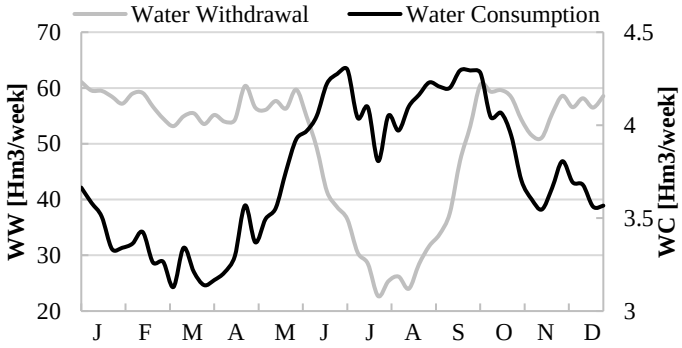

Figure 10-24: Weekly water withdrawal (WW) and consumption (WC) volumes (Hm^3/week) averaged across the 30 years and aggregated at the IP scale. They refer to the climate change scenario.

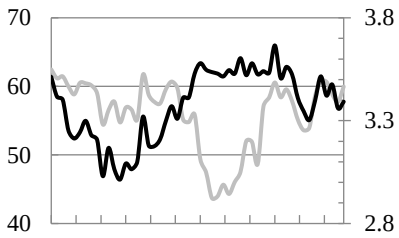

Figure 10-9: Weekly water withdrawal and consumption volumes (Hm^3/week) in control period.

Another difference with the control period curves can be assessed: during July, water consumption does not hold constant anymore but decreases. Since under climate change river water temperature reaches the maximum legal upper bound of 28°C, thermal power plants are forced by the sharp strictness of cooling constraints to not produce at all. Exception is not even made for the ones equipped with a cooling tower (i.e. the ones consuming water to produce electricity). This has a direct consequence on the weekly pattern of power production, divided per generation source type (Figure 10-25, compare to Figure 10-5).

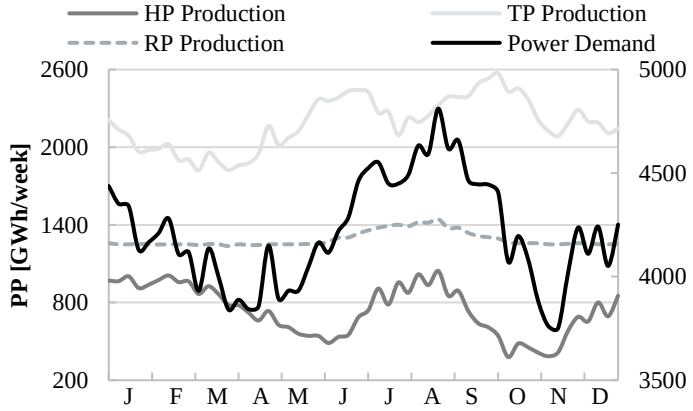

Figure 10-25: Weekly power production (PP) and power demand (PD) averaged across 30 years and aggregated at the Peninsula level (GWh/week). They refer to climate change scenario. Power production has been divided into hydropower (HP), thermal (TP) and residual power (RP) production. **Carefully note** that there is a primary and a secondary axis on the graph, with two different scales.

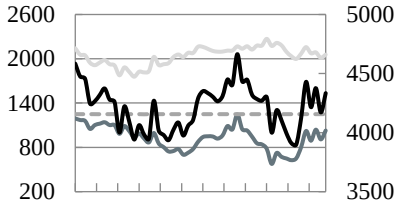

Figure 10-5: Weekly power production and power demand (GWh/week) in control period.

Even if the summer power demand still increases under climate change, thermal production decreases. In order to meet the demand, more residual thermal power is thus produced (3% more), i.e. it does not hold constant anymore throughout the average year, but it grows in July/August. This pattern is reflected by two factors: (i) the 5% increase in residual power production costs under climate change (Table 10-7); (ii) the shadow price

temporal variation of the power demand constraint, which still stays constant for most of the average year and equal to 57 €/MWh. Exception is made for the summer months when it rises up to 58.10 €/MWh (the price of the sixth generation segment in the residual supply curve). Thus, the model finds it optimal to produce electricity by following the supply curve up to the sixth step during July/August under climate change (it would always stop at the fifth segment in control period).

Overall, the share of total electricity production per generation source type is summarized in Figure 10-26 for future climate (compare to Figure 10-1). Thermal production (i.e. all the modelled thermal power plants) belongs to both 'Nuclear' and 'Other Thermal' categories, while residual thermal power to 'Other Thermal' only.

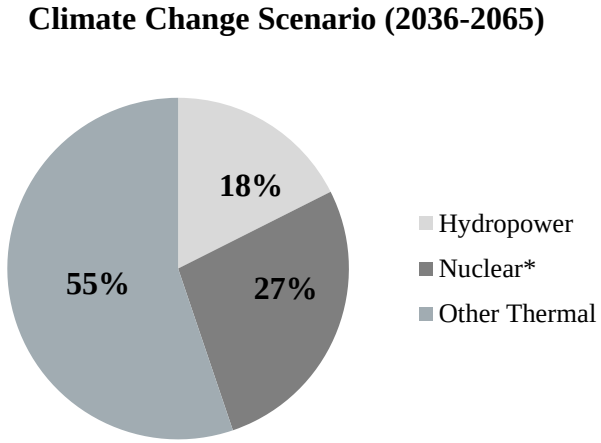

*The nuclear production share obtained as an output of the implemented model was updated by adding the yearly average production of the nuclear power plant along the sea that was not directly modelled (i.e. Trillo) (OMIE, 2016).

Figure 10-26: Share of the yearly average modelled electricity production under climate change. Productions have been divided by generation source type (i.e. hydropower, nuclear and other thermal).

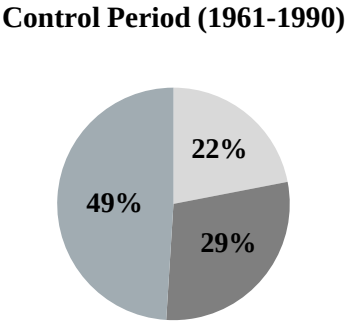

Figure 10-1: Share of the yearly average modelled electricity production in control period.

It can be noticed that under climate change: (a) hydropower production decreases by 20%; (b) nuclear production decreases by 7%; (c) generation from modelled coal and CCGT thermal power plants increases by 23%. In general, thermal and residual thermal generations increase by 7% and 3% respectively (Table 10-7). Thus, the entire thermal sector produces 6% more. Lehner et al. (2005) and Pereira-Cardenal et al. (2014) achieved similar results. The former demonstrated that hydropower is likely to produce 19% less by the 2020s in both Spain and Portugal. The latter calculated a 21% (15% - 32%) reduction in hydropower generation and a 6.7% increase in thermal power generation.

The spatial variation of thermal production can be mapped as thermal production rate (%) (Figure 10-27 for climate change, compare to Figure 10-16 for control period).

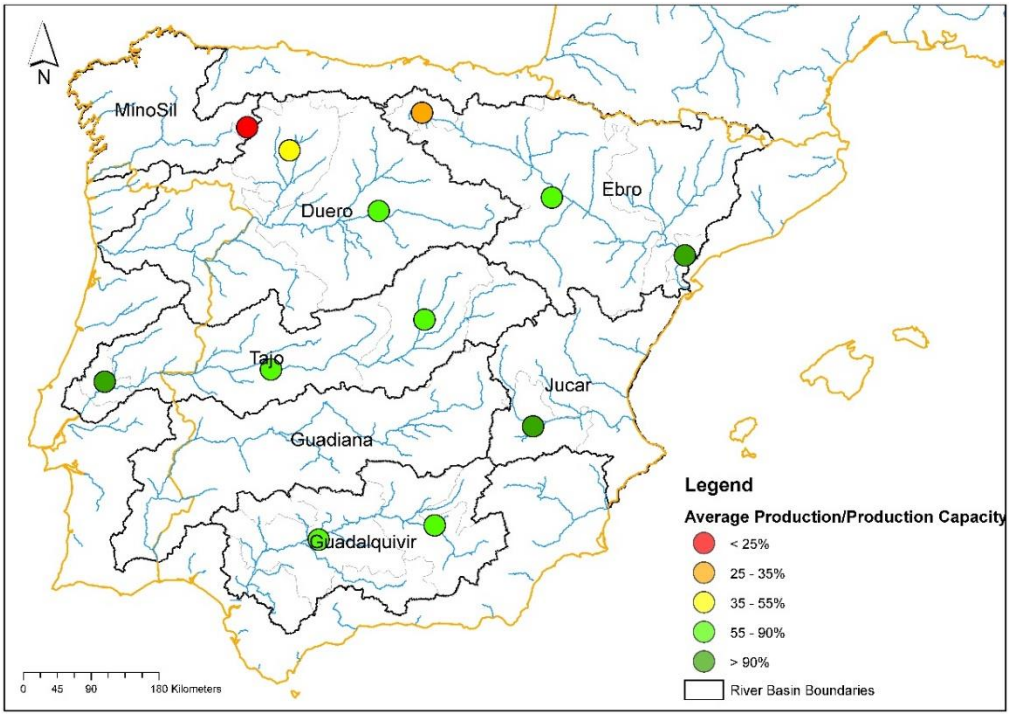

Figure 10-27: Production rate (%) of the modelled thermal power plants, averaged at a yearly scale. This percentage was computed as average production over production capacity of a single generator. It refers to climate change scenario.

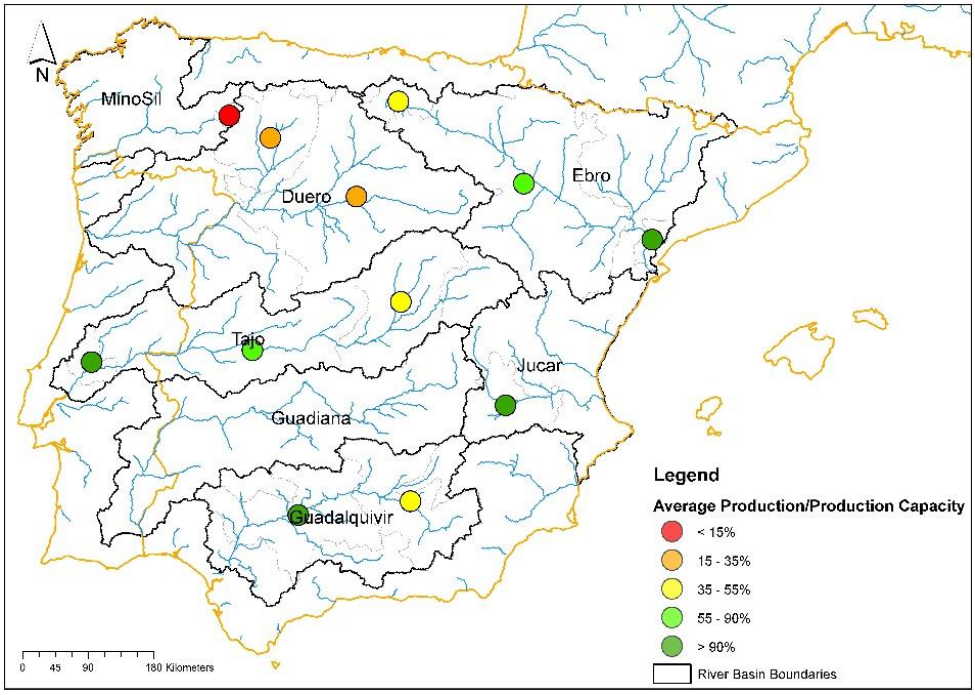

Figure 10-16: Production rate (%) of the modelled thermal power plants in control period.

As can be observed, in future climate there is a more even distribution of thermal production across the IP, i.e. an equalization of the thermal power plants over the Peninsula. Most of them starts producing at more than 55% of their production capacity, whereas in control period only few generators were selected to produce most of the electricity.

In control period, the "prioritized" power plants are indiscriminately equipped with once-through or cooling tower technology, since thermal production is not significantly limited by cooling constraints. Among the generators with a cooling tower (i.e. beta very close to 1), all the ones producing at full capacity present: (a) a low value for the ratio of thermal power discharged into the river and transformed into electricity ($\frac{Hw\ River}{Hw\ Production}$); (b) no cooling limitations. A low ratio means that, if two power plants both have a cooling tower, the one with a better gross efficiency will be chosen to produce more. Thus, the most efficient generators are selected, as can be noticed in Table 10-9 (rows highlighted in green). However, some power plants producing at more than 80% of their capacity present a high ratio, which simply means that they are once-through (but still very efficient; rows highlighted in red).

Table 10-9: 15 modelled thermal power plants throughout the IP in control period. The column 'Ratio' refers to the production rate (%). The rows highlighted in green identify the most efficient power plants equipped with a cooling tower, which are producing at full capacity. The rows highlighted in red show the once-through generators producing the most.

CONTROL PERIOD					
TPP Name	**% of weeks with cooling water constraints**	**Ratio**	**Gross Efficiency (%)**	**Beta (/)**	$\frac{\boldsymbol{Hw\ River}}{\boldsymbol{Hw\ Production}}$
Aceca	0.00	18%	0.43	1.00	0.58%
Jose and Trillo	0.00	100%	0.34	0.99	1.96%
Almaraz	58.65	88%	0.36	0.27	131.87%
Pego	0.00	**95%**	0.45	1.00	**0.42%**
Escatron and Castelnou	3.65	**82%**	0.69	0.60	**18.01%**
Escucha Teruel	0.06	26%	0.38	0.89	17.33%
Castejon and Arrubal	0.00	53%	0.50	1.00	0.45%
Asco	4.23	**100%**	0.35	0.99	**1.89%**
Santa Maria de Garona	91.22	42%	0.34	0.27	140.89%
Velilla	1.99	24%	0.38	0.76	38.94%
La Robla	0.00	18%	0.38	1.00	0.34%
Puertollano	0.00	52%	0.44	1.00	0.41%
Puente Nuevo	2.69	**90%**	0.38	0.21	**128.87%**
Cofrentes	9.42	**100%**	0.34	0.99	**1.98%**
Compostilla and Anllares	24.10	14%	0.38	0.75	41.27%
TOTAL	**12.8**	**66%**	-	-	-

Under climate change, the production shifts from once-through to generators equipped with a cooling tower, as can be deduced from Table 10-10 (rows highlighted in green/red), once it is compared with Table 10-9. Nevertheless, most of the power plants produce at more than 55% of their capacity.

Table 10-10: 15 modelled thermal power plants throughout the IP under climate change. The column 'Ratio' refers to the production rate (%), whereas 'ΔRatio' to the difference between production rates in future climate and control period. The rows highlighted in green identify the increased production of power plants with a cooling tower, the ones in red the decreased production of once-through generators.

CLIMATE CHANGE SCENARIO						
TPP Name	**% of weeks with cooling water constraints**	**Ratio**	**ΔRatio**	**Gross Efficiency (%)**	**Beta (/)**	$\frac{Hw\ River}{Hw\ Production}$
Aceca	3.27	51%	**+33%**	0.43	**1.00**	0.58%
Jose and Trillo	3.97	96%	-4%	0.34	0.99	1.96%
Almaraz	77.37	71%	**-17%**	0.36	**0.27**	131.87%
Pego	1.41	95%	0%	0.45	1.00	0.42%
Escatron and Castelnou	23.59	78%	-4%	0.69	0.60	18.01%
Escucha Teruel	3.27	38%	+12%	0.38	0.89	17.33%
Castejon and Arrubal	0.13	60%	**+7%**	0.50	**1.00**	0.45%
Asco	17.05	100%	0%	0.35	0.99	1.89%
Santa Maria de Garona	95.90	29%	-13%	0.34	0.27	140.89%
Velilla	6.22	59%	+35%	0.38	0.76	38.94%
La Robla	0.26	52%	**+34%**	0.38	**1.00**	0.34%
Puertollano	5.77	63%	**+11%**	0.44	**1.00**	0.41%
Puente Nuevo	13.21	86%	**-4%**	0.38	**0.21**	128.87%
Cofrentes	21.28	100%	0%	0.34	0.99	1.98%
Compostilla and Anllares	54.55	26%	+12%	0.38	0.75	41.27%
TOTAL	**19.8**	**70%**	**+4%**	-	-	-

As expected, once-through power plants (rows highlighted in red) present a lower production rate than in control period, while the ones with a cooling tower (rows highlighted in green) produce more (i.e. have a higher rate). This change in the production is mainly due to cooling constraints, which become more binding. For instance, the percentage of weeks with active constraints is non-zero for all the power plants and is 55% higher than in control period at the IP scale.

The increased strictness of thermal cooling constraints under climate change can also be assessed by analyzing the spatial and temporal variations of their shadow prices, thus comparing control and future climate patterns.

Shadow Prices

At first, a spatial variation of cooling constraints shadow price was analyzed by comparing control and future climate outputs. The former period has already been represented in Figure 10-15, whereas the latter is displayed in Figure 10-28.

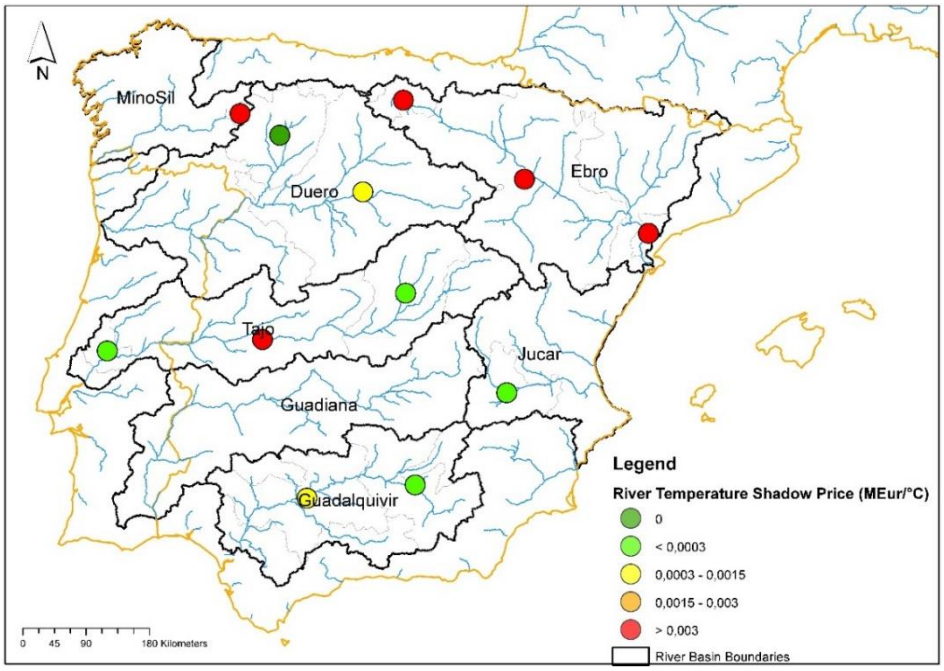

Figure 10-28: River water shadow price [M€/°C] of the modelled thermal power plants, averaged at a yearly scale. It refers to climate change scenario.

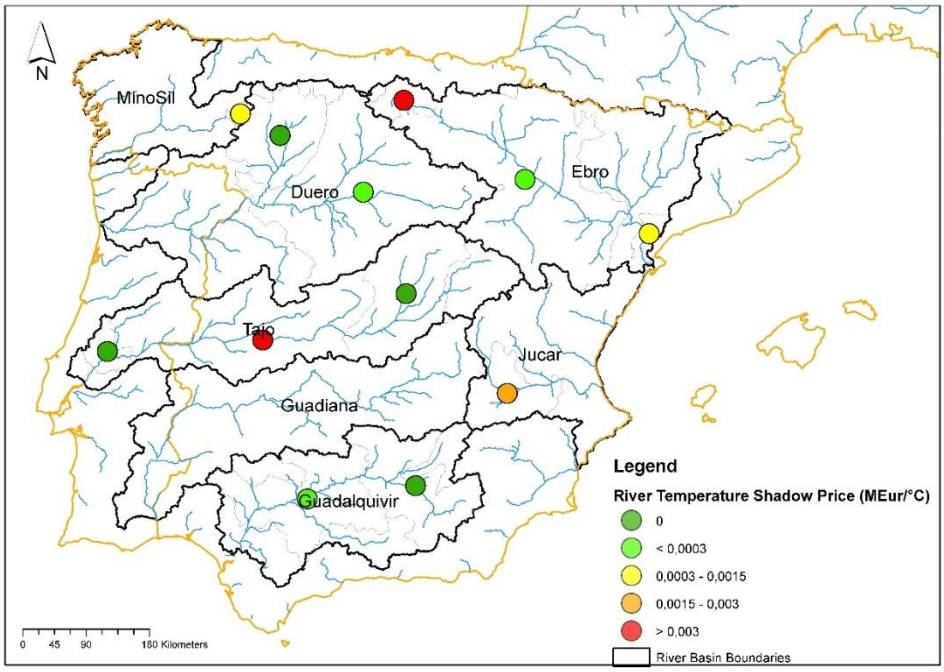

Figure 10-15: River water shadow price [M€/°C] of the modelled thermal power plants, averaged at a yearly scale. It refers to control period.

As can be deduced from the higher shadow prices [M€/°C] in Figure 10-28 and the increased percentage of weeks with active limitations on thermal production in Table 10-10, cooling constraints become more binding under climate change. In particular, the power plants that were already constrained in control period (e.g. Compostilla-Anllares in Miño-Sil) become even more limited (from 0.0008 to 0.006 M€/°C in its corresponding shadow price value), while the ones without any cooling restrictions (e.g. Puertollano in the upstream Guadalquivir) become constrained (from 0 to <0.0003 M€/°C in its corresponding shadow price value).
At the Peninsula level, cooling constraints shadow price increases by 3% (from 1.45 to 1.50 M€/°C), while the percentage of weeks with active cooling restrictions goes from 12.8% to 19.8% under climate change.

Furthermore, a temporal variation of weekly cooling constraints shadow price aggregated at the IP scale was investigated. Figure 10-29 shows the climate change outputs, whereas control period has already been presented in Figure 10-14.

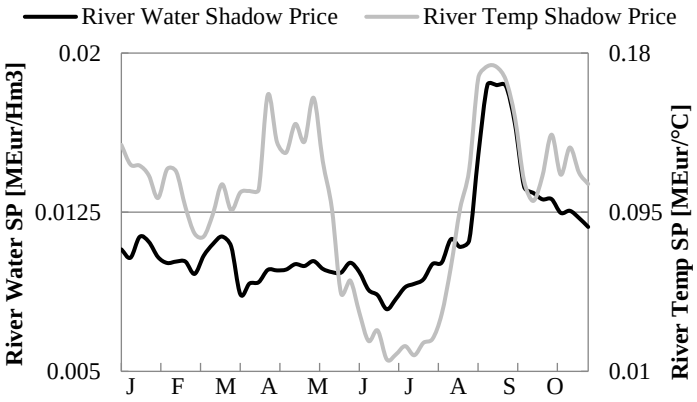

Figure 10-29: Temporal variation of weekly river water [M€/Hm^3] and river temperature [M€/°C] shadow prices. They have been averaged across the 30 years and aggregated at the Peninsula level. They refer to climate change scenario.

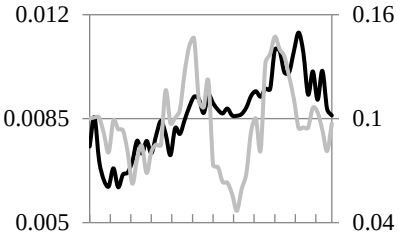

Figure 10-14: Temporal variation of weekly river water [M€/Hm^3] and river temperature [M€/°C] shadow prices. They refer to control period.

Both curves present similar patterns. However, the absolute values of both shadow prices in future climate are higher due to less water availability and higher water temperatures. Two main differences between control period and climate change outcomes can be observed:

i. River water shadow price [M€/Hm^3] does not hold constant anymore during summer, but it presents a minimum peak under climate change. This decrease is due to very high water temperatures forecasted in July (up to 28°C), which drive the shadow price pattern down. Power demand increase and water availability decrease are not significant enough to compensate this downward trend;

ii. The minimum peak in river water temperature shadow price [M€/°C] reaches a lower value under climate change. Even if the production shifts to the power plants with a cooling tower, the water temperature in July still reaches the 28°C legal limit, thus no thermal generator is allowed to produce electricity during this time slot (water consumption decreases as observed in Figure 10-24). As a consequence, the river temperature shadow price gets closer to zero.

The spatial variation of water availability shadow price in control and climate change scenario was also compared. The former period has already been presented in Figure 10-10, the latter is displayed in Figure 10-30.

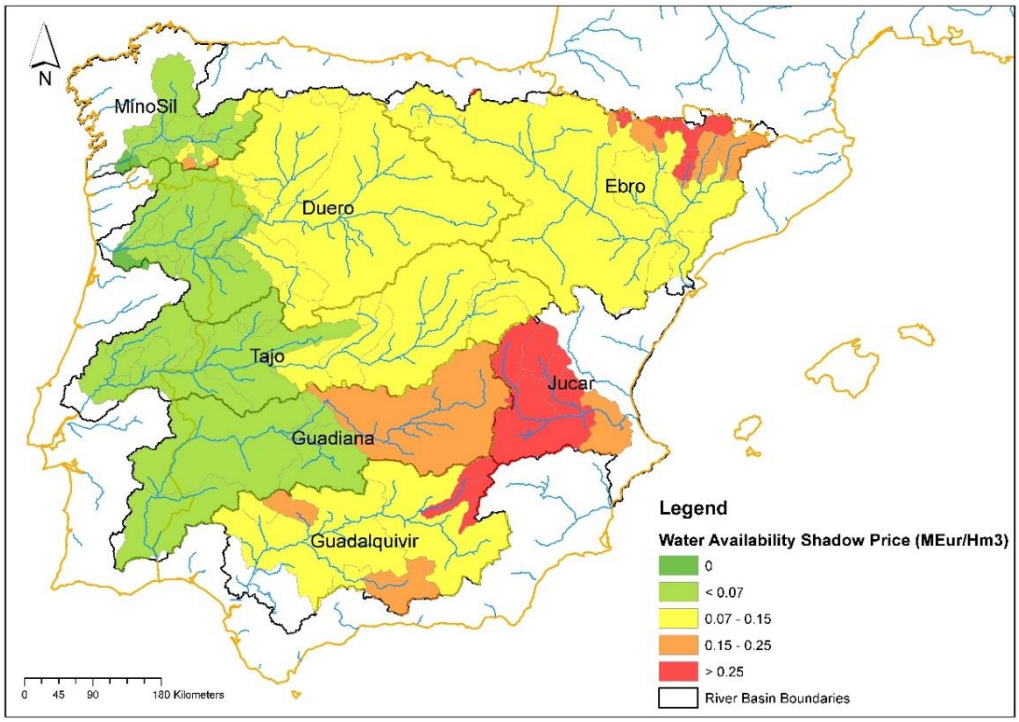

Figure 10-30: Spatial variation of water availability shadow price (M€/Hm^3), averaged at a yearly scale. It refers to climate change scenario.

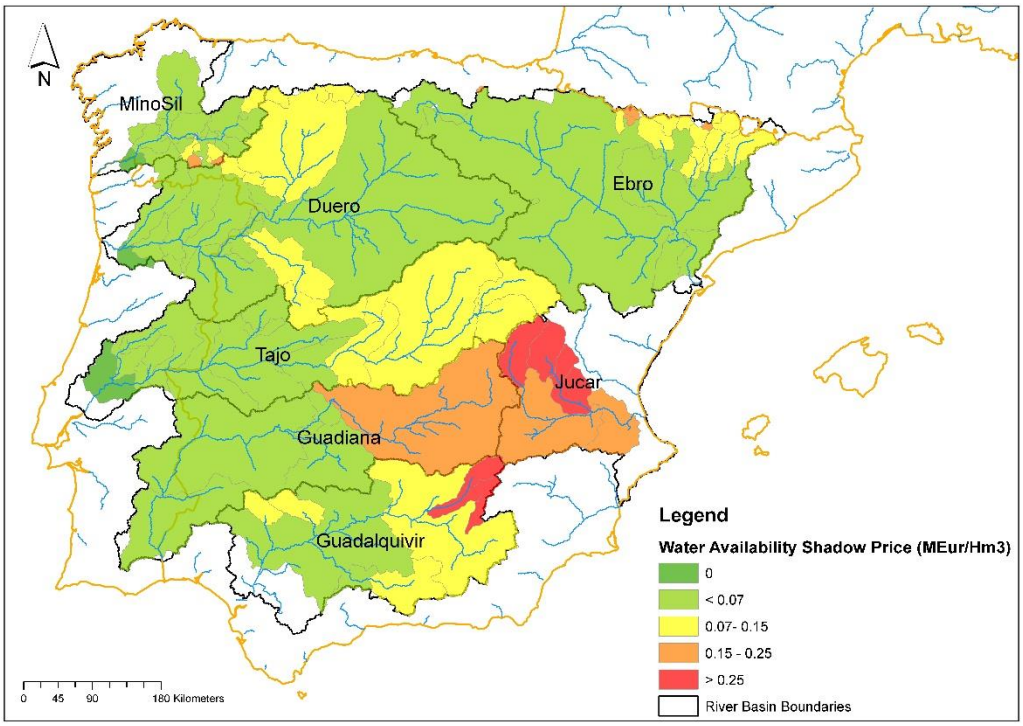

Figure 10-10: Spatial variation of water availability shadow price (M€/Hm^3), averaged at a yearly scale. It refers to control period.

Under climate change and at a yearly average scale, the only watersheds where agriculture is curtailed in favor of the downstream users are: (a) the red and orange ones in the Ebro; (b) the red ones in the Guadalquivir; (c) the three small, upstream ones in the Jucar. For instance, they all present a water availability shadow price that is higher than the irrigation curtailment cost of the corresponding river basin. In all the other watersheds, agriculture can be sometimes curtailed during certain weeks of the average year. The Ebro is the only basin that experiences more irrigation curtailment in future climate than in control period, whereas climate change does not worsen the situation in either Guadalquivir or Jucar.

Moreover, under climate change, agriculture still drives the total shadow price in the downstream watershed where all the users (i.e. agriculture, thermal and hydropower) are located simultaneously. For instance, it is responsible for more than 90% of the water availability shadow price in these watersheds, thus it is still prioritized.

From a broad perspective, water availability shadow price increases under climate change in most of the river basins. The main reason lies in a general decrease in the inflow (thus, water availability) from March to December.

The temporal variation of water availability and cooling water consumption shadow prices present the same pattern in both control and climate change scenario (i.e. they both peak from June to August). The only difference is that in future climate they reach a higher peak value, since even less water is available in summer compared to control period.

Thermal Cooling Constraints Impacts

If the model is optimized over climate change scenario without cooling constraints and compared with the future climate outputs just discussed in the previous section, the same considerations already made for the control period can be applied.

The only exception is in the residual power production cost. If cooling constraints are not active, this cost decreases by 5% compared to the climate change scenario with binding cooling constraints (the control period presented a 0% variation, see Section 10.3). For instance, if thermal power production is not limited, there is no need to produce with the sixth step of the residual supply curve, since the missing gap to meet power demand can be filled by the modelled thermal power plants only.

10.5 Sensitivity Analysis

Firstly, the sensitivity of the optimal total costs of the system to the change in the parameters values have been analyzed. Afterwards, the impact on several model outcomes (e.g. thermal power production) has been discussed.

All the following graphs present a percentage decrease/increase of some input parameters values on the x-axis. 100 refers to their reference value, used in the first optimization of the system. Higher percentages indicate an increase (up to 110%), whereas lower a decrease (down to 90%) in their original values.

Total Costs

Three out of four parameters (i.e. inflow, thermal efficiency and thermal marginal costs) lead to a linear variation in the optimal total costs of the system. An increase in the first two determines a linear decrease in the cost function value, whereas an increase in the last one causes a linear increase. An increase in the fourth parameter (i.e. river water temperature) induces an exponential growth in the total costs.

In Figure 10-31a, lower inflow leads to higher total costs, since both agriculture curtailment and thermal power production costs rise. Residual thermal generation cost is not affected by a change in the inflow, i.e. residual power production holds constant across the five different inflow scenarios.

Figure 10-31b shows that total costs are not linearly proportional to water temperature. For instance, a 5% increase in this parameter value will have a moderate impact, whereas a 10% increase will start to augment the costs significantly. The reason for this exponential growth lies in the thermal cooling constraints implemented. The river water temperature reaches the 28°C legal limit only when its value is increased by at least 10%. In this case, the thermal power plants along this stream are forced to not generate electricity at all. Their missing production has to be compensated either by hydropower or through the more expensive residual thermal supply curve.

In Figure 10-31c, when the thermal marginal costs are higher than their reference value, the total costs consequently increase. This growth is mainly driven by a rise in the residual thermal production costs. For instance, the model finds it optimal to start producing with the more expensive generation segments in the residual supply curve, rather than with the modelled thermal power plants, whose production thus decreases.

Figure 10-31d shows that thermal efficiency has a moderate impact on the total costs of the system. In the most extreme scenario characterized by a 20% decrease in thermal efficiency values, total costs only increase by 2% compared to the reference case.

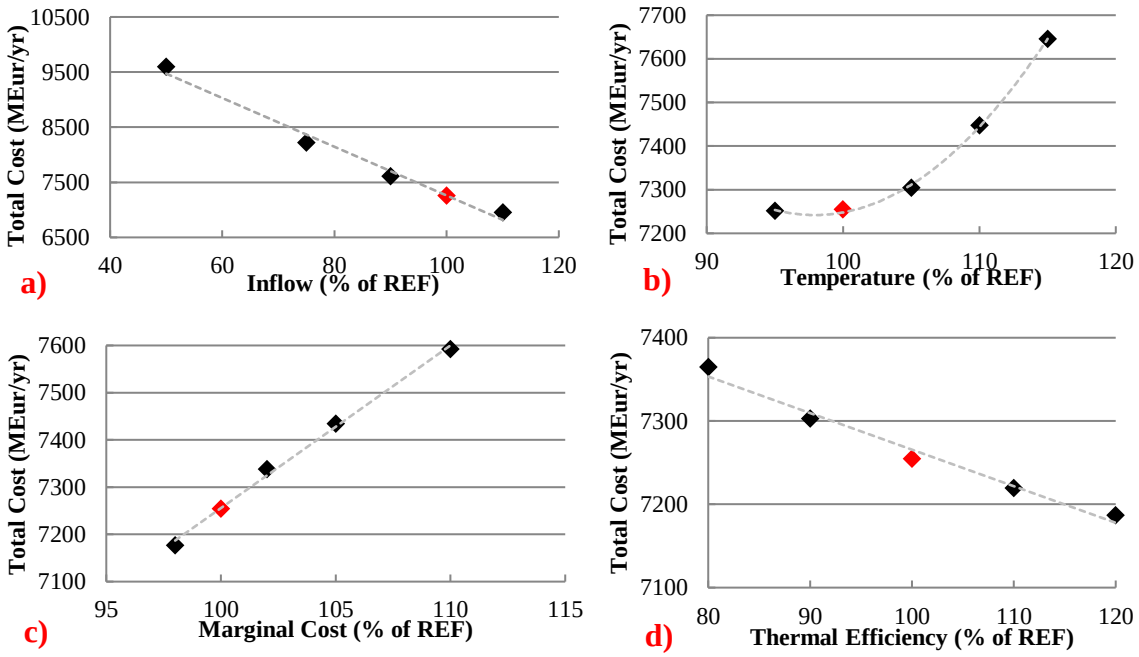

Figure 10-31: Total costs variation (M€/yr) depending on the decrease/increase of: (a) inflow values. The red dot identifies the reference inflow value; (b) river water temperature values. The red dot identifies the reference temperature value; (c) thermal marginal costs values. The red dot identifies the reference marginal costs value; (d) thermal efficiency values. The red dot identifies the reference efficiency value.

In the following paragraphs, the impacts of the same four parameters on more sectorial model outputs (e.g. thermal power production) will be discussed.

Inflow

The consequences of inflow variation can also be assessed at the thermal cooling water and hydropower production level (Figure 10-32 and Figure 10-33 respectively).

As can be noticed, less inflow results in less hydropower production, thus higher thermal production. For instance, power demand has to be fulfilled at each time step. To compensate the lower water availability, electricity generation is shifted to the thermal power plants withdrawing less water. Therefore, cooling water consumption increases and water withdrawn decreases as the inflow becomes less and less, as can be observed in Figure 10-32.

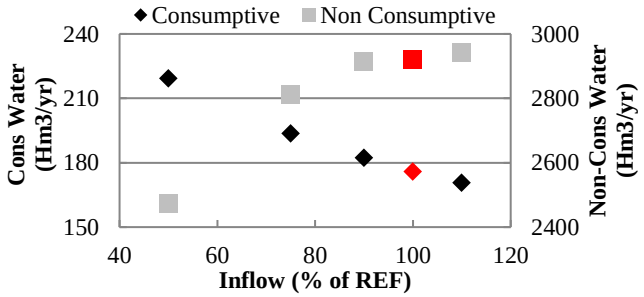

Figure 10-32: Consumptive and non-consumptive thermal cooling water variation (Hm^3/yr), depending on the decrease/increase of inflow values. The red dots identify the reference cooling water volumes values.

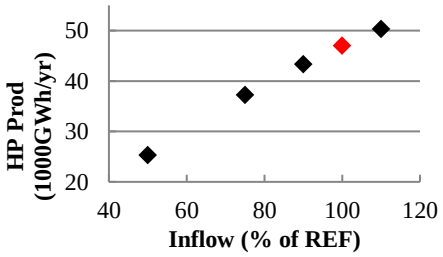

Figure 10-33: Hydropower production variation (1000GWh/yr) depending on the decrease/increase of inflow values. The red dot identifies the reference inflow value.

When the inflow decreases, water allocation to agriculture is also reduced. For example, irrigation water deficit increases by 100% when the inflow is reduced to 50% of its reference value.

Temperature

The impacts of temperature change on power production are quite significant: Figure 10-34 refers to thermal power production, while Figure 10-35 to the weekly relative storage in the Tajo and Ebro river basins.

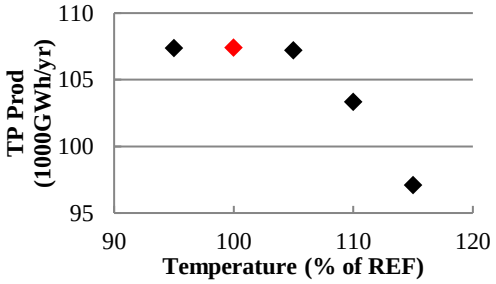

Figure 10-34: Thermal power production variation (1000GWh/yr), depending on the decrease/increase of water temperature values. The red dot identifies the reference temperature value.

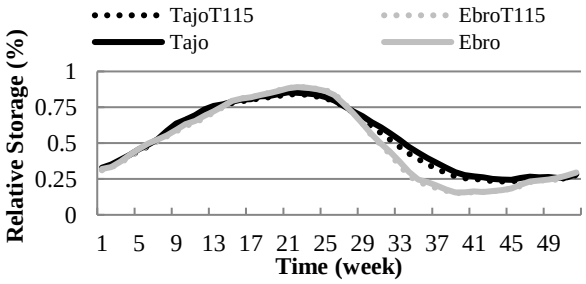

Figure 10-35: Relative storage (%) curves of the Tajo and Ebro river basins, averaged across the 30 years. The dotted lines identify the hydropower storage pattern when the water temperature is 15% higher than its reference value. The thick curves refer to the original optimization outcome.

As already deduced from the total costs variation, once the river water temperature becomes at least 10% higher than its reference value, the thermal power plants along

certain rivers stop producing due to cooling constraints restrictions. Thus, thermal production decreases (Figure 10-34). On a yearly average, the missing thermal generation is compensated by residual thermal, whereas hydropower holds constant. For instance, the impact of temperature increase on average relative storage is very small at the basin level (Figure 10-35). This parameter does not affect agriculture either.

Thermal Production Marginal Costs

The increase in the production marginal costs of the modelled thermal power plants directly affects their production, as can be observed in Figure 10-36.

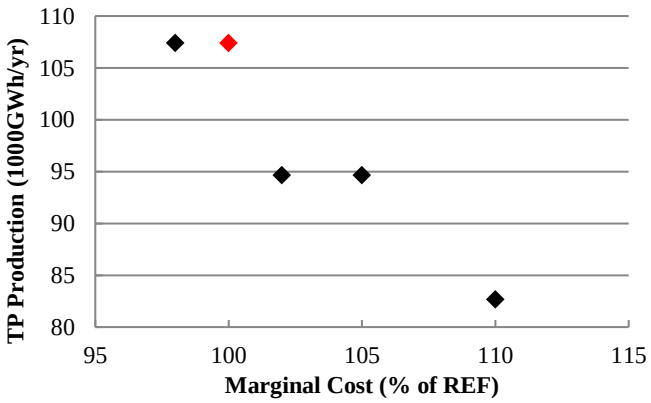

Figure 10-36: Thermal power production variation of the modelled generators (1000GWh/yr), depending on the decrease/increase of thermal marginal costs values. The red dot identifies the reference marginal costs value.

This step-pattern of the thermal power production curve originates from the residual thermal supply one, which was implemented as a 10 consecutive steps function. If one of its steps is characterized by a lower production price than the one of the modelled coal and CCGT generators, the model will always choose to produce first following the supply curve up to this step, rather than using the modelled thermal generators. Thus, as the production cost of the implemented power plants increases (i.e. becomes higher than the price of the up-next step in the supply curve), their production decreases (Figure 10-36).

Thermal Efficiency

Thermal efficiency has a limited impact not only on total costs but also on other model outputs. For example, the variation of withdrawn water volumes due to thermal efficiency decrease/increase is displayed in Figure 10-37.

As can be observed, cooling water withdrawals increase by 30% when the total thermal efficiency decreases by 20%; thermal production of the modelled power plants holds constant. However, thermal generation cost grows, showing that nuclear power plants (which are cheaper than coal and CCGT ones) have reduced their activity. For example, Santa Maria de Garona lowers its yearly production down to 1350 GWh/yr (from 1700 GWh/yr).

This also indicates how a switch from coal to CCGT power plants, which have a higher thermal efficiency, could reduce cooling water withdrawals, thus the strictness of thermal cooling constraints.

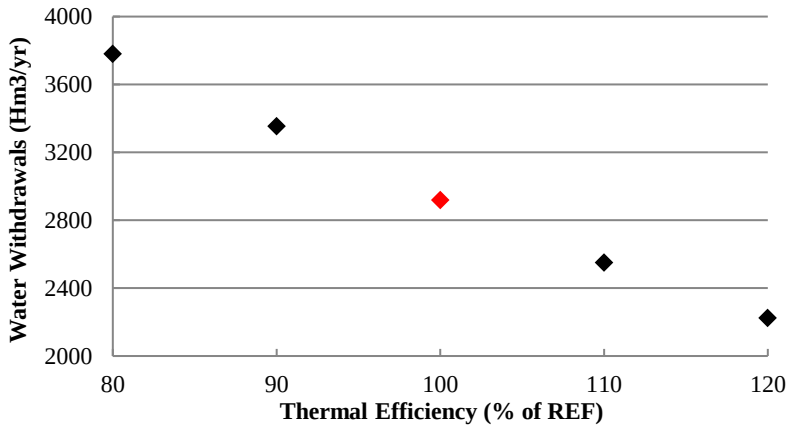

Figure 10-37: Variation of withdrawn water volumes (Hm^3/yr) depending on the decrease/increase of thermal efficiency values. The red dot identifies the reference efficiency value.

Part VI

Conclusions

Chapter 11

Conclusions

The purpose of this thesis was to find a proper method to further improve the modelling of the water-energy nexus in the IP in order to analyze the effects of thermal cooling constraints on both thermal and overall energy production, as well as on its water-power coupled system. The consequences of thermal generation restrictions were to be assessed both in control period (1961-1990) and under climate change scenario (2036-2065).

In order to achieve the goal of the study, a more spatially detailed representation of the water-power system already developed by Pereira-Cardenal et al. (2013) was needed. This was successfully achieved by developing a deterministic flow path model, implementing the spatial and temporal interactions between water and energy systems. The model was optimized over both control and future climate in order to assess and compare the impacts of cooling constraints in both time periods. Moreover, several outcomes of the two optimizations were compared in order to estimate some of the potential effects of climate change, especially on thermal production limited by cooling water requirements.

Within the first optimization framework (i.e. control period), it was found that thermal cooling constraints do not have a very significant impact on the model outcomes.
Irrigation is not curtailed more than in the case without any cooling constraints. For instance, agriculture users are usually prioritized at a yearly average temporal scale, regardless of binding or not binding cooling restrictions; thus, they should not be affected by these limitations.
As far as hydropower production is concerned, it holds constant (22% of the total), thus it is not influenced by cooling constraints. However, when these restrictions are not active, relative reservoir storages are generally kept lower across the IP. Since less (more) consumptive (non-consumptive) water volumes are required by thermal generators within this scenario, more water is left available in the river for other users. In conclusion, there is no more need to store significant amounts of water in the reservoirs before June in order to fulfill high thermal consumptive demands in summer. This is also reflected by a lower peak in the temporal variation curve of water availability shadow price, aggregated at the Peninsula level.
As for thermal power production, the only thermal generators that are significantly affected by cooling restrictions are two nuclear ones (Almaraz and Santa Maria de Garona). They present the highest river water temperature shadow prices among all the power plants in the IP (1.11 and 0.33 M€/°C respectively) and are constrained 59% and

91% of the weeks in the average year. When cooling constraints are not active, no thermal power plant is limited anymore, thus the model finds it optimal to make all the nuclear ones produce first at full capacity, at the expenses of coal and CCGT that generate less power. This leads to a substantial decrease in the total thermal production costs (thus total costs), since nuclear is the cheapest generation technology.

Under climate change scenario, it was assessed that thermal cooling constraints become more binding, since both river temperature shadow prices [M€/°C] and the percentage of weeks with active limitations on thermal production increase. In particular, the power plants that were already constrained in control period become even more limited, while the ones without any cooling restrictions become constrained. At the Peninsula level, cooling constraints shadow price increases by 3%, while the percentage of weeks with active cooling restrictions goes from 12.8% to 19.8%. The reason why cooling constraints become stricter lies in the higher water temperatures and lower water availability of future climate; this holds particularly true in summer. As a consequence, residual thermal power does not hold constant anymore during this time frame but it increases.
From a broad perspective, under climate change: (i) hydropower production decreases by 20%, due to lower inflows. However, hydropower reservoirs do not significantly change their release and storage policies compared to control period; (ii) modelled thermal power plants generation increases by 7%. Even if thermal generators are more limited, they have to supply for the lack of hydropower production; (iii) residual thermal power production rises by 3%; (iv) agriculture deficit grows from 12.5% in control period up to 29% (i.e. agriculture curtailment costs increase by 184% their initial value). Nevertheless, irrigation users are still prioritized at a yearly average temporal scale; (v) water availability shadow price increases in most of the river basins, due to a general decrease in the inflow (thus, water availability) from March to December.

When the model is optimized over climate change scenario without cooling constraints and compared with the future climate outputs just discussed, the same considerations already made for control period can be applied.

11.1 Future Research

Several assumptions were made in order to simplify the system implemented, due to the limited time frame of this thesis project. Possible further researches are thus recommended to both overcome these limitations and make a step forward towards a deeper understanding and modelling of the integrated water-energy nexus.

Firstly, a deterministic optimization of the model has been performed. Therefore, many uncertain input data were assumed to be deterministically known and treated as such, e.g. inflow time series, total power demand, residual power supply and irrigation water demand functions. This holds true for both control period and climate change scenario.

Moreover, the average CFs derived from the four RCMs on which climate change scenario is based represent another source of uncertainty that was treated deterministically. In order to reduce the effects of uncertainty, a Model Predictive Control (MPC) strategy could be employed. This would imply an optimization repeated online at each time step and for every uncertain input, which would be very computationally expensive because of the large dimension of the system.

The temporal aggregation of the power system represents another major source of uncertainty. As already discussed in Section 9.2.3, a modelling weekly time step was employed, despite the significant variation of hourly electricity production and prices within a single week (refer to Figure 7-1a). If an hourly discretization was applied, the power system (inclusive of residual power supply and demand functions) could be represented more realistically and pumped-storage hydropower could be taken into account. However, the problem would be computationally infeasible. Pereira-Cardenal et al. (2013) already faced the same issue and proposed some potential solutions, e.g. keep weekly time steps and: (a) split each week into a few load segments with a certain demand profile; (b) determine hydropower revenue functions per time step.

The last source of uncertainty is the model structure: (i) the implementation of agriculture as a surface water user only; (ii) the representation of the power system without any electricity transmission lines constraints.
The former simplification could be overcome by adding groundwater abstractions for irrigation in the model. In the system implemented, the rainfall-runoff model already includes groundwater storage, which is thus treated as a natural, rechargeable source for surface water. Since all the groundwater becomes part of the inflow to the watersheds, groundwater pumping is modelled as fully sustainable. In order to overcome this limitation, several reservoir nodes could be added to the flow path implementation of the water system, representing groundwater storage. A sustainability constraint would have to be added in order to not incur groundwater over-exploitation by agriculture. A downside of this procedure would be the increased dimension of the system.
The latter simplification results in an unbalanced power production across the entire IP. In the model implemented and optimized over both control period and climate change scenario, two river basins (Tajo and Ebro) produce most of the electricity. For instance, they generate 130% more than the power demand in the basin (Figure 11-1). Their excessive production is used to fulfill the power demand in the other five basins, which generate up to 80% less than their actual demand. However, it might not be feasible for the existing power transmission lines in the Peninsula to transfer electricity across several river basins indiscriminately.

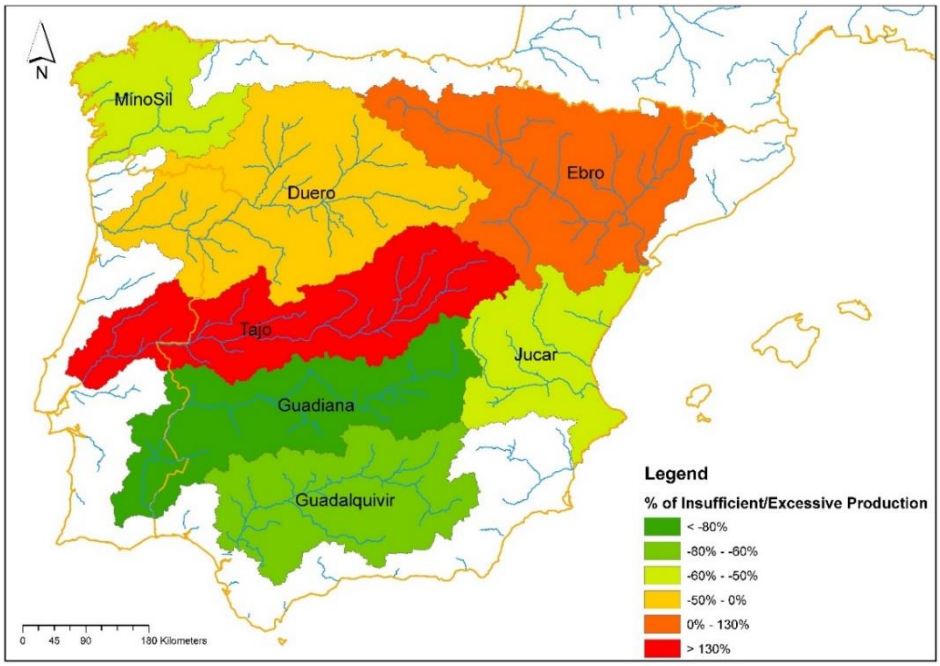

Figure 11-1: Percentage of power production compared to power demand in each river basin, averaged at a yearly time scale. If the percentage is negative, production is lower than demand, vice versa for positive ratios. It refers to control period optimization.

This limitation could be faced by implementing a flow path model of the power system, which would run parallel to the water system one. These two models would interact at each time step, in order to transfer energy from the water to the power system. Moreover, the new power flow path would feasibly represent the electricity flow through the transmission lines across the entire IP.

The modelled system should also be expanded in order to include more characterizing elements of the water-energy nexus in the IP (e.g. domestic and other industrial water users, an accounting mechanism for greenhouse gas emissions) and assess a more realistic tradeoff among them.

Despite the assumptions and simplifications made, the proposed method demonstrated to be suitable for assessing: (a) the impacts of thermal cooling constraints on thermal and total power production, in both control and future climate; (b) the effects of climate change on the entire system; (c) more broadly, the spatio-temporal interactions between water and energy systems in the IP. It also proved to be flexible and be able to include other elements of the water-energy nexus (e.g. electricity transmission lines, domestic water users).

Chapter 12

References

Al-Sunaidy, A. and Green, R., 2006. Electricity Deregulation in OECD (Organization for Economic Cooperation and Development) Countries. *Energy*, 31, pp. 769-87

Arunkumar, S. and Yeh, W. W-G., 1973. *Probabilistic Models in the Design and Operation of a Multipurpose Reservoir System: A Research Contribution to the Water Resources Center, University of California, and Office of Water Resources Research, USDI. Contribution 144.* Davis: California Water Resources Center, University of California

Barros, M. T. L., Tsai, F. T-C., Yang, S., Lopes, J. E. G. and Yeh, W. W.-G., 2003. Optimization of Large-Scale Hydropower System Operations. *Journal of Water Resources Planning and Management*, 129(3), pp. 178-88

Barros, M. T. L., Zambon, R. C., Barbosa, P. S. F. and Yeh, W. W.-G., 2008. Planning and Operation of Large-Scale Water Distribution Systems With Preemptive Priorities. *Journal of Water Resources Planning and Management*, 134(3), pp. 247-56

Bear, J. and Levin, O., 1966. *Optimal Utilization of an Aquifer as an Element of a Water-Resources System.* Haifa: Technion-I.I.T., Hydrodinamics & Hydraulic Engineering Laboratory, Operations Research Center

Bear, J. and Levin, O., 1967. The Optimal Yield of an Aquifer. *International Association of Hydrological Sciences*, pp. 401-12

Bear, J. and Levin, O., 1970. Optimal Utilization of an Aquifer as an Element of a Water-Resource System: Research Period 1967-68. In: Levin, O., ed. 1970. *Selected Works in Operations Research and Hydraulics*. Haifa: Israel Institute of Technology. pp. 64-279

Bear, J., Levin, O. and Buras, N., 1964. *Optimal Utilization of Aquifers as Elements of Water-Resources Systems: Progress Report.* Haifa: Technion, Israel Institute of Technology, Technion Research and Development Foundation

Bellman, R., 1957. *Dynamic Programming.* Princeton: Princeton University Press

Berga Casafont, L., 2003. Presas y Embalses en la España del Siglo XX. *Revista de Obras Pùblicas,* 3438, pp. 37–40

Booker, J. E. and Young, R. A., 1994. Modelling Intrastate and Interstate Markets for Colorado River Water Resources. *Journal of Environmental Economics and Management*, 26(1), pp. 66-87

Braat, L. C. and Lierop, W. F. J., 1987. *Integrated Economic-Ecological Modelling*. New York: Elsevier Science Publishers B V

Braga, B., Yen, W. Jr., Becker, L. and Barros, M., 1991. Stochastic Optimization of Multiple-Reservoir-System Operation. *Journal of Water Resources Planning and Management*, 117(4), pp. 471-81

Bright, E. A., Coleman, P. R., King, A. L. and Rose, A. N., 2008. *LandScan 2007*. Oak Ridge: Oak Ridge National Laboratory

Briscoe, J., 2005. Water as an Economic Good. In: Brouwer, R. and Pearce, D. W., eds. 2005. *Cost Benefit Analysis and Water Resources Management*. Cheltenham: Edward Elgar Publishing. Ch.3

Brouwer, R. and Hofkes, M., 2008. Integrated Hydro-Economic Modelling: Approaches, Key Issues and Future Research Directions. *Ecological Economics,* 66, pp. 16-22

Bruns, B. R., Ringler, C. and Meinzen-Dick, R. S., 2005. *Water Rights Reform: Lessons for Institutional Design*. Washington D.C.: International Food Policy Research Institute

Byers, E. A., Hall, J. W. and Amezaga, J. M., 2014. Electricity Generation and Cooling Water Use: UK Pathways to 2050. *Global Environmental Change,* 25, pp. 16-30

Cai, X. M., McKinney, D. C. and Lasdon, L. S., 2003a. Integrated Hydrologic-Agronomic-Economic Model for River Basin Management. *Journal of Water Resources Planning and Management*, 129(1), pp. 4-17

Characklis, G. W., Kirsch, B. R., Ramsey, J., Dillard, K. E. M. and Kelley, C. T., 2006. Developing Portfolios of Water Supply Transfers. *Water Resources Research*, 42(5), pp. n/a-n/a

Cheng, W.-C., Hsu, N.-S., Cheng, W.-M., and Yeh, W. W.-G., 2009. A Flow Path Model for Regional Water Distribution Optimization. *Water Resources Research*, 45(9), pp. 1-12

CNE, 2008. *Precios y Costes de la Generaciòn de Electricidad*. [pdf] Madrid: Comisión Nacional de Energia. Available at:

<http://energia.cnmc.es/cne/doc/publicaciones/cne82_08.pdf> [Accessed 30 March 2016]

Colman, J., 2013. *The Effects of Ambient Air and Water Temperature on Power Plant Efficiency*. M.Sc. Thesis. Duke University

Committee on Education, 1992. The Dublin Statement on Water and Sustainable Development. In: United Nations, *International Conference on Water and the Environment (ICWE)*. Dublin, Ireland, 26-31 January 1992. [online] Available at: <http://www.wmo.int/pages/prog/hwrp/documents/english/icwedece.html> [Accessed 31 March 2016]

Conejo, A. J., Carriòn, M. and Morales, J. M., 2010. *Decision Making Under Uncertainty in Electricity Markets.* New York: Springer

Confederaciòn Hidrogràfica del Duero, 2016. *Mapa de Estaciones con Datos Historicos*. [online] Available at: <http://81.33.18.208/saica/DatosHistoricos/tabid/110/Default.aspx> [Accessed 1 February 2016]

Crawley, P. D. and Dandy, G. C., 1993. Optimal Operation of Multiple-Reservoir System. *Water Resources Planning and Management*, 119(1), pp. 1-17

Davies, E. G. R., Kyle, P. and Edmonds, J. A., 2013. An Integrated Assessment of Global and Regional Water Demands for Electricity Generation to 2095. *Advances in Water Resources*, 52, pp. 296-313

De-Castro, M., Martìn-Vide, J. and Alonso, S., 2005. *El Clima de España: Pasado, Presente y Escenarios de Clima Para el Siglo XXI, Impactos del Cambio Climàtico en España*. Madrid: Ministerio Medio Ambiente

Directive 2006/44/EC of the European Parliament and of the Council of 6 September 2006 on the Quality of Fresh Waters Needing Protection or Improvement in order to Support Fish Life

Dooge, J. C. I., 2009. *Fresh Surface Water*. Oxford: EOLSS Publishers/UNESCO

Dudley, B. J. and Scott, B. W., 1993. Integration Irrigation Water Demand, Supply, and Delivery Management in a Stochastic Environment. *Water Resources Research*, 29(9), pp. 3093-3101

Eaton, J., 2012. Record Heat, Drought Pose Problems for U.S. Electric Power. *National Geographic News*, [online] 17 August. Available at: <http://news.nationalgeographic.com/news/energy/2012/08/120817-record-heat-droughtpose-problems-for-electric-power-grid/> [Accessed 6 April 2016]

EC JRC, 2001. *Integrated Pollution Prevention and Control (IPPC) Reference Document on the Application of Best Available Techniques to Industrial Cooling Systems*. [pdf] Sevilla: European IPPC Bureau, European Commission Join Research Centre. Available at: <http://eippcb.jrc.ec.europa.eu/reference/BREF/cvs_bref_1201.pdf> [Accessed 30 March 2016]

Electrical Engineering Portal (EEP), 2012. *An Overview of Combined Cycle Power Plant*. [online] (25 August 2012) Available at: <http://electrical-engineering-portal.com/an-overview-of-combined-cycle-power-plant> [Accessed 12 May 2016]

Endesa Educa, 2014. *Informacion General de la Central Termica de Compostilla*. [online] Available at: <http://www.endesaeduca.com/Endesa_educa/recursos-interactivos/instalaciones-electricas/informacion-compostilla> [Accessed 15 February 2015]

EPRI, 2002. *Water & Sustainability (Volume 3): U.S. Water Consumption for Power Production – The Next Half Century*. Palo Alto: EPRI

Erickson, T. R. and Stefan, H. G., 1996. *Correlation of Oklahoma Stream Temperatures with Air Temperatures*. Project Report 398. University of Minnesota, St. Anthony Falls Laboratory

European Environment Agency (EEA), 2012. *Elevation Map of Europe*. [online] (29 November 2012) Available at: <http://www.eea.europa.eu/data-and-maps/data/digital-elevation-model-of-europe#tab-gis-data> [Accessed 23 March 2016]

Eurostat Statistics Explained, 2012. *Glossary: Gross Electricity Generation*. [online] (14 September 2012) Available at: <http://ec.europa.eu/eurostat/statistics-explained/index.php/Glossary:Gross_electricity_generation> [Accessed 12 May 2016]

FAO, 2016. *AQUASTAT*. [online] (1 June 2016) Available at: <http://www.fao.org/nr/water/aquastat/water_res/index.stm#cp> [Accessed 6 June 2016]

Feeley, T. J., Skone, T. J., Stiegel, G. J., McNemar, A., Nemeth, M., Schimmoller, B., Murphy, J. T. and Manfredo, L., 2008. Water: A Critical Resource in the Thermoelectric Power Industry. *Energy*, 33, pp. 1-11

Fisher, F. M., Arlosoroff, S., Eckstein, Z., Haddadin, M., Hamati, S. G., Huber-Lee, A., Jarrar, A., Jayyousi, A., Shamir, U. and Wesseling, H., 2002. Optimal Water

Management and Conflict Resolution: The Middle East Water Project. *Water Resources Research*, 38(11), 1243

Fisher, F. M., Huber-Lee. A. and Amir, I., 2005. *Liquid Assets: An Economic Approach for Water Management and Conflict Resolution in the Middle East and Beyond.* Washington D.C.: Resources for the Future

Flörke, M., Teichert, E. and Bärlund, I., 2011. Future Changes of Freshwater Needs in European Power Plants. *Management of Environmental Quality: an International Journal*, 22(1), pp. 89-104

Fowler, H. J., Blenkinsop, S. and Tebaldi, C., 2007. Linking Climate Change Modelling to Impact Studies: Recent Advances in Downscaling Techniques for Hydrological Modelling. *International Journal of Climatology*, 27, pp. 1547-78

Förster, H. and Lilliestam, J., 2009. Modelling Thermoelectric Power Generation in View of Climate Change. *Regional Environmental Change*, 10, pp. 327-38

Gale, D., 2007. Linear Programming and the Simplex Method. *Notices of the American Mathematical Society*, 54(3), pp. 364-69

Gentleman, A., 2003. France Faces Nuclear Power Crisis. *The Guardian*, [online] 13 August. Available at: <http://www.theguardian.com/news/2003/aug/13/france.internationalnews> [Accessed 6 April 2016]

Gisser, M and Mercado A., 1973. Economic Aspects of Ground Water Resources and Replacement Flows in Semiarid Agricultural Areas. *American Journal of Agricultural Economics*, 55(3), pp. 461-66

Gisser, M and Mercado A., 1972. Integration of the Agricultural Demand Function for Water and the Hydrologic Model of the Pecos Basin. *Water Resources Research*, 8(6), pp. 1373-84

Gleick, P. H., 1993a. Water and Conflict – Freshwater Resources and International Security. *International Security*, 18(1), pp. 79-112

Gleick, P. H., 1994. Water and Energy. *Annual Review of Energy and the Environment*, 19, pp. 267-99

Global Energy Observatory, 2016. *Power Plants*. [online] Available at: <http://globalenergyobservatory.org/index.php#> [Accessed 1 February 2016]

Godoy, J., 2006. European Heat Wave Shows Limits of Nuclear Energy. *Inter Press Service*, [online] 26 July. Available at:

<http://www.ipsnews.net/2006/07/environment-heat-wave-shows-limits-of-nuclear-energy/> [Accessed 6 April 2016]

Gonzàlez-Hidalgo, J. C., Brunetti, M. and De-Luis, M., 2011. A New Tool for Monthly Precipitation Analysis in Spain: MOPREDAS Database [Monthly Precipitation Trends December 1945–November 2005]. *International Journal of Climatology*, 31, pp. 715-31

Goor, Q, Kelman, R. and Tilmant, A., 2011. Optimal Multipurpose-Multireservoir Operation Model with Variable Productivity of Hydropower Plants. *Journal of Water Resources Planning and Management*, 137(3), pp. 258-67

Hamlet, A. F., Lee, S.-Y., Mickelson, K. E. B. and Elsner, M. M., 2010. Effects of Projected Climate Change on Energy Supply and Demand in the Pacific Northwest and Washington State. *Climatic Change*, 102, pp. 103-128

Hardy, L., Garrido, A. and Juana, L., 2012. Evaluation of Spain's Water-Energy Nexus. *Water Resources Development*, 28(1), pp. 151-70

Hardy, L. and Garrido, A., 2010. *Anàlisis y Evaluaciòn de las Relaciones Entre El Agua y La Energìa en España*. Madrid: Observatorio del Agua

Harou, J. J., Pulido-Velazquez, M., Rosenberg, D. E., Medellìn-Azuara, J., Lund, J. R. and Howitt, R. E., 2009. Hydro-Economic Models: Concepts, Design, Applications, and Future Prospects. *Journal of Hydrology*, 375, pp. 627-43

Hayek, F. A., 1950. *The Counter-Revolution of Science: Studies on the Abuse of Reason.* Indianapolis: Liberty Fund Publishers

Haylock, M. R., Hofstra, N., Tank, A. M. G. K., Klok, E. J., Jones, P. D. and New, M., 2008. A European Daily High-Resolution Gridded Dataset of Surface Temperature and Precipitation for 1950-2006. *Journal of Geophysical Resource*, 113 (D20), pp. n/a-n/a

Hightower, M. and Pierce, S. A., 2008. The Energy Challenge. *Nature*, 452(20), pp. 285-86

Hoffman, A., 2010. The Water-Energy Conundrum: Can We Satisfy the Need for Both? *Journal of Energy Security*, [online] Available at: <http://ensec.org/index.php?option=com_content&view=article&id=266:the-water-energy-conundrum-can-we-satisfy-the-need-for-both&catid=110:energysecuritycontent&Itemid=366> [Accessed 23 March 2016]

Hollinshead, S. P. and Lund, J. R., 2006. Optimization of Environmental Water Purchases With Uncertainties. *Water Resources Research*, 42(8), pp. W08403

Howe, C. W., Schurmeier, D. R. and Shaw, W. D. JR., 1986. Innovative Approaches to Water Allocation: The Potential for Water Markets. *Water Resources Research*, 22(4), pp. 439-45

Hsu, N.-S., Cheng, W.-C., Cheng, W.-M., Wei, C.-C. and Yeh, W. W.-G., 2008. Optimization and Capacity Expansion of a Water Distribution System. *Advances in Water Resources*, 31, pp. 776-86

Instituto Nacional de Estadistica, 2008. *Estadisticas e Indicadores del Agua*. [online] Available at: <http://www.ine.es/revistas/cifraine/0108.pdf> [Accessed 19 April 2016]

International Energy Agency (IEA), 2008. *Energy Efficiency Indicators for Public Electricity Production from Fossil Fuels*. [pdf] Paris: IEA Publications. Available at: <https://www.iea.org/publications/freepublications/publication/En_Efficiency_Indicators.pdf> [Accessed 19 April 2016]

International Energy Agency (IEA), 2008. *World Energy Outlook 2008*. [pdf] Paris: IEA Publications. Available at: <http://www.worldenergyoutlook.org/media/weowebsite/2008-1994/weo2008.pdf> [Accessed 23 March 2016]

International Energy Agency (IEA), 2010. *Power Generation from Coal. Measuring and Reporting Efficiency Performance and CO_2 Emissions*. [pdf] Paris: IEA Publications. Available at: <https://www.iea.org/ciab/papers/power_generation_from_coal.pdf> [Accessed 19 April 2016]

International Energy Agency (IEA), 2015. *Key World Energy STATISTICS*. [pdf] Paris: IEA Publications. Available at: <https://www.iea.org/publications/freepublications/publication/KeyWorld_Statistics_2015.pdf> [Accessed 30 March 2016]

International Water Management Institute, 2007. *Water for Food, Water for Life: A Comprehensive Assessment of Water Management in Agriculture*. London: Earthscan and Colombo: International Water Management Institute

IPCC, 2007. *Climate Change 2007: Impacts, Adaptation and Vulnerability. Contribution of Working Group II to the Fourth Assessment Report of the Intergovernmental Panel on Climate Change*. In: Parry, M. L., Canziani, O. F., Palutikof, J. P., van der Linden, P. J. and Hanson, C. E., (Eds.), Cambridge University Press, Cambridge, United Kingdom, 976 pp.

IPCC, 2014. *Climate Change 2014: Mitigation of Climate Change. Working Group III Contribution to the Fifth Assessment Report of the Intergovernmental Panel on Climate Change*. In: Edenhofer, O., Pichs-Madruga, R., Sokona, Y., Farahani, E., Kadner, S., Seyboth, K., Adler, A., Baum, I., Brunner, S., Eickemeier, P., Kriemann, B., Savolainen, J., Schlömer, S., von Stechow, C., Zwickel, T. and Minx, J. C., (Eds.), Cambridge University Press, Cambridge, United Kingdom and New York, NY, USA

IPCC, 2014. *Climate Change 2014: Impacts, Adaptation and Vulnerability. Part A: Global and Sectoral Aspects. Contribution of Working Group II Contribution to the Fifth Assessment Report of the Intergovernmental Panel on Climate Change.* In: Field, C. B., Barros, V. R., Dokken, D. J., Mach, K. J., Mastrandrea, M. D., Bilir, T. E., Chatterjee, M., Ebi, K. L., Estrada, Y. O., Genova, R. C., Girma, B., Kissel, E. S., Levy, A. N., MacCracken, S., Mastrandrea, P. R. and White, L. L., (Eds.), Cambridge University Press, Cambridge, United Kingdom and New York, NY, USA

Isaac, M. and van Vuuren, D. P., 2009. Modeling Global Residential Sector Energy Demand for Heating and Air Conditioning in the Context of Climate Change. *Energy Policy*, 37(2), pp. 507-21

Jacob, D., Van den Hurk, B. J. J. M., Andrae, U., Elgered, G., Fortelius, C., Graham, L. P., Jackson, S. D., Karstens, U., Kopken, C., Lindau, R., Podzun, R., Rockel, B., Rubel, F., Sass, B. H., Smith, R. N. B. and Yang, X., 2001. A Comprehensive Model Inter-Comparison Study Investigating the Water Budget During the BALTEX-PIDCAP Period. *Meteorology and Atmospheric Physics*, 77(1), pp. 19-43

Jaeger, E. B., Anders, I., Luthi, D., Rockel, B., Schar, C. and Seneviratne, S. I., 2008. Analysis of ERA40-driven CLM Simulations for Europe. *Meteorologische Zeitschrift*, 17(4), pp. 349-67

Joskow, P. L., 2006. Introduction to Electricity Sector Liberalization: Lessons Learned from Cross-Country Studies. In: Sioshansi, F. P. and Pfaffenberger, W., eds. 2006. *Electricity Market Reform: An International Perspective*. Oxford: Elsevier Ltd. pp. 1-32

Joskow, P. L., 2006. Regulation of Natural Monopoly. In: Polinsky, A. M. and Shavell, S., eds. 2007. *Handbook of Law and Economics*. Amsterdam: Elsevier. Ch.16

King, C. W., Holman, A. S. and Webber, M. E., 2008. Thirst for Energy. *Nature Geoscience*, 1, pp. 283-86

Kirshen, P., Ruth, M. and Anderson, W., 2008. Interdependencies of Urban Climate Change Impacts and Adaptation Strategies: A Case Study of Metropolitan Boston USA. *Climatic Change*, 86, pp. 105–22

Koch, H., Vögele, S., Kaltofen, M. and Grünewald, U., 2012. Trends in Water Demand and Water Availability for Power Plants – Scenario Analyses for the German Capital Berlin. *Climatic Change,* 110, pp. 879-99

Koch, H. and Vögele, S., 2009. Dynamic Modelling of Water Demand, Water Availability and Adaptation Strategies for Power Plants to Global Change. *Energy*, 68, pp. 2031-39

Koch, H. and Vögele, S., 2013. Hydro-Climatic Conditions and Thermoelectric Electricity Generation – Part I: Development of Models. *Energy,* 63, pp. 42-51

Kristiansen, T., 2004. Financial Risk Management in the Hydropower Industry Using Stochastic Optimization. *Advanced Modelling and Optimization*, 6, pp. 17-24

Labadie, J. W., 2004. Optimal Operation of Multireservoir Systems: State-of-the-Art Review. *Journal of Water Resources Planning and Management*, 130, pp. 93-111

Langford, T. E. L., 1990. *Ecological Effects of Thermal Discharges*. London: Elsevier Applied Sciences

Langins, J., 2004. *Conserving the Enlightenment: French Military Engineering from Vauban to the Revolution.* Cambridge: MIT Press

Lefkoff, L. J. and Gorelick, S. M., 1990b. Simulating Physical Processes and Economic Behavior in Saline, Irrigated Agriculture – Model Development. *Water Resources Research*, 26(7), pp. 1359-69

Lehner, B., Czisch, G. and Vassolo, S., 2005. The Impact of Global Change on the Hydropower Potential of Europe: A Model-based Analysis. *Energy Policy*, 33, pp. 839-55

Lòpez-Bustins, J. A., Martìn-Vide, J. and Sànchez-Lorenzo, A., 2008. Iberia Winter Rainfall Trends Based Upon Changes in Teleconnection and Circulation Patterns. *Global Planetary Change*, 63, pp. 171-76

Lorenzo-Lacruz, J., Moràn-Tejeda, E., Vicente-Serrano S. M. and Lòpez-Moreno, J. I., 2013. Streamflow Droughts in the Iberian Peninsula Between 1945 and 2005: Spatial and Temporal Patterns. *Hydrology and Earth System Sciences*, 17, pp. 119-34

Loucks, D. P., Van Beek, E., Stedinger, J. R., Dijkman, J. P., and Villars, M. T., 2005.*Water Resources Systems Planning and Management: An Introduction to Methods, Models and Applications*. Paris: UNESCO

Lund, J. R., Cai, X. and Characklis, G. W., 2006. Economic Engineering of Environmental and Water Resource Systems. *Journal of Water Resources Planning and Management*, 132(6), pp. 399-402

Macknick, J., Newmark, R., Heath, G. and Hallett, K. C., 2012. Operational Water Consumption and Withdrawal Factors for Electricity Generating Technologies: A Review of Existing Literature. *Environmental Research Letters*, 7(4), 10 pp.

Maulbetsch, J. S. and DiFilippo, M. N., 2006. Cost and value of water use at combined cycle power plants. California Energy Commission, PIER Energy-Related Environmental Research, CEC-500-2006-034

Mays, W. M. and Tung, Y.-K., 2002. *Hydrosystems Engineering and Management*. Highlands Ranch: Water Resources Publlications

McDermott, G. R. and Nilsen, O. A., 2014. Electricity Prices, River Temperatures, and Cooling Water Scarcity. *Land Economics*, 90(1), pp. 131-48

McKinney, D., Cai, X., Rosegrant, M. W., Ringler, C. and Scott, C. A., 1999. *Modelling Water Resources Management at the Basin Level: Review and Future Directions.* Colombo: International Water Management Institute

Medellìn-Azuara, J., Mendoza-Espinosa, L. G., Lund, J. R., Harou, J. J. and Howitt, R. E., 2009. Virtues of Simple Hydro-Economic Optimization: Baja-California, Mexico. *Journal of Environmental Management*, 90, pp. 3470-78

Mediterranean Water Scarcity and Drought Working Group, 2007. *Mediterranean Water Scarcity and Drought Report*. [pdf] Brussels: Mediterranean Water Scarcity and Drought Working Group. Available at: <http://www.emwis.net/topics/WaterScarcity/PDF/MedWSD_FINAL_Edition> [Accessed 30 March 2016]

MIBEL, 2016. *MIBEL*. [online] Available at: <http://www.mibel.com/index.php?mod=pags&mem=detalle&relmenu=9&relcategoria=1026&idpag=67> [Accessed 15 April 2016]

Miczek, J. E., 2008. Drought Could Shut Down Nuclear Power Plants. *Associated Press*, [online] 23 January. Available at: <http://www.nbcnews.com/id/22804065/ns/weather/t/drought-could-shut-down-nuclear-power-plants/#.VwT2Q49OJPY> [Accessed 6 April 2016]

Mikosch, T. V., Resnick, S. I. and Robinson, S. M., 2006. Linear Programming: The Simplex Method. In: *Springer Series in Operations Research and Financial Engineering*. New York: Springer. Ch. 2

MMA, 2007. *El Agua en la Economia Española: Situación y Perspectivas*. Madrid: Ministerio del Medio Ambiente

MMA, 2005. *Evaluación Preliminar de los Impactos en España por Efecto del Cambio Climático*. Madrid: Ministerio del Medio Ambiente

Mohseni, O., Stefan, H. G. and Erickson, T. R., 1998. A Nonlinear Regression Model for Weekly Stream Temperatures. *Water Resources Research*, 34(10), pp. 2685-92

Mousavi, H. and Ramamurthy, A. S., 2000. Optimal Design of Multi-Reservoir Systems for Water Supply. *Advances in Water Resources*, 23(6), pp. 613-24

Mukherjee, N., 1996. Water and Land in South Africa: Economywide Impacts of Reform - A Case Study for the Olifants River. Trade and Macroeconomics Division (TMD) Discussion Paper No. 12. International Food policy Research Institute, Washington D.C.

Nakiâcenoviâc, N., 2000. *Emission Scenarios. Special Report on Emissions Scenarios. A Special Report of Working Group III of the Intergovernmental Panel on Climate Change*. Cambridge: Cambridge University Press

Nandalal, K. D. W. and Bogardi, J. J., 2007. *Dynamic Programming Based Operation of Reservoirs: Applicability and Limits.* Cambridge: Cambridge University Press

Nash, J. E. and Sutcliffe, J. V., 1970. River Flow Forecasting through Conceptual Models, I-A. *Journal of Hydrology*, 10, pp. 282-90

Needham, J. T., Watkins, D. W. Jr., Lund, J. R. and Nanda, S. K., 2000. Linear Programming for Flood Control in the Iowa and Des Moines Rivers. *Journal of Water Resources Planning and Management*, 126(3), pp. 118-27

NETL, 2011. *Estimating Freshwater Needs to Meet Future Thermoelectric Generation Requirements – 2011 Update*. [pdf] South Park Township: U.S. Department of Energy, National Energy Technology Laboratory. Available at: <http://www.netl.doe.gov/energy-analyses/pubs/WaterNeeds2011.pdf> [Accessed 15 February 2016]

Noel, J. E., Gardner, B. D. and Moore, C. V., 1980. Optimal Regional Conjunctive Water Management. *American Journal of Agricultural Economics*, 62(3), pp. 489-98

Noel, J. E. and Howitt, R. E., 1982. Conjunctive Multibasin Management – An Optimal-Control Approach. *Water Resources Research*, 18(4), pp. 753-63

Olsson, G., 2012. *Water and Energy – Threats and Opportunities*. London: IWA Publishing

OMIE, 2016. *Resultados del Mercado. Operador del Mercado Iberico de Electricidad – Polo Español*. [online] Available at: <http://www.omie.es/files/flash/ResultadosMercado.swf> [Accessed 15 April 2015]

Pagnamenta, R., 2009. France Imports UK Electricity as Plants Shut. *The Times*, [online] 3 July. Available at: <http://www.thetimes.co.uk/tto/business/industries/utilities/article2198065.ece> [Accessed 6 April 2016]

Pereira, M. V. F. and Pinto, L. M. V. G., 1991. Multistage Stochastic Optimization Applied to Energy Planning. *Math Program*, 52, pp. 359-75

Pereira-Cardenal, S. J., Bauer-Gottwein, P., Arnbjerg-Nielsen, K. and Madsen, H., 2013. *A Framework for Joint Management of Regional Water-Energy Systems*. Ph.D. Thesis, DTU Environment, Kgs. Lyngby.

Pereira-Cardenal, S. J., Madsen, H., Arnbjerg-Nielsen, K., Riegels, N., Jensen, R., Mo, B., Wangensteen, I. and Bauer-Gottwein, P., 2014. Assessing Climate Change Impacts on the Iberian Power System Using a Coupled Water-Power Model. *Climatic Change*, 126, pp. 351-64

Pereira-Cardenal, S. J., Mo, B., Riegels, N. D., Arnbjerg-Nielsen, K. and Bauer-Gottwein, P., 2014. Optimization of Multipurpose Reservoir Systems Using Power Market Models. *Journal of Water Resources Planning and Management*, 141(8), pp. 04014100

Pilgrim, J. M., Fang, X. and Stefan, H. G., 1995. *Correlation of Minnesota Stream Water Temperatures with Air Temperatures*. Project Report 382. University of Minnesota, St. Anthony Falls Laboratory

Pùblico, 2011. *Medio Ambiente ve "riesgo" en la refrigeraciòn de Garoña*. [online] (07 April 2011) Available at: <http://www.publico.es/ciencias/medio-ambiente-ve-riesgo-refrigeracion.html> [Accessed 06 June 2016]

Pulido-Velazquez, M., Andreu, J., Sahuquillo, A. and Pulido-Velazquez D., 2008. Hydro-Economic River Basin Modelling: The Application of a Holistic Surface-Groundwater Model to Assess Opportunity Costs of Water Use in Spain. *Ecological Economics*, 66, pp. 51-65

Pulido-Velazquez, M., Andreu, J. and Sahuquillo, A., 2006. Economic Optimization of Conjunctive Use of Surface Water and Groundwater at the Basin Scale. *Journal of Water Resources Planning and Management*, 132(6), pp. 454-67

Quiroga, S., Garrote, L., Iglesias, A., Fernàndez-Haddad, Z., Schlickenrieder, J., de Lama, B., Mosso, C., and Sànchez-Arcilla, A., 2011. The Economic Value of Drought Information for Water Management Under Climate Change: A Case Study in the Ebro Basin. *Natural Hazards and Earth System Sciences*, 11, pp. 643-57

Randall, D., Cleland, L., Kuehne, C., Link, G. and Sheer, D., 1997. Water Supply Planning Simulation Model Using Mixed-Integer Linear Programming "Engine". *Journal of Water Resources Planning and Management*, 123(2), pp. 116-24

Rani, D. and Moreira M. M., 2009. Simulation-Optimization Modelling: A Survey and Potential Application in Reservoir Systems Operation. *Journal of Water Resources Management*, 24(6), pp. 1107-38

REE, 2014. *Boletìn Mensual. Febrero 2014*. [online] Available at: <http://www.ree.es/sites/default/files/downloadable/ree_febrero_2014.pdf> [Accessed 15 April 2016]

Ringler, C., von Braun, J. and Rosegrant, M. W., 2004. Water Policy Analysis for the Mekong River Basin. *Water International*, 29(1), pp. 30-42

Rio Carrillo, A. M. and Frei, C., 2009. Water: A Key Resource in Energy Production. *Energy Policy*, 37, pp. 4303-12

Rosegrant, M. W., Ringler, C., McKinney, D., Cai, X., Keller, A. and Donoso, G., 2000. Integrated Economic-Hydrologic Water Modelling at the Basin Scale: The Maipo River Basin. *Agricultural Economics*, 24(1), pp. 33-46

Rothlauf, F., 2011. *Design of Modern Heuristics – Principles and Application*. Berlin: Springer

Saad, M. P., Bigras, A. and Turgeon, R. D., 1996. Fuzzy Learning Decomposition for the Scheduling of Hydroelectric Power Systems. *Water Resources Research*, 32(1), pp. 179-86

Sadoff, C. and Grey, D., 2002. Beyond the River: The Benefits of Cooperation on International Rivers. *Water Policy*, 4, pp. 389-403

Savic, D., 2002. Single-Objective vs. Multiobjective Optimization for Integrated Decision Support. [online] Available at:

<http://www.iemss.org/iemss2002/proceedings/pdf/volume%20uno/399_savic.pdf > [Accessed 21 April 2016]

Scanlon, B. R., Duncan, I. and Reedy, R. C., 2013. Drought and the Water-Energy Nexus in Texas. *Environmental Research Letters*, 8(4), 045033 (14pp)

Schaefli, B., Hingray, B. and Musy, A., 2007. Climate Change and Hydropower Production in the Swiss Alps: Quantification of Potential Impacts and Related Modelling Uncertainties. *Hydrology and Earth System Sciences*, 11, pp. 1191-1205

Serageldin, I., 1995. Water Resources Management: A New Policy for a Sustainable Future. *International Journal of Water Resources Development*, 11(3), pp. 221-32

Serrat-Capdevila, A. and Valdés, J., 2007. An Alternative Approach to the Operation of Multinational Reservoir Systems: Application to the Amistad & Falcon System (Lower Rio Grande/Rio Bravo). *Journal of Water Resources Management*, 21(4), pp. 677-98

SHERPA, 2008. *Strategic Study for Development of Small Hydropower in the European Union*. [pdf] Available at: <http://www.esha.be/fileadmin/esha_files/documents/SHERPA/Strategic_Study_for_Development_of_SHP_in_EU.pdf> [Accessed 6 May 2016]

Sioshansi, F. P., 2008. Introduction: Electricity Market Reform – Progress and Remaining Challenges. In: Sioshansi, F. P., ed. 2008. *Competitive Electricity Markets: Design, Implementation, Performance*. Amsterdam: Elsevier. pp. 1-23

Sohn, P., 2011. River Temperature Forces Nuclear Plant to 50 Percent Power. *Times Free Press*, [online] 4 August. Available at: <http://www.timesfreepress.com/news/news/story/2011/aug/04/river-temperature-forces-plant-to-50-percent/55574/> [Accessed 6 April 2016]

Spanish National Institute of Statistics, 2008. *Water Statistics – The National Institute of Statistics' Brochure*. [INEbase > Agriculture and Environment > Water > Statistics on Water Usage > Results] INEbase [online] Available through: Instituto Nacional de Estadistica <http://www.ine.es/en/inebmenu/indice_en.htm> [Accessed 11 April 2016]

Stage, S. and Larsson, Y., 1961. Incremental Cost of Water Power. *Transactions of the American Institute of Electrical Engineers*, 80(3), pp. 361-64

Stucki, V. and Sojamo, S., 2012. Nouns and Numbers of the Water-Energy-Security Nexus in Central Asia. *International Journal of Water Resources Development*, 28(3), pp. 399-418

TEPCO, 2010. *Thermal Power Generation*. [online] (31 March 2010) Available at: <https://www4.tepco.co.jp/en/corpinfo/ir/kojin/generation/thermal-e.html> [Accessed 18 April 2016]

The World Data Bank, 2016. *World Development Indicators*. [Data > By Country > Spain > Databank] The World Data Bank [online] Available through: World DataBank <http://data.worldbank.org/> [Accessed 11 April 2016]

Tilmant, A., Goor, Q. and Pinte, D., 2009. Agricultural-to-Hydropower Water Transfers: Sharing Water and Benefits in Hydropower-Irrigation Systems. *Hydrology and Earth System Sciences*, 13, pp. 1091-101

Tilmant, A., Pinte, D. and Goor, Q., 2008. Assessing Marginal Water Values in Multipurpose Multireservoir Systems via Stochastic Programming. *Water Resources Research*, 44(12), pp. 1-17

Tu, M. Y., Hsu, N. S. and Yeh, W. W-G., 2003. Optimization of Reservoir Management and Operation with Hedging Rules. *Journal of Water Resources Planning and Management*, 129(2), pp. 86-97

Turgeon, A. and Charbonneau, R., 1998. An Aggregation-Disaggregation Approach to Long-Term Reservoir Management. *Water Resources Research*, 34(12), pp. 3585-94

U.S. Department of Energy, 2006. *Energy Demands on Water Resources – Report to Congress on the Interdependency of Energy and Water*. Washington D.C.

US Energy Information Administration, 2011. *Independent Statistics and Analysis, International Energy Statistics*. [online] Available at: <https://www.eia.gov/> [Accessed 6 April 2016]

US Energy Information Administration, 2016. *Frequently Asked Questions – What Is the Difference between Electricity Generation Capacity and Electricity Generation?* [online] (23 February 2016) Available at: <https://www.eia.gov/tools/faqs/faq.cfm?id=101&t=3> [Accessed 12 May 2016]

USGS (US Geological Survey), 2010. *Estimated Use of Water in the United States in 2010*. [online] Available at: <http://pubs.usgs.gov/circ/1405/pdf/circ1405.pdf> [Accessed 24 March 2016]

Valor, E., Meneu, V. and Caselles, V., 2001. Daily Air Temperature and Electricity Load in Spain. *Journal of Applied Meteorology and Climatology*, 40, pp. 1413-21

van der Linen, P. and Mitchell, J. F.B., 2012. *Climate Change and its Impacts: Summary of research and results from the ENSEMBLES project*. Exeter: Met Office Hadley Centre

van Meijgaard, E., van Ulft, L., van de Berg, W., Bosveld, F., van den Hurk, B., Lenderink, G. and Siebesma, A., 2008. *The KNMI Regional Atmospheric Climate Model RACMO Version 2.1*. De Bilt: KNMI

Van Vliet, M. T. H., Wiberg, D., Leduc, S. and Riahi, K., 2016. Power-generation System Vulnerability and Adaptation to Changes in Climate and Water Resources. *Nature Climate Change*, [online] Available at:

<http://www.nature.com/nclimate/journal/vaop/ncurrent/full/nclimate2903.html> [Accessed 23 March 2016]

Van Vliet, M. T. H., Yearsley, J. R., Ludwig, F., Vögele, S., Lettenmaier, D. P. and Kabat, P., 2012. Vulnerability of US and European Electricity Supply to Climate Change. *Nature Climate Change*, [online] Available at: <http://www.nature.com/nclimate/journal/v2/n9/full/nclimate1546.html> [Accessed 6 April 2016]

Vassolo, S. and Döll, P., 2005. Global-Scale Gridded Estimates of Thermoelectric Power and Manufacturing Water Use. *Water Resources Research*, 41(4), pp. n/a-n/a

Vedula, S. and Mujumdar, P. P., 1992. Optimal Reservoir Operation for Irrigation of Multiple Crops. *Water Resources Research*, 28(1), pp. 1-9

Vicuna, S., Leonardson, R., Hanemann, M. W., Dale, L. L. and Dracup, J. A., 2008. Climate Change Impacts on High Elevation Hydropower Generation in California's Sierra Nevada: A Case Study in the Upper American River. *Climatic Change*, 87, pp. S123-37

Vörösmarty, C. J., Green, P., Salisbury, J. and Lammers, R. B., 2000. Global Water Resources: Vulnerability from Climate Change and Population Growth. *Science*, 289, pp. 284-88

Wang, L., Fang, L. and Hipel, K. W., 2007. Mathematical Programming Approaches for Modelling Water Rights Allocation. *Journal of Water Resources Planning and Management*, 133(1), pp. 50-9

Wangensteen, I., 2012. *Power System Economics—The Nordic Electricity Market*. Trondheim: Tapir Academic Press

Weber, R., 2010. The Simplex Algorithm. In: Gowers, T., Barrow-Green, J. and Leader, I., eds. 2008. *Princeton Companion to Mathematics*. Princeton: Princeton University Press. Ch. III.84

Wikipedia, 2016. *Simplex Algorithm*. [online] Available at: <https://en.wikipedia.org/wiki/Simplex_algorithm> [Accessed 22 April 2016]

Williams, J. H. and Ghanadan, R., 2006. Electricity Reform in Developing and Transition Countries: A Reappraisal. *Energy*, 31, pp. 815-44

Wolfgang, O., Haugstad, A., Mo, B., Gjelsvik, A., Wangensteen, I. and Doorman, G., 2009. Hydro Reservoir Handling in Norway Before and After Deregulation. *Energy*, 34, pp. 1642-51

World Nuclear Association, 2016. *Reactor Database*. [online] Available at: < http://www.world-nuclear.org/information-library/facts-and-figures/reactor-database.aspx?source=%7B%22query%22%3A%7B%22filtered%22%3A%7B%22filter%22%3A%7B%22bool%22%3A%7B%22must%22%3A%5B%7B%22terms%22%3A%7B%22reactor.country.exact%22%3A%5B%22Spain%22%5D%7D%7D%5D%7D%7D%2C%22query%22%3A%7B%22match_all%22%3A%7B%7D%7D%7D%7D%2C%22size%22%3A25%2C%22sort%22%3A%5B%7B%22index.sort_name.exact%22%3A%7B%22order%22%3A%22asc%22%7D%7D%5D%7D> [Accessed 1 February 2016]

Wriedt, G., Van der Velde, M., Aloe, A. and Bouraoui, F., 2009. Estimating Irrigation Water Requirements in Europe. *Journal of Hydrology*, 373, pp. 527-44

WWAP (United Nations World Water Assessment Programme), 2014. *The United Nations World Water Development Report 2014: Water and Energy*. Paris: UNESCO

Yakowitz, S., 1982. Dynamic-Programming Applications in Water-Resources. *Water Resources Research*, 18, pp. 673-96

Young, R. A. and Loomis, J. B., 2014. *Determining the Economic Value of Water. Concepts and Methods*. 2nd ed. New York: RFF Press

Appendix A

Supplements for Case Study: ArcGIS

A.1 Hydropower Watersheds Delineation in ArcGIS 10

In order to digitally delineate the 123 hydropower watersheds constituting the modelled area in ArcGIS 10, the following procedure was followed.

Firstly, the required data was obtained, which includes a Digital Elevation Model (DEM), a stream network and a hydropower plants file for the area of interest (IP in this case). The former was provided by the European Environment Agency (2012), whereas the last two were obtained from Pereira-Cardenal et al. (2013)'s ArcGIS dataset. Then, the following steps were carried out:

1) Creation of a **depressionless DEM**:
   The ***Fill*** tool in the ***ArcToolbox > Spatial Analyst Tools > Hydrology*** toolbox was used to remove any imperfections (sinks) in the DEM. A sink is a cell that does not have an associated drainage value, which in turn indicates the direction of the water flowing out of a cell. Drainage values are assigned during the creation process of a flow direction grid (Step 2).
   The following parameters were entered the ***Fill*** tool:

   Input Surface Raster: DEM grid

   Output Surface Raster: DEM filled (in the same working directory as the input surface raster)

2) Creation of a **flow direction grid**:
   A flow direction grid assigns a value to each cell to indicate the direction of flow, i.e. the direction that flowing water will follow from that particular cell according to the underlying topography of the landscape.
   The ***Flow Direction*** tool in the ***ArcToolbox > Spatial Analyst Tools > Hydrology*** toolbox was used and the following parameters were given as input:

   Input Surface Raster: DEM filled (Step 1)

   Output Flow Direction Raster: DEM flow (in the same working directory as the input surface raster)

3) Creation of a **flow accumulation grid**:

A flow accumulation grid determines each cell's flow accumulation value by the number of upstream cells flowing into it, based on landscape topography.
The ***Flow Accumulation*** tool in the ***ArcToolbox > Spatial Analyst Tools > Hydrology*** toolbox was used and the following parameters were given as input:

Input Flow Direction Raster: DEM flow (Step 2)

Output Flow Direction Raster: DEM accumulation (in the same working directory as the input flow direction raster)

4) Snapping **pour points**:
After loading the shapefile containing pour point (i.e. hydropower reservoirs) locations, the ***Snap Pour Point*** tool in the ***ArcToolbox > Spatial Analyst Tools > Hydrology*** toolbox was used in order to: (i) snap the loaded pour points to the closest cell of high flow accumulation to account for any error during placement; (ii) convert the pour points to raster format for input to the Watershed tool (Step 5).
The following parameters were entered the ***Snap Pour Point*** tool:

Input Raster or *Feature Pour Point Data:* Hydropower Reservoirs Shapefile

Input Accumulation Raster: DEM accumulation (Step 3)

Output Raster: DEM snapped (in the same working directory as the input accumulation raster)

Snap Distance: 2500 m. The snap distance identifies the specified distance (in map units, i.e. meters) that the tool will use to search for the cell with the highest flow accumulation value around the pour points. The snap distance is based on the resolution of the data and it required some trial and error to determine its best value

5) **Watersheds Delineation**:
The ***Watershed*** tool in the ***ArcToolbox > Spatial Analyst Tools > Hydrology*** toolbox was used and the following parameters were given as input:

Input Flow Direction Raster: DEM flow (Step 2)

Input Raster or *Feature Pour Point Data:* Hydropower Reservoirs Shapefile (Step 4)

Output Raster: HP Watersheds Raster (in the same working directory as the input raster)

6) Conversion of **watershed rasters to polygons**:
The ***Raster to Polygon*** tool in the ***ArcToolbox > Conversion Tools > From Raster*** toolbox was used and the following parameters were given as input:

Input Raster: HP Watersheds Raster (Step 5)

Output Polygon Features: HP Watersheds (in the same working directory as the input raster)

A.2 Crop Water Demand per Watershed in ArcGIS 10

In order to downscale the annual *CWD* data for the whole IP to each watershed in ArcGIS 10, the following procedure was followed.

Firstly, the required data was obtained, which includes a raster *CWD* dataset over the entire Peninsula and a shapefile containing the 123 watersheds delineation. The former was acquired from Wriedt et al. (2009)'s dataset for Europe, the latter from Pereira-Cardenal et al. (2013)'s ArcGIS dataset. Then, a zonal statistics table was calculated through the ***Zonal Statistics as a Table*** tool in the ***ArcToolbox > Spatial Analyst Tools > Zonal*** toolbox. This tool aggregated the value of the *CWD* raster within each zone delineated by the watershed shapefile and reported the results to a table. The following parameters were entered the ***Zonal Statistics as a Table*** tool:

Input Raster or Feature Zone Data: Watersheds shapefile

Zone Field: Watershed ID

Input Value Raster: CWD

Output Table: CWD per watershed

Statistics Type (Optional): Sum.

The same procedure can be applied to the computation of irrigated area [km^2] per watershed. The only difference is in the input value raster entering the ***Zonal Statistics as a Table*** tool:

Input Raster or Feature Zone Data: Watersheds shapefile

Zone Field: Watershed ID

Input Value Raster: Irrigated Area

Output Table: Irrigated Area per watershed

Statistics Type (Optional): Sum

Appendix B

Supplements for Case Study: Input Data

B.1 Rainfall-Runoff Model

The downscaling procedure of Pereira-Cardenal et al. (2013)'s runoff dataset consisted of three subsequent steps, of which the first two were carried out in the software ArcGIS 10:

1. Computation of runoff intensity [$m^3/sec/km^2$] from Pereira-Cardenal et al. (2013)'s rainfall-runoff model output;
2. Integration of runoff intensity (Step 1) over each watershed area [km^2]. A simulated runoff series [m^3/sec] was thus calculated per watershed;
3. Weekly aggregation of the runoff computed at Step 2.

B.2 Evaluation of Air-River Water Temperature Function

Linear regression models have been broadly applied to successfully simulate stream temperatures with air temperatures above 0°C (e.g. Pilgrim et al., 1995; Erickson et al., 1996). However, Mohseni et al. (1998) stated that at the highest and lowest air temperatures, the water/air temperature relationship does not usually remain linear. In particular, they found out that the weekly water/air temperature relationship well follows the profile of a continuous S-shaped function, which was also applied to this study. Among this broad class of functions, a logistic one was chosen since its parameters are the most stable; among different types of logistic functions, the following was selected as its parameters are more stable than others' (Mohseni et al., 1998):

$$T_r = \mu + \frac{\alpha - \mu}{1 + e^{\gamma(\beta - T_a)}} \quad \text{(B-1)}$$

where T_r and T_a are estimated river temperature (°C) and measured air temperature (°C) respectively. The four parameters α, β, γ and μ all have a physical meaning (Table B-1). Their numerical values were estimated using both air and water temperature observations of the Duero. These data were measured by several stations along the river and collected from Confederaciòn Hidrogràfica del Duero (2016) for all the years from 2007 up to 2014 (2011 and 2013 did not have any recorded data).

Figure B-1 displays the S-shaped curve fitting the data, later employed to estimate water temperature time series of the seven rivers in the IP.

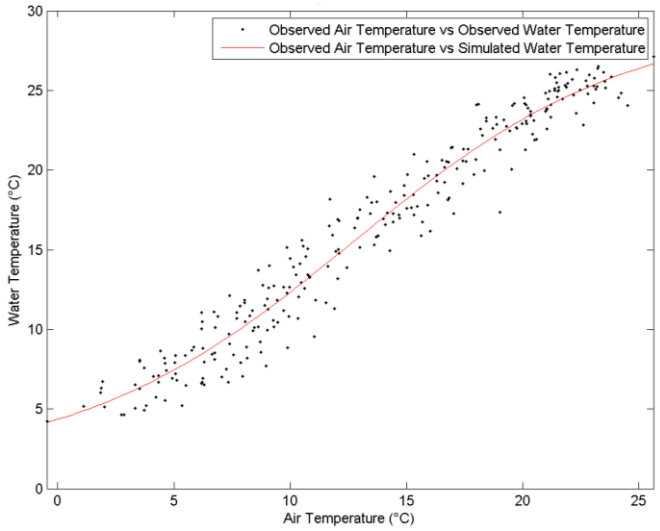

Figure B-1: Logistic function fitting the air-water temperature observations of the Duero. The black dots identify the measurements, whereas the red line shows the goodness of fit of the logistic function to the data. The values of the four parameters characterizing this curve are summarized in Table 13-1. Data source: Confederaciòn Hidrogràfica del Duero (2016).

Table B-1: Physical meaning and estimated numerical values of the four parameters constituting the logistic function implemented in the model.

Param	Definition	Numerical Value
α	Estimated max river temperature	29.49 [°C]
β	Air temperature at the inflection point	12.66 [°C]
γ	Steepest slope of the function	0.17 [-]
μ*	Estimated min river temperature	1.3925 [°C]

*Added to generate nonzero minimum water temperatures.

The red line fitting the observations graphically represents the aforementioned logistic function equation and is characterized by the four estimated parameters values summarized in Table B-1. It also gives a visual idea of the goodness of fit between the estimated function and the air-water temperature measurements.
Mathematically, the goodness of fit was estimated through the Nash-Sutcliffe coefficient (NSC)[15] (Nash et al., 1970), which resulted to be equal to 0.9547 (an NSC equal to 1 represents a perfect fit).

Because of lack of data, it was assumed that all the river basins present the same air-water temperature pattern. Thus, the estimated parameters for the Duero (but river-specific air temperature data) were employed to estimate the water temperature of all the rivers in the IP, through a three-steps procedure:

1. Collection of air temperature data for the seven river basins from MIKE (Pereira-Cardenal et al. (2013)'s dataset);

[15]It is also known as the coefficient of determination or the efficiency of the fit and is specified as follows (Mohseni et al., 1998): $NSC = 1 - \sum_{i=1}^{n}\left(T_{sim_i} - T_{obs_i}\right)^2 / \sum_{i=1}^{n}(\overline{T_{obs}} - T_{obs_i})^2$. T_{sim} is the estimated water temperature of the Duero (identified by the red curve in Figure B-1), T_{obs} its observed water temperature and $\overline{T_{obs}}$ its average observed water temperature.

2. Estimation of the rivers water temperature through the air temperature measurements (Step 1) and the air-water temperature sigmoid function, characterized by the estimated parameters in Table B-1;
3. Weekly aggregation of the rivers water temperature computed at Step 2.

B.3 Hydropower Reservoirs

The three main parameters characterizing the 116 modelled actual hydropower plants were computed as follows:

- **Local energy equivalent *y*** [KWh/m^3] of a single hydropower reservoir:

$$y = \rho * \varphi * h * \eta * \gamma \quad \text{(B-2)}$$

  where ρ is the water density [kg/m^3], φ is the gravitational constant [m/s^2], *h* is the reservoir head [m], η is the plant's efficiency and γ is the appropriate conversion factor.
  Pereira-Cardenal et al. (2013) have already computed all the *y* values for all the modelled hydropower plants in the IP. Thus, the same data were used in this study without any changes;

- **Installed capacity** [MW] of a single hydropower reservoir. It was converted into maximum turbinated flow [Hm^3/week] according to the following formula:

$$MaxTF = \left(\frac{InstCap*24*7}{y*10\text{^}(-3)}\right) * 10\text{^}(-6) \quad \text{(B-3)}$$

  where *MaxTF* is the maximum turbinated flow of a given hydropower plant, *InstCap* is its installed capacity turned into [MWh/week] and *y* is its local energy equivalent transformed into [MWh/m^3]. In the end, the ratio is converted from [m^3/week] to [Hm^3/week];

- **Maximum and minimum storage** [Hm^3] of a single hydropower reservoir. The latter has been subtracted from the former in order to obtain only one storage capacity [Hm^3] per hydropower plant.

B.4 Irrigation Demand

Irrigation water demand per watershed was computed through a four-steps procedure:

1. Collection of precipitation data [mm/day] for the seven river basins from MIKE (Pereira-Cardenal et al. (2013)'s dataset) and its aggregation into [mm/week];
2. Computation of irrigated area [km^2] per watershed. The irrigated surface data for the whole IP was obtained from Wriedt et al. (2009)'s raster dataset. It was then downscaled to each watershed area, following the same procedure presented in Appendix A.2;

3. Integration of the precipitation [mm/week] (Step 1) over each watershed irrigated area [km^2] (Step 2). The volume of precipitation feeding the crops per watershed was thus calculated [Hm^3/week];
4. Subtraction of the precipitation volume computed at Step 3 from weekly *CWD* data, in order to obtain *IWD* [Hm^3/week] per watershed.

B.5 Thermal Power Plants

The thermal power plants modelled are characterized by several parameters.
Among them, **thermal efficiency (%)** was calculated on a gross output basis using net calorific values (NVC) (IEA, 2008). 'Gross output' refers to the overall 'generated' power, without any deduction for the power plant's own-use; the NCV assumes that water in the combustion products is not condensed, so latent heat is not recovered (IEA, 2010).
In particular, nuclear thermal efficiencies were computed as follows:

$$Eff_n = \frac{DC}{TC} * 100\% \quad \text{(B-4)}$$

where Eff_n is the thermal efficiency (%) of a particular nuclear thermal power plant, *DC* is its Design Capacity or Gross Capacity (MW) and *TC* is its Thermal Capacity (MWt).
This equation was directly inferred from the definition of thermal efficiency given by IEA (2010): "'Thermal efficiency' is strictly defined as the useful output energy for a given quantity of gross input heat energy".

B.6 Thermal Power Plants Aggregation

Table B-2: Characteristics of the 15 aggregated thermal power plants modelled in this study.

Aggregated TPP Name	Design Capacity [MW]	Fuel Type	Type of Cooling	*e* [-]	*b* [-]	Marginal Cost [€]	Main River*
Almaraz	2093	Nuclear	Once-through	0.36	0.27	0.018	1
Asco	2068	Nuclear	Cooling tower	0.35	0.99	0.018	1
Castejon+Arrubal	2055	CCGT	Cooling tower	0.50	1.00	0.057	1
Escatron+ Castelnou	1929	Mix	Mix	0.69	0.60	0.057	1
Acceca	1579	Mix	Cooling tower	0.43	1.00	0.057	1
Pego	1458	Mix	Cooling tower	0.45	1.00	0.057	1
Jose and Trillo	1226	Nuclear	Mix	0.34	0.99	0.018	1
Escucha Teruel	1210	Coal	Mix	0.38	0.89	0.057	0
Cofrentes	1102	Nuclear	Cooling tower	0.34	0.99	0.018	1
Compostilla+ Anllares	1058	Coal	Mix	0.38	0.75	0.057	1
Puertollano	670	Mix	Cooling tower	0.44	1.00	0.057	0
La Robla	655	Coal	Cooling tower	0.38	1.00	0.057	0
Velila	516	Coal	Mix	0.38	0.76	0.057	0
Santa Maria de Garona	466	Nuclear	Once-through	0.34	0.27	0.018	1
Puente Nuevo-3	324	Coal	Once-through	0.38	0.21	0.057	0

*1 means that the thermal power plant is located on the main river, 0 is not.

B.7 Residual Thermal Power Supply Curve

Marginal costs (i.e. production costs) of each non-modelled power producer at different production levels are needed in order to construct the residual thermal power supply curve. However, in a competitive power market this information is strictly confidential and not

available to the general public. Therefore, it is generally deduced from the hourly market results data collected (i.e. production (MWh) and price (€/MWh), which represent the marginal cost of the marginal producer (Pereira-Cardenal et al., 2014)). These data can be seen as points of the supply curve. In particular, daily data from 2008 up to 2015 (OMIE, 2016) were used to calculate weekly power production and the corresponding average price of residual thermal generators (Figure B-2). As Pereira-Cardenal et al. (2014) stated, data from 2009 were not taken into account, since they presented a different pattern than the other years (i.e. lower electricity prices). This could be due to a significantly lower global oil price in 2009 (US$ 57.2/barrel compared to US$ 88.7/barrel on average in the other years), which also affects the price of natural gas.

Since the purpose is to model the remaining 50% of thermal power production, special regime[16] and hydropower contributions were subtracted from the dataset, before computing the supply curve through a linear regression. This was achieved using the electricity production per category data from OMIE (2016). The modelled 50% of thermal power production was also subtracted. This was done by multiplying the entire thermal power production by a factor of 0.5 and keeping the same corresponding average market price. This procedure assumes that the modelled thermal generators are uniformly spread across the power production and price dataset.

[16]Group of generation technologies that includes approximately 60% renewable and is always cleared regardless of the market price (Pereira-Cardenal et al., 2014).

In the end, a residual thermal power supply curve was obtained and displayed in Figure B-2.

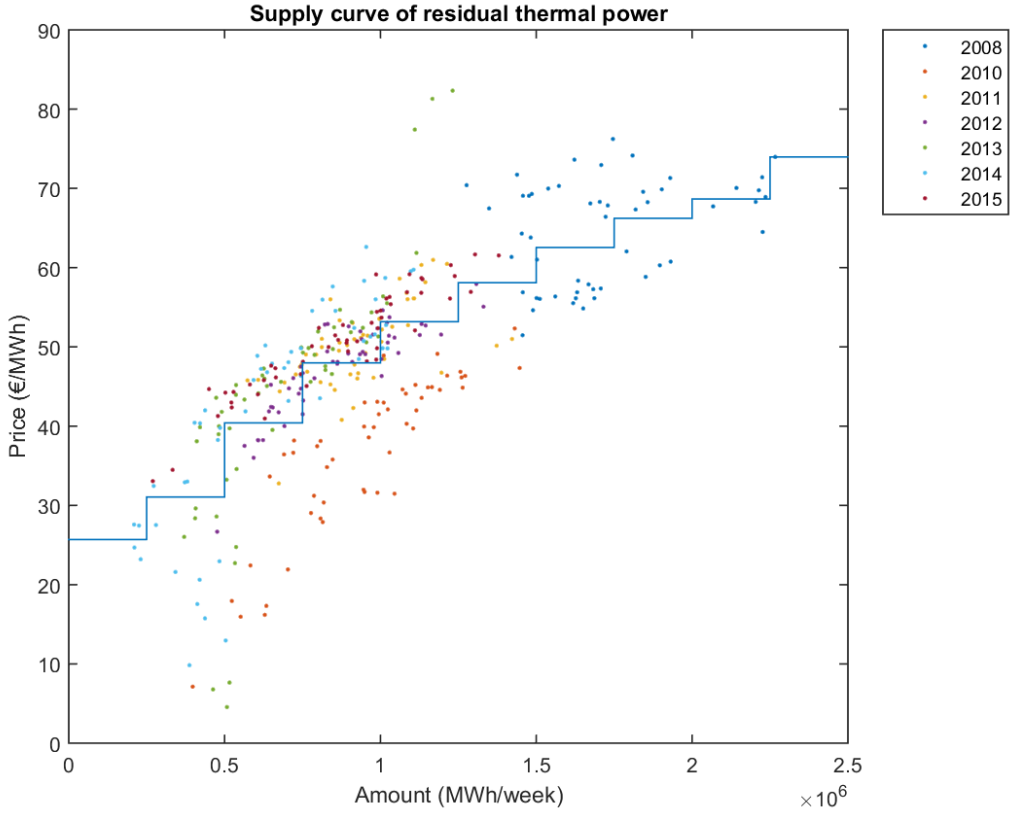

Figure B-2: Residual thermal power supply curve. The colored dots represent the weekly averaged market clearing results from 2008 up to 2015. 2009 was excluded. The x-axis presents the amount of electricity [MWh/week] sold on the market, while the y-axis the clearing price [€/MWh]. Special regime, hydropower and half of the thermal production have been subtracted.

B.8 Climate Change

Figure B-3 and Figure B-4 display the monthly precipitation and temperature CFs over the IP respectively.

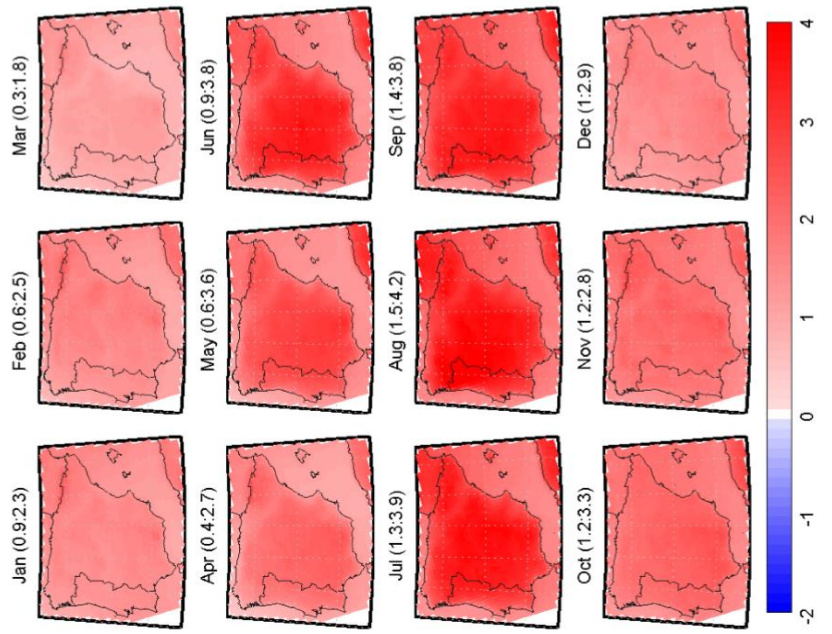

Figure B-4: Temperature change factors 2036-2065 (future scenario) v. 1961-1990 (control scenario) [°C]. The numbers in parenthesis show the minimum and maximum CFs value calculated (Pereira-Cardenal et al., 2013).

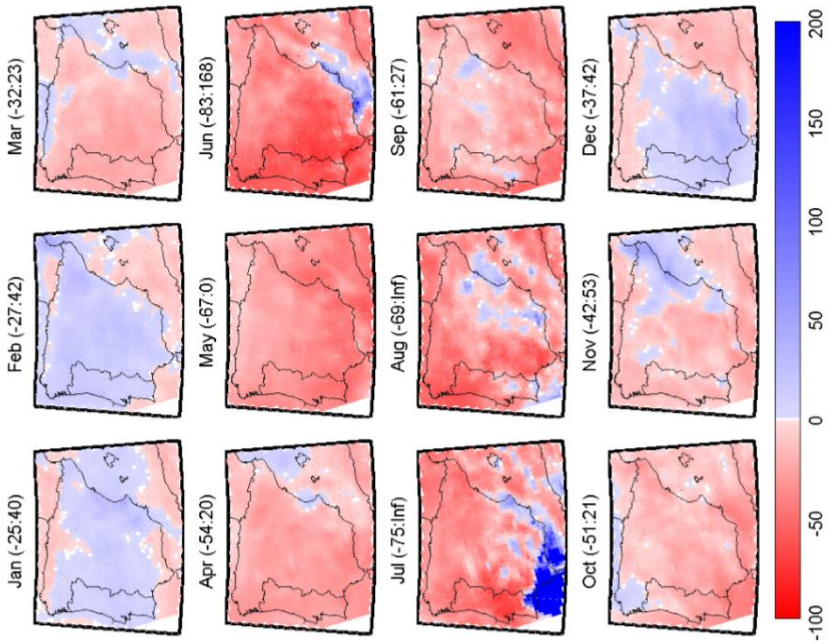

Figure B-3: Precipitation change factors 2036-2065 (future scenario) v. 1961-1990 (control scenario) [%]. The numbers in parenthesis show the minimum and maximum CFs value calculated (Pereira-Cardenal et al., 2013).

Appendix C

Supplements for Models and Methods

C.1 Network and Flow Path Matrix Construction

Firstly, an explanatory example of how the implemented flow path model works is presented. A simple case is considered, characterized by: (a) two in line watersheds; (b) one hydropower plant (HPP) delimiting the upstream watershed; (c) a basin outlet delineating the downstream watershed; (d) one thermal power plant (TPP) in the downstream watershed; (e) one agricultural demand per watershed. Figure C-1 shows both the conceptual model and the flow path representation.

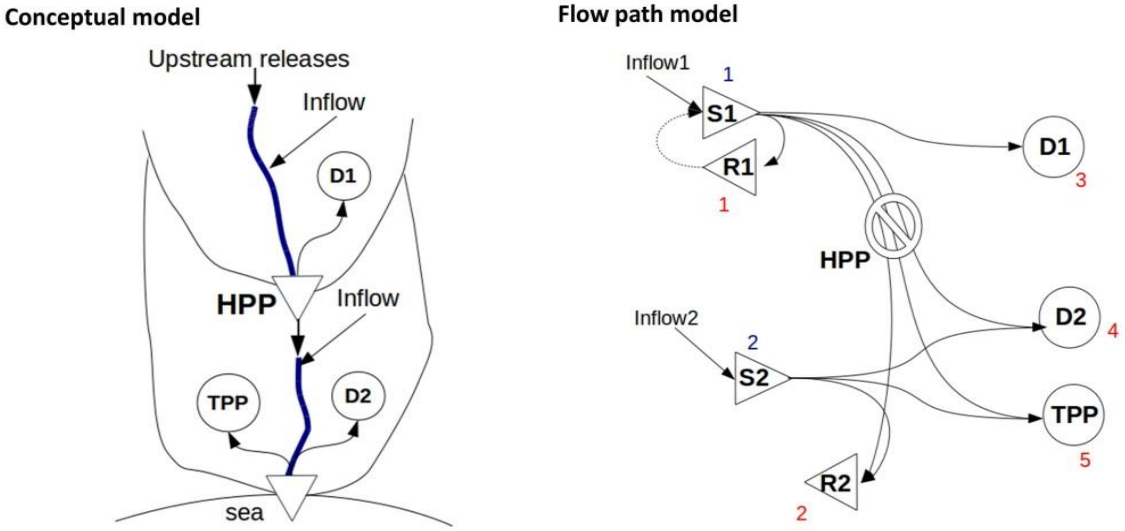

Figure C-1: Conceptual and flow path-based model of a fictitious river basin. The two black thin lines represent the two watersheds, whereas the blue thick one the main river. In the flow path model, the red numbers (1, 2, 3, 4, 5) identify the sink nodes, whereas the blue ones (1, 2) the source nodes.

In this simplified, flow path-based water distribution system, it can be observed that each upstream source node is connected to the downstream receiving ones through a different flow path (i.e. black continuous arrow). Overall, eight flow paths represent this distribution network. The source nodes are represented by the two reservoirs (S1 and S2), whereas the sink ones are the two demands (D1 and D2), the hydropower reservoir (R1), the thermal power plant (TPP) and the sea (R2). As already mentioned in Section 9.2.1, the runoff is not considered as a source node, thus a dotted black arrow flowing into the two reservoirs symbolizes it.

This sample model representation can be extended to all the river basins of the IP. For instance, the type of sources and sinks implemented at a basin scale remains unchanged compared to the simplified, smaller scale considered above. The only difference is the number of flow paths, sources and sinks, which increases significantly at a bigger scale.

Network and Flow Path Matrix

A network matrix was created in order to represent the node-to-node linkage in the water distribution system, i.e. the spatial connection between source and sink nodes. In this study, a network matrix M made of ones and zeros was built per river basin (seven matrices in total), whose dimensions are *i x j* and where:

$$M_{i,j} = \begin{cases} 1, & \forall\ sink\ node\ j\ downstream\ of\ source\ node\ i \\ 1, & \forall\ sink\ node\ j\ equal\ to\ source\ node\ i \\ 0, & otherwise \end{cases}$$

$$where\ i \in [1, \dots, So]\ ;\ j \in [1, \dots, Si] \qquad \text{(C-1)}$$

The rows of M represent the source nodes *i* (i.e. hydropower and synthetic reservoirs), whereas the columns denote the sinks *j* (i.e. hydropower reservoirs, sea, water demands and thermal power plants) in each catchment. The total number of sources and sinks in each basin is *So* and *Si* respectively. Thus, the dimensions of M change from one river basin to the other, according to the number of sources and sinks located in each one of them.

The seven network matrices have been automatically generated in Matlab using Pereira-Cardenal et al. (2013)'s Connectivity Matrices CM as a starting point. Their connectivity matrices only refer to the hydropower and fictitious reservoirs in each river basin and are made of zeros, ones (on the main diagonal only) and negative ones. There are seven CMs provided (one per river basin), each one of which has been built as follows:

$$CM_{i,j} = \begin{cases} -1, & \forall\ row\ node\ i\ connected\ downstream\ to\ column\ node\ j\ (\forall\ i \neq j) \\ 1, & \forall\ row\ node\ i\ equal\ to\ column\ node\ j\ (\forall\ i = j) \\ 0, & otherwise \end{cases}$$

$$where\ i, j \in [1, \dots, p]^2 \qquad \text{(C-2)}$$

Thus, every CM is a *p x p* matrix, where *p* is the number of hydropower and synthetic reservoirs in a certain river basin. The order of the reservoirs on the rows and columns of a single CM is the same.

The network matrix, mathematically representing the simplified flow path model in Figure C-1, is summarized in Table C-1.

Table C-1: Network matrix M mathematically implementing the simplified flow path-based scheme presented in Figure C-1.

			Sinks ID				
			1	2	3	4	5
			HPP (R1)	Sea (R2)	D1	D2	TPP
Sources ID	1	HPP (S1)	1	1	1	1	1
	2	Sea (S2)	0	1	0	1	1

As can be noticed, a reservoir sink, water demand and thermal power plant belonging to a certain watershed are considered as sinks with regard to the reservoir source located in the same watershed. This means that a reservoir delineating a watershed can supply water also to the sinks in its same watershed, and not only to the downstream ones. For example, if source S2 is considered, its sinks are embodied by the sea (R2), water demand D2 and thermal power plant TPP, which are all located in the same watershed as the source S2 itself.

After computing the network matrices, a Flow Path (FP) matrix is calculated in order to define all the possible flow paths in each river basin of the water distribution network. Thus, seven FP matrices have been computed in total. All the feasible water delivery routes in one catchment are evaluated by looping through the rows in M (i.e. sources) and searching for sinks (columns) either in the same watershed or in the ones downstream. The so-computed FP matrix has two columns (sources and sinks respectively) and as many rows as all the possible flow paths (i.e. delivery routes or links) identified in a certain river basin. Each row presents a source ID and a sink ID in the first and second column respectively, as the ones identified in Table C-1.

This FP matrix generation methodology is based on five assumptions: (i) the water can follow only one possible route to flow from a source to one of its sink nodes; (ii) the water flows from a certain source to all its potential sinks in one time step; (iii) there are no loops in the water distribution system (see Section 9.2.1); (iv) the hydropower turbines do not consume any water; (v) the FP matrix does not include the carryover storage temporal arc, since it is meant to describe the physical distribution network only. The carryover storage will be taken into account in the constraint set, discussed in Section 9.2.3.

The FP matrix, mathematically representing the simplified flow path model displayed in Figure C-1, is summarized in Table C-2.

Table C-2: Flow Path (FP) matrix, mathematically implementing the simplified flow path-based scheme discussed in Figure C-1. The sources ID and the sinks ID are the blue and red ones used in Table C-1 respectively.

Sources ID	Sinks ID
1	1
1	2
1	3
1	4
1	5
2	2
2	4
2	5

As can be noticed, all the sinks with regard to source 1 are evaluated before moving onto the next source.

C.2 Linear Programming

Marginal Costs

Table C-3 summarizes the numerical values of the marginal costs multiplying the decision variables in the objective function and employed in the model.

Table C-3: Summary of the numerical values of the costs appearing in the objective function and used in this study.

Marginal Costs			
FPC	0		
IDCC (€/m³)	0.32	Tajo	River Basin
	0.24	Ebro	
	0.14	Duero	
	0.25	Guadalquivir	
	0.28	Guadiana	
	0.36	Jucar	
	0.38	Miño-Sil	
TFC	0		
TC (€/MWh)	18	Nuclear	Fuel Type
	57	Coal/CCGT	
RC (€/MWh)	25.70	250,000	Generator Capacity (MWh/week)
	31.06	250,000	
	40.41	250,000	
	47.97	250,000	
	53.17	250,000	
	58.10	250,000	
	62.54	250,000	
	66.23	250,000	
	68.66	250,000	
	73.96	250,000	

Construction of Constraints Matrices

Figure C-2 shows the A, A_{eq} and b, b_{eq} matrices associated to the example presented in Appendix C.1. They reflect the equality and inequality constraints discussed in Section 9.2.3 and are built for a single time step and a single basin.

Aeq	**Allocations**								**Deficits**		**TF**	**Waste heat**		**beq**
Constraints / decision variables	*11*	*12*	*13*	*14*	*15*	*22*	*24*	*25*	*d1*	*d2*	*TF*	*Hw*		
*mass balance 1**	1	1	1	1	1	0	0	0	0	0	0	0		Inflow1
*mass balance 2**	0	0	0	0	0	1	1	1	0	0	0	0		Inflow2
demand deficit 1	0	0	1	0	0	0	0	0	1	0	0	0		dem1
demand deficit 2	0	0	0	1	0	0	1	0	0	1	0	0	·x =	dem2
cooling water consumption	0	0	0	0	1	0	0	1	0	0	0	$\frac{-b}{\rho \cdot Le^*}$		0
power equilibrium	0	0	0	0	0	0	0	0	0	0	y	e		Pdem

A														**b**
Constraints / decision variables	*11*	*12*	*13*	*14*	*15*	*22*	*24*	*25*	*d1*	*d2*	*TF*	*Hw*		
HPP max storage	1	0	0	0	0	0	0	0	0	0	0	0		HPScap
HPP available flow	-1	-1	-1	-1	-1	0	0	0	0	0	1	0		0
max turbinated flow	0	0	0	0	0	0	0	0	0	0	1	0	·x <	HPcap
max waste heat	0	0	0	0	0	0	0	0	0	0	0	1		TPcap·(1-e)/e
cooling water req.	0	-1	0	-1	0	-1	-1	-1	0	0	0	$\frac{1-b}{\rho \cdot cp \cdot dT} + \frac{b}{\rho \cdot Le^*}$		0

Figure C-2: *A*, *Aeq* and *b*, *beq* matrices associated to the example in Appendix C.1. *d1* and *d2* stand for demand deficits, *TF* turbinated flow and H_w waste heat decision variables. *y* is the energy equivalent of the HPP and *e* is the thermal efficiency of the TPP.

*Carryover storage is not represented, since a single time step is modelled.

River Basin and Time Step Aggregation

Aeq and *A* matrices are constructed time step per time step, basin per basin. The example refers to the building procedure of *Aeq* matrix only. However, the same considerations can be applied to *A* matrix also. The only exception is represented by the carryover storage and the power equilibrium constraint, which do not appear in the *A* matrix.

Since different river basins are hydrologically independent, the constraints are applied to each basin independently. Power equilibrium constraint represents the only exception, as it links different basins together. Thus, *Aeq* matrix is firstly built basin per basin, then it is aggregated over several basins. In the end, power market equality constraint is added at the last line of the aggregated *Aeq* matrix, as displayed in Figure C-3.

Afterwards, *Aeq* and *A* matrices have to be aggregated over different time steps.

Most of the time-dependent elements in the constraints (e.g. inflow, water and power demand) are in the *beq* matrix. Thus, only the few time varying elements in the *Aeq* matrix have to be updated at each time step (here, only water temperature). In the end, the global *Aeq* matrix is constructed by assembling the individual time step matrices, as shown in Figure C-3.

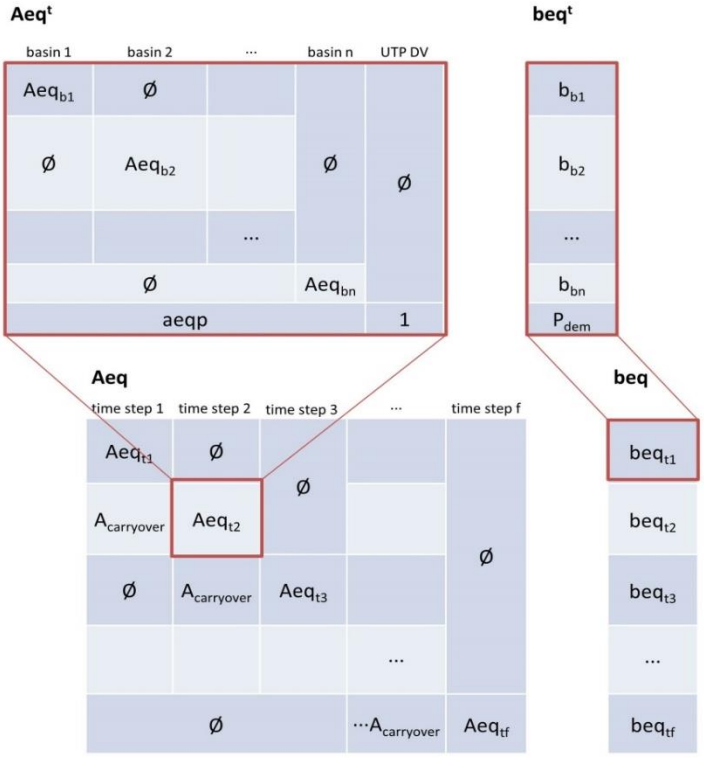

Figure C-3: Construction of the global equality constraint matrix (Aeq and beq) basin per basin and time step per time step. *Ø* represents an empty matrix, *UTP DV* the unconstrained thermal power production decision variable (which consists of several decision variables), while *aeqp* the power market equilibrium equality constraint.

The only connection between subsequent time steps is the carryover storage, which is the water made available from a given HPP sink to the same HPP source from one time step to the next one (according to the mass balance equality constraint). The first time step differs from the others as there is no carryover from a previous time step; an initial storage can be set instead. Similarly, a final storage can be forced at the last time step.

Appendix D

Supplements for Results and Discussion

D.1 Climate Change

CLM

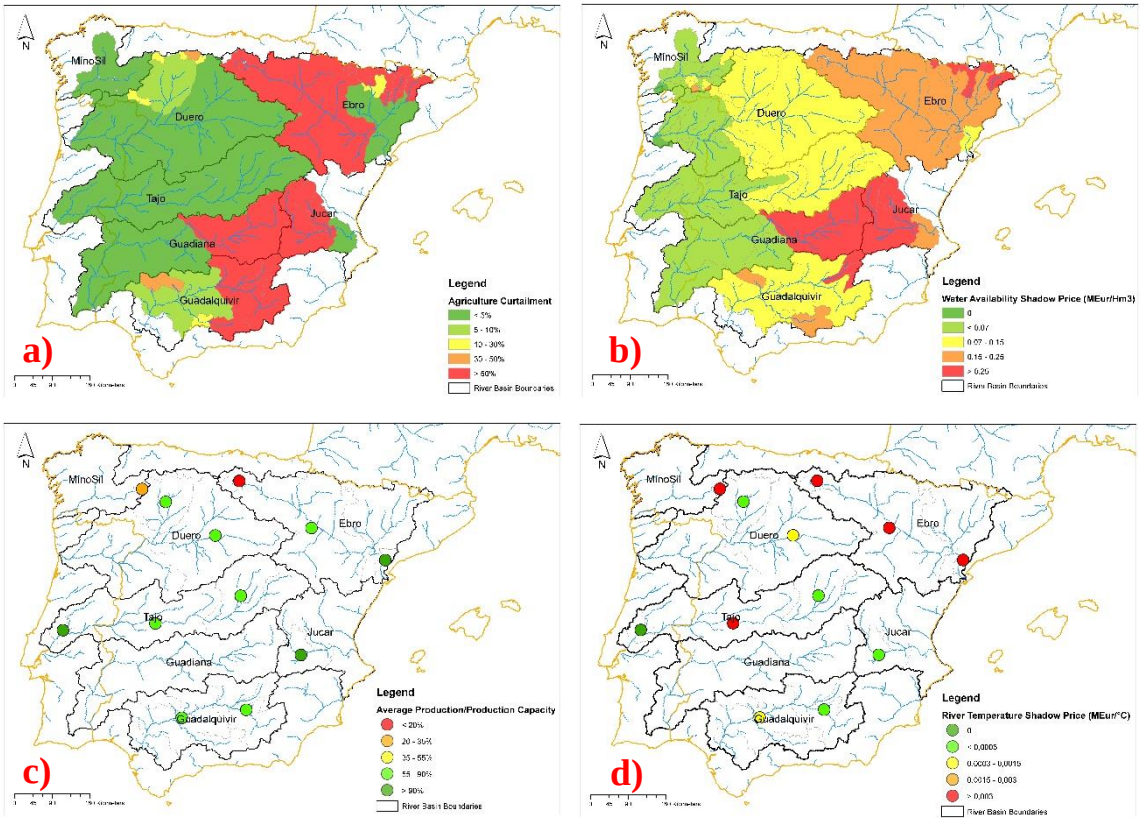

Figure D-1: a) Agriculture curtailment (%) per watershed; (b) Water availability shadow price (M€/Hm^3) per watershed; Ratio between average production and production capacity of each modelled thermal power plant; (d) River water temperature shadow price (M€/°C) per modelled thermal generator.

RACMO

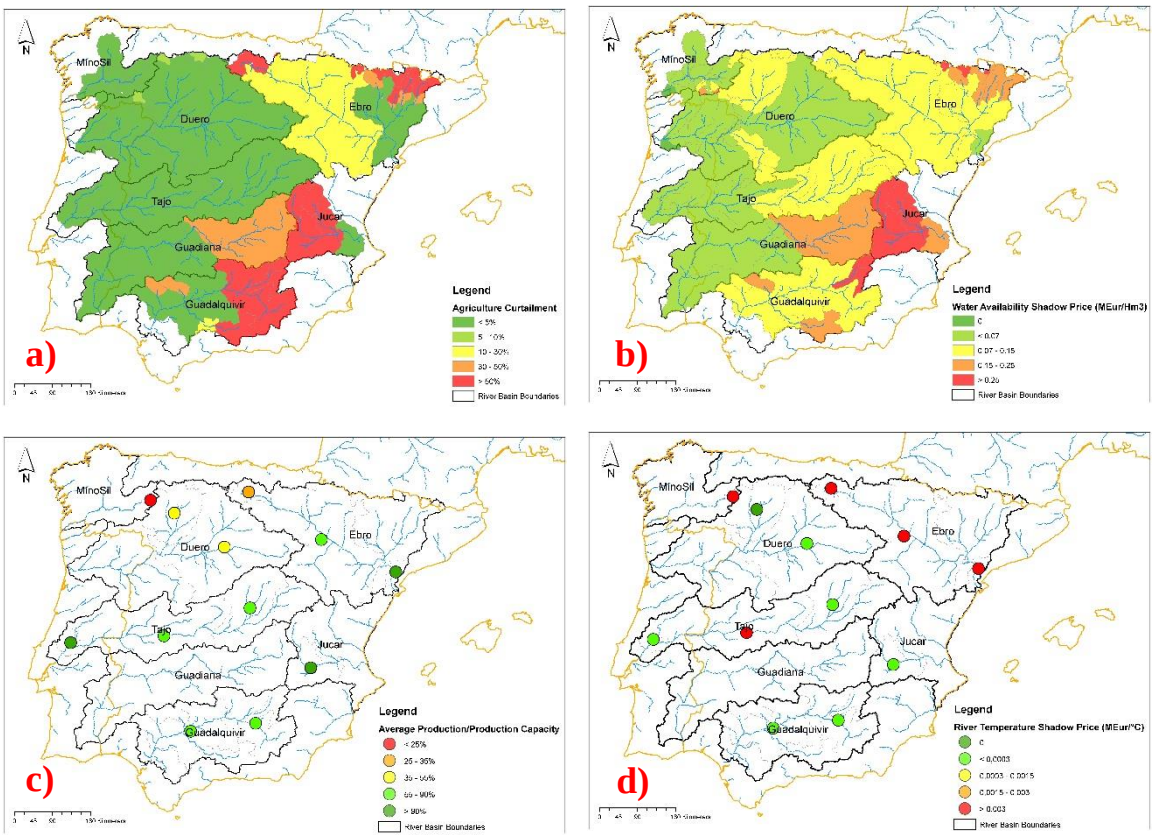

Figure D-2: a) Agriculture curtailment (%) per watershed; (b) Water availability shadow price (M€/Hm^3) per watershed; Ratio between average production and production capacity of each modelled thermal power plant; (d) River water temperature shadow price (M€/°C) per modelled thermal generator.

REMO

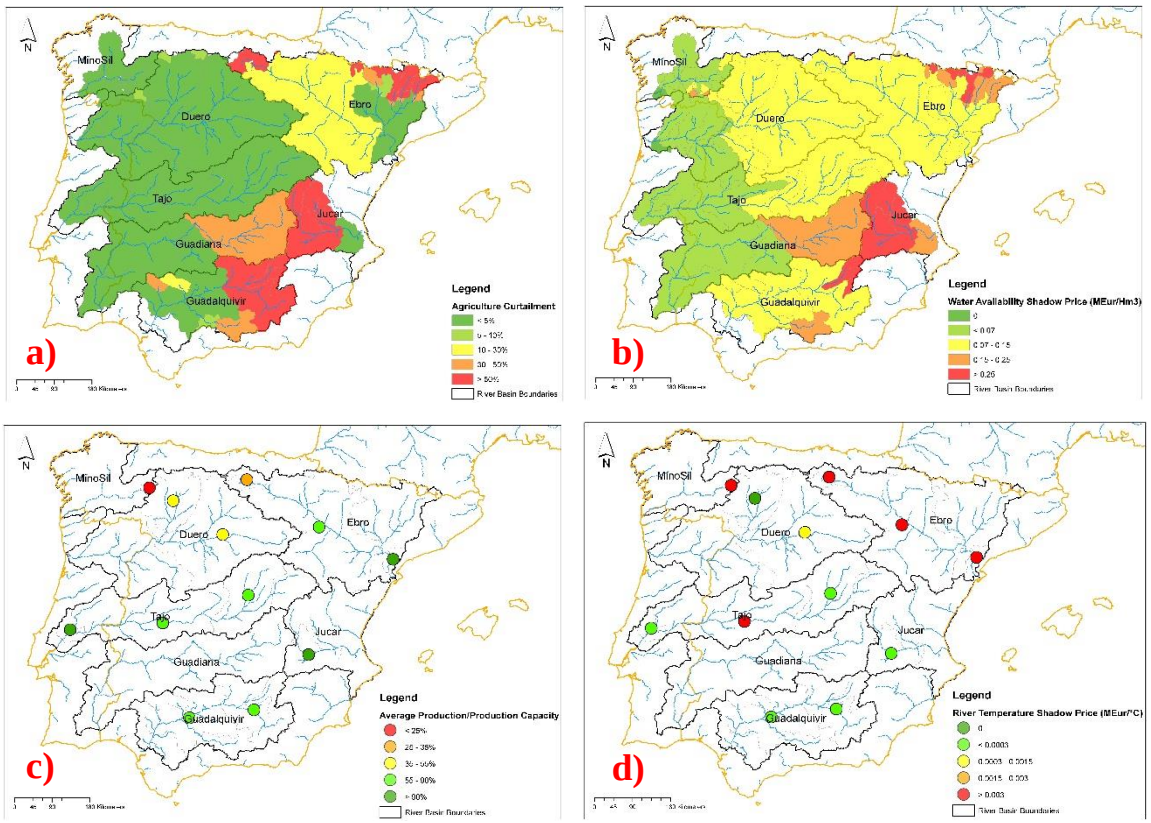

Figure D-3: a) Agriculture curtailment (%) per watershed; (b) Water availability shadow price (M€/Hm^3) per watershed; Ratio between average production and production capacity of each modelled thermal power plant; (d) River water temperature shadow price (M€/°C) per modelled thermal generator.